UNIVERSITY OF CAPE TOWN

MASTERS DISSERTATION

Rapidity evolution of observables at high energies using the gaussian truncation

Author:
Daniel ADAMIAK

Supervisor:
Assoc/Prof. H WEIGERT

A thesis submitted in fulfilment of the requirements for the degree of Master of Science

in the Department of Physics

November 27, 2018

UNIVERSITY OF CAPE TOWN

Abstract

Faculty of Science
Department of Physics

Master of Science

Rapidity evolution of observables at high energies using the gaussian truncation

by Daniel ADAMIAK

Today, the biggest predictive uncertainties in the Standard Model arise from theoretical uncertainties in quantum-chromo-dynamics contributions to cross-sections measured at high-energy collider experiments. At high energies, the quantum-chromo-dynamics of particle collisions is well described through the use of the colour-glass condensate. In this domain, the interaction of coloured objects with the CGC medium is well explained through the use of path-ordered colour rotations, called Wilson Lines, as well as their correlators. The rapidity evolution of these correlators is given by the JIMWLK equation. However, this leads to an infinite hierarchy of coupled differential equations, which are impossible to solve in a closed form and truncations become necessary. The most common truncation relies on the large Nc limit, which is relatively crude and subtly breaks gauge invariance. To get around this, we can perform a gauge invariant truncation of this hierarchy in the form of the Gaussian truncation for the correlators of these Wilson lines. Initial comparison to HERA data for the total and rapidity gap cross-sections show a noticeable improvement in comparison to data which only depend on the dipole correlator. We extend this method to incorporate observables that depend on more complicated correlators and present the machinery for how to compute their rapidity dependence with the Gaussian truncation.

Acknowledgements

I'm blessed to have been able to complete this Masters. I am eternally grateful to my parents, without whom I wouldn't be here today. This work would not have been possible without my supervisor, Heribert Weigert, who has guided me through the world of saturation physics and JIMWLK and who is as kind as his knowledge is deep. On top of this, all of my colleagues deserve thanks, who served as fonts knowledge and pillars of support. In no particular order, Lizelle Niit, Robert Moerman, Jonathan Rayner, William Grunow, Luke Lippstreu, Nicole Moodley, Robert Hambrock and Judy Alcock-Zeilinger. I am the better for having known you all.

I'd also like to thank Stephan Peigne for insightful discussions on the induced gluon spectrum. I'd like thank Javier Albacete for providing numerical data. Finally, I'd like to thank the Harry Crossley foundation for funding this endeavour.

Contents

Chapter 1

Introduction

With the collider at CERN reaching an astonishing centre of mass energy of 13 TeV [1], the experimental uncertainties on the particle production spectra are ever shrinking beyond the accuracy of theoretical predictions. The onus is now on theorists to come up with more precise predictions. The area with the largest uncertainties is quantum-chromo-dynamics (QCD), the physics of the strong force. This is unsurprising because QCD is just so resistant to the physicist's tool kit.

The underlying source of this difficulty arises from the non-Abelian nature of QCD. What does this mean? For quantum field theory (QFT), the underlying mathematics of particle physics, the general thrust of how we get information about the world is through the use of Lagrangians. A Lagrangian is an expression constructed out from the kinetic and potential energies of a particular system of particles that encodes both all the dynamics the particles undergo and the inherent symmetries thereof. The equations of motion are hard to solve exactly, so one then uses perturbative expansions to the solution to obtain dynamics. These perturbative expansions are similar to Taylor series, in that we expand in some small parameter and neglect higher order terms. See [2] or [3] for an introduction to the subject. This doesn't really work for QCD.

QCD is non-Abelian because the symmetry it encodes is $SU(3)$, which is non-Abelian. A direct consequence of this is that the gluons, the force mediator for QCD, can self-interact, which introduces a host of non-linearities. In particular, the strong coupling constant, which is the parameter one would naïvely expand in, runs. This means the coupling actually changes its value at different energies. At small energies, this coupling is large and perturbation theory is not applicable. At large energies the coupling is small, perfect for perturbation theory. However, there may be terms that grow as the coupling shrinks, compensating for the couplings small size and leaving perturbation theory inapplicable. In other words, care must be taken before applying perturbation theory. A phenomenon that occurs for many observables is that the gluon "current" is very large. By current we mean the number of gluons the projectile will interact with. This has the effect of compensating for the small strong coupling and we can no longer use the leading order term to approximate the full calculation.

Instead, one is forced to identify new degrees of freedom which either depend on a different, small parameter, or that can be re-summed exactly. There is no universal strategy for treating all of QCD this way, but different kinematic limits can be explored which permit simplifying assumptions. Consider the case where an electron is being scattered off a proton at high energies (Say, 13 TeV). In what is known as the Regge limit, the proton can be considered to consist entirely of low momentum gluons in state known as the Colour Glass Condensate (CGC). The Regge limit will be explained

in more detail in chapter 2, but, briefly, here are some consequences of the limit. First, because the proton consists mostly of gluons, indirect gluon exchanges with the electron contribute the most to the observable. Indirect, because the electron first emits a photon that splits into a quark anti-quark pair that may then exchange gluons. It turns out that all n-gluon exchanges with this quark anti-quark pair contribute more to the observable than even the two photon exchange. Second, because these gluons are soft, i.e. possess low momentum, the quark anti-quark pair will not deviate from their trajectories as they pierce the target proton. In summary, the only relevant interaction in this regime can be through a colour exchange mediated by the gluons. In other words, the dominant contribution to observables comes from these colour exchanges. The objects that describes these colour exchanges are known as Wilson lines and their correlators. It is these objects that we must master in order make predictions for QCD in the Regge limit.

An additional argument for why Wilson line correlators dominate this aspect of QCD can be made by considering the factorization of hard and soft processes. The observables that we calculate and measure get contributions from interactions across the whole range of momentum scales. What Wilson lines can be shown to do is re-sum all of the soft gluon interactions. This is true, regardless of what QCD regime we are working in. However, in the regime where the Regge limit is applicable, most of the interactions that contribute to the observables are soft. In other words, the observable is dominated by soft process. Since these soft processes are captured by Wilson lines, they must effectively describe the observables in question.

Now that we have identified the relevant degrees of freedom, there remains the question of how to calculate these Wilson line correlators. An integro-differential equation has been constructed, the solution of which is the energy dependance of these correlators. This equation is known as the JIMWLK equation [4] and marks a revolutionary point in our understanding of QCD process. The initial condition, as is the case with all differential equations, needs to be prescribed, and, in our case, measured. Unfortunately, the JIMWLK equation is incredibly difficult to solve and full numeric simulations of it are computationally prohibitive. The problem, again, arises because JIMWLK appropriately captures the non-Abelian nature of QCD process and there is just no free lunch for these kinds of QFTs. The manner by which veterans of the CGC get around this is through trading simplicity in the evolution equation against the degree to which evolution equation remains faithful to all the QCD processes. This can be done in a number of different ways, usually through neglecting part of the non-linearities in the evolution equation. What concerns us specifically is a clever method of simplifying JIMWLK known as the Gaussian truncation.

The Gaussian truncation is a method of truncating the JIMWLK equation, making it exactly solvable, while preserving important properties of Wilson line correlators that other contemporary methods don't [5]. As a consequence of gauge invariance, Wilson lines possess what we call the coincident limit property. A Wilson line composed with an anti-Wilson line that both possess the same transverse coordinate dependence, in other words are coincident, must cancel and become gauge equivalent to one. This is the property that is usually lost that the Gaussian truncation preserves. So far, the Gaussian truncation has only been used to numerically predict the simplest Wilson line correlator, the dipole correlator [5].

The Gaussian truncation is the focus of this thesis. We will extend the work in [5], producing a numerical scheme to calculate any Wilson line correlator using the Gaussian truncation. This scheme can calculate correlators of any complexity, including correlators that are neglected in other contemporary truncation schemes.

The thesis is arranged as follows. The first chapter after this introduction will explore the implications of the Regge limit and clarify the assumptions required to make our calculations work.

The third chapter will discuss Wilson lines. We will explore various contexts in which they arise, from the mathematical definition to physical interpretation. We will also discuss various properties of Wilson lines here.

The fourth chapter will be a detailed derivation of the JIMWLK equation for all Wilson line correlators, as this is what one uses to calculate Wilson line correlators. A physical interpretation is extracted as well. After going through an example calculation where we find the evolution equation for the dipole correlator, we discuss a contemporary technique for solving the JIMWLK equation, as well as its strengths and weaknesses.

The fifth chapter will be a detailed derivation and discussion of the Gaussian truncation. We go through how it used to calculate the dipole and more complicated correlators. We also discuss how the Gaussian truncation encodes information about JIMWLK.

The next two chapters explore implementing the numerics of the Gaussian truncation. We present an algorithm and the results thereof. We then explore various limiting cases of the different correlators, checking that the numerics reproduce what we expect analytically.

The penultimate chapter is a detailed derivation of the induced gluon spectrum, an observable important in energy loss effects that depends on Wilson line correlators that we present a method for calculating using the Gaussian truncation.

Chapter 2

Regge and Eikonal Limits

The non-Abelian and non-perturbative nature of QCD make it very difficult to deal with. A common strategy employed is to work in certain kinematic limits that simplify the calculations. For example, the parton distribution functions which describe the partonic content of the proton are derived via the DGLAP equations [6], which are only valid in the Bjorken limit [7]. All of the results of interest to this thesis are applicable in the Regge limit. This is what lets us talk about the CGC and to argue that Wilson lines are the main actors on the stage. Here we will explore precisely what this limit entails and the implications for how we may interpret the resulting physics.

First, one needs to define the kinematic variables that go into the Regge limit. Consider the case of Deep Inelastic Scattering (DIS), shown in figure [2.1], where we probe a proton with an electron via photon exchange

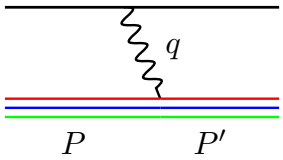

FIGURE 2.1: Feynman diagram for deep inelastic scattering. An electron, represented by the black line, exchanges a photon of momentum q with a proton of momentum P, leaving the proton with momentum P'.

Here the black line is an electron and the coloured lines are the quarks comprising the incoming proton of 4-momentum P. They exchange a photon of 4-momentum q, leaving the proton with momentum $P - q = P'$. Since the exchanged photon is virtual, it actually has a negative invariant mass. We define $Q^2 := -q^2$ to account for this. Q^2 also determines the resolution of the interaction. While the partons in the proton are point-like in our theory, experimentally they appear as small as the wavelength of the photon used to measure them. From these one can define the following Mandelstam variables

$$t := (P - P')^2 = q^2 \tag{2.1}$$

$$\hat{s} := (P + q)^2 \tag{2.2}$$

Mandelstam variables are convenient because they are Lorentz invariants, they are constant in all reference frames. The hat on $\hat{s}$ denotes that it is the invariant energy of a *partonic interaction*, specifically the interaction of the photon and the quark, and not the

energy of the electron-proton system. Finally, the Regge limit is defined as the following

$$\left|\frac{t}{\hat{s}}\right| \to 0. \tag{2.3}$$

Let's change variables again to understand just what this limit implies for the physical picture. We introduce a variable that plays a pivotal role in this thesis, Bjorken-x:

$$x_{bj} := \frac{Q^2}{2P^\mu q_\mu}. \tag{2.4}$$

Bjorken-x can carry the interpretation of the fraction of the proton's momentum taken by the photon. In the Regge limit, x_{bj} behaves like so,

$$x_{bj} = \frac{Q^2}{2P^\mu q_\mu} = \frac{|t|}{\hat{s} - m_P^2 + Q^2} \to \left|\frac{t}{\hat{s}}\right|, \tag{2.5}$$

where m_P is the mass of the proton. In other words, x_{bj} goes to zero in the Regge limit. To invoke the Regge limit more precisely, we fix the transferred momentum, Q^2 and let the interaction energy, $\hat{s}$, go to infinity. This has the effect of fixing the resolution and making a decrease in x_{bj} synonymous with an increase in energy. At this point we can ask the question: how does the energy and resolution affect the make-up of the proton? The resolution determines the apparent size of the constituent parton and the energy determines the ability for quark anti-quark ($q\bar{q}$) pairs to form. A representation of this behaviour is given in figure [2.2].

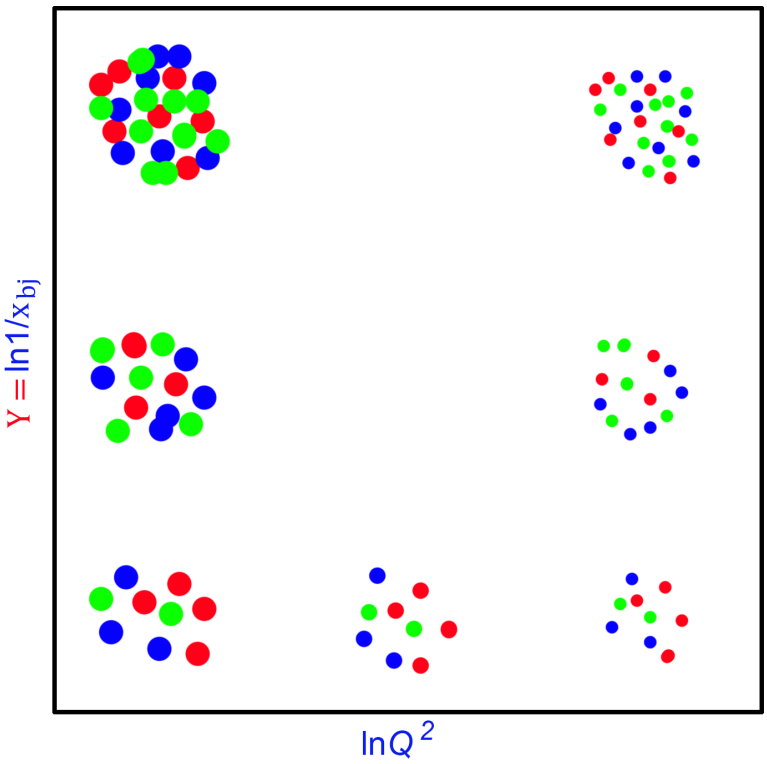

FIGURE 2.2: The rapidity, Y, is related to the energy of the process and the space-like momentum, Q^2, sets the resolution of the process. This figure shows a figurative make-up of a proton at different energies and resolutions.

Here, Y is rapidity. It is related to x_{bj} by

$$Y = \ln(1/x_{bj}). \tag{2.6}$$

Hence, an increasing energy, $\hat{s}$, leads to a decreasing x_{bj}, which in turn leads to an increasing rapidity. Therefore, we can talk about increasing rapidity as being synonymous with increasing energy. Figure [2.2] displays the effect on the proton make-up at different resolutions and energies. Increasing the resolution shrinks the apparent size of the partons, but increasing the energy allows for the increase of pair production of partons. In the Bjorken limit, one fixes the energy but at the same time increases the resolution. This simplifies things, because then the proton can be modelled as a dilute collection of non-interacting partons. It is in this context in which DGLAP is derived, which will be spoken about below. We, on the other hand, are interested in the top, left-hand corner of figure [2.2]. Here it is impossible to treat the partons as non-interacting. In fact, they overlap and become hard to distinguish. This allows for different simplifications to be made as we can treat the proton as continuous colour field instead of as a collection of distinguishable particles.

We are almost at the point where we can motivate the CGC. The make-up of the proton is determined by the parton distribution functions (PDFs)[8]. These functions are derived using the DGLAP equations and, while they are not valid for small x_{bj}, they do hint that the distribution of a nucleon is dominated by gluons.

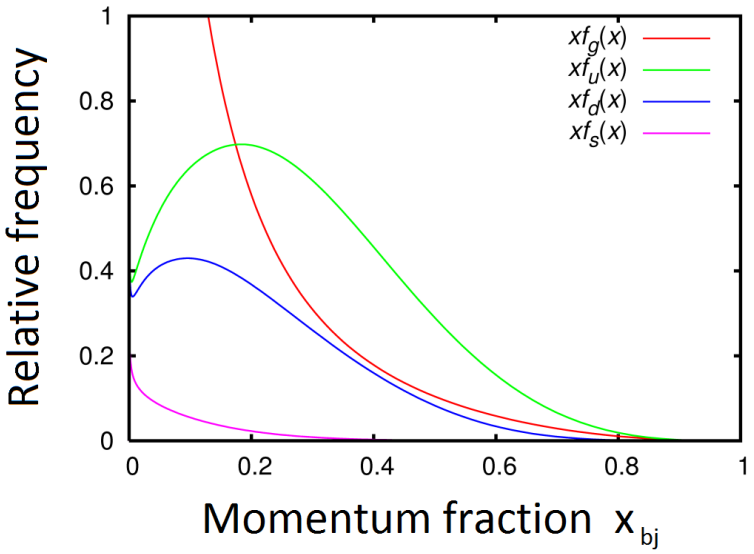

FIGURE 2.3: Parton Distribution function

The Regge limit gives us the following: the target proton in DIS seems to be made of dense and overlapping gluons and it is this state of matter that is dubbed the colour glass condensate.

In the next chapter, we will show that the eikonal limit leads to the presence of Wilson lines. We will also explore and explain the various contexts in which Wilson lines appear as well as some of their properties.

Chapter 3

Wilson Lines

In the context of the CGC, we make the claim that we can replace the partonic interactions between the projectile and target with objects, called Wilson lines, that encode the colour rotations of the partons as they traverse the target. This chapter will attempt to justify this claim, but also help familiarize the reader with a number of contexts in which Wilson lines naturally arise. The mathematical definition of Wilson lines is that they are elements of the special unitary group, $SU(N_c)$, that arise from path ordered matrix exponentials of elements of the special unitary algebra, $su(N_c)$:

$$U_R(\boldsymbol{x})_{[\gamma;b,a]} = \mathcal{P}\exp\left[ig\int_0^1 ds\frac{d\gamma^\mu}{ds}A^a_\mu(\gamma(s))T^a_R\right] \tag{3.1}$$

where γ is a path parametrized by $s \in [0,1]$ with $\gamma(0) = a$ and $\gamma(1) = b$, $T \in su(N_c)$ R is the representation of the generator, g is the coupling constant and A is the gauge field. By gauge field, we mean that A^a is a set coefficients in the linear combination of generators, A^aT^a, that are determined from the gluon configuration of the proton target. $\mathcal{P}$ is the path ordering symbol, denoting path ordering from the lower limit of the integral, 0, to the upper limit, 1. In the context of saturation physics, which is what we'll be dealing with in this work, it sufficient to work with straight paths along the x^- light-cone direction.

$$U_R(\boldsymbol{x})_{[b,a]} = \mathcal{P}\exp\left[ig\int_a^b dx^- A^{+a}(x^-,\boldsymbol{x})T^a_R\right] \tag{3.2}$$

Where a and b are the start and end of the path respectively. Whether the integral is done in the x^- direction and the coordinate degrees of freedom are the transverse coordinates is a matter of context, but it is what we will use throughout this work.

In all representations, the generators, T^a_R, are Hermitian. A Wilson line in the fundamental representation is the object we associate with quarks. Due to these objects being Hermitian, taking the Hermitian conjugate of a Wilson line changes the sign of the i, but leaves the generators unchanged. The path ordering is also reversed. This is because, in the Dyson expansion of the path ordered exponential, each term consists of the product of matrices which, when transposed, reverse order. In other words, a daggered Wilson line is that same Wilson line but along the reverse path.

$$\begin{aligned} U^\dagger_F(\boldsymbol{x})_{[b,a]} &= \overline{\mathcal{P}}exp\left[-ig\int_a^b dx^- A^{+a}(x^+,\boldsymbol{x})t^a\right] \\ &= \mathcal{P}exp\left[ig\int_b^a dx^- A^{+a}(x^+,\boldsymbol{x})t^a\right] \\ &= U_F(\boldsymbol{x})_{[a,b]}, \end{aligned} \tag{3.3}$$

where $\overline{\mathcal{P}}$ denotes reverse or anti-path ordering, ordering from the upper limit of the integral, b, to the lower limit, a. When a path ordered integral is transposed, its ordering is reversed. Regular path ordering may be restored by swapping the order of integration. Equation (3.3) also carries the interpretation of an anti-quark travelling along the forward path. If one were to use the adjoint representation instead of the fundamental, as explained in section 3.3, then the Wilson line represents a hard gluon in a background of soft gluons.

Another property that these Wilson lines possess as a consequence of being path-ordered exponentials is **Composition**: The product of two Wilson lines where one ends where the other begins is just the Wilson line along the entire path. I.e.

$$U_{c,b}U_{b,a} = U_{c,a}, \tag{3.4}$$

with paths $[c, b]$ and $[b, a]$, and $c > b > a$. This can be thought of as the defining property of path ordered functions. Since the exponentials making each Wilson line are themselves path ordered and the two paths are ordered with respect to each other, they can then be conjoined under one path ordering symbol. This statement can also be proven explicitly with reference to the Baker-Campbell-Hausdorff formula.

Proof:
This is a property of path ordered exponentials. Consider two path ordered exponentials, with paths $[c, b]$ and $[b, a]$, and $c > b > a$. Their product is as follows

$$\mathcal{P}e^{ig\int_b^c dx_1 A(x_1)}\mathcal{P}e^{ig\int_a^b dx_2 A(x_2)} = \mathcal{P}e^{ig\int_b^c dx_1 A(x_1)+ig\int_a^b dx_2 A(x_2)} \tag{3.5}$$

Baker-Campbell-Hausdorff implies that in this exponential there must be higher order terms dependent on the commutator of the two exponents. However, if the components do commute, then 3.5 reduces to the simple sum of exponents that we are familiar with[9]. In fact, path ordering enforces this condition. In the Dyson series of this exponential, the commutator term enters like so:

$$\mathcal{P}\int_b^c\int_a^b dx_1 dx_2 [A(x_1), A(x_2)],$$

where take advantage of the fact that $b \leq x_1 \leq c$, $a \leq x_2 \leq b$, thus $x_2 \leq x_1$, and path ordering to deduce

$$\begin{aligned} & \mathcal{P} \int_b^c \int_a^b dx_1 dx_2 [A(x_1), A(x_2)] \\ = \; & \mathcal{P} \int_b^c \int_a^b dx_1 dx_2 A(x_1) A(x_2) - \mathcal{P} \int_b^c \int_a^b dx_1 dx_2 A(x_2) A(x_1) \\ = \; & \int_b^c \int_a^b dx_1 dx_2 A(x_1) A(x_2) - \int_b^c \int_a^b dx_1 dx_2 A(x_1) A(x_2) \\ = \; & 0. \end{aligned} \tag{3.6}$$

From this we can conclude that operators commute under path ordering, which implies that the product of path ordered exponentials is the exponential of the sum. Hence we can compose path ordered exponentials.

In the next few subsections we will explore the interpretations of Wilson lines and the context in which they arise.

3.1 Wilson Line Interpretations

This section is meant to bolster one's intuition of Wilson lines by explaining why and how they appear in different contexts.

3.1.1 As Group elements of SU(N)

The generators that sit in the exponent of the Wilson line are generators of the Lie algebra, $su(N_c)$. Lie algebra elements are mapped to the Lie group via the exponential map. Given that Wilson lines are in fact exponentials of Lie algebra elements, makes them members of the Lie group, $SU(N_c)$.

The special unitary group, $SU(N_c)$, is a sub-group of the general linear group, GL(N_c). The general linear group is the group of $N_c \times N_c$ matrices, while the special unitary group is the group of matrices subjected to the following constraints: For all $U \in SU(N_c)$

$$|det(U)| = 1 \tag{3.7}$$

and

$$UU^\dagger = \mathbb{1}. \tag{3.8}$$

The second property is vital to the purpose of this thesis. In equation [(3.2)], we constructed the Wilson line to have a transverse coordinate dependence and we shall find Wilson lines often enter into observables as the trace of the product of Wilson lines, e.g. tr$(U_{\boldsymbol{x}} U_{\boldsymbol{y}}^\dagger)$. One can then ask, what happens in the coincident limit, $\boldsymbol{y} \to \boldsymbol{x}$?

$$U_{\boldsymbol{x}} U_{\boldsymbol{y}}^\dagger \underset{\boldsymbol{y} \to \boldsymbol{x}}{\to} U_{\boldsymbol{x}} U_{\boldsymbol{x}}^\dagger = \mathbb{1}. \tag{3.9}$$

This is known as the coincident limit property of Wilson lines, where correlators of Wilson lines simplify in very particular ways when the particles they represent are too close to each other to resolve separately.

This is the crucial property whose consequences for correlators we try to preserve in this thesis. The most common technique for calculating Wilson line correlators numerically is the large N_c limit, which loses this property beyond leading order in N_c. In chapter 5 we will discuss a numerical technique for giving us access to any Wilson line correlator while preserving the coincident limit property.

The Lie Derivative

At this point it is convenient to also discuss the generators of translations across the group manifold of SU(N_c). The operator that generates translations is that which, when exponentiated, takes us from one point on the manifold to another. As a simple example, consider a function in flat space, $f(x) : \mathbb{R}^n \to \mathbb{R}$.

If we want to find the value of the function f at some new position, $x_0 + \epsilon$, we could make reference to the Taylor expansion of f,

$$\begin{aligned} f(x_0+\epsilon) &= f(x) + \epsilon^\mu \nabla_\mu f(x) + \frac{1}{2!}(\epsilon^\mu \nabla_\mu)^2 f(x) + ... \Big|_{x=x_0} \\ &= \sum_{n=0}^{\infty} \frac{1}{n!}(\epsilon^\mu \nabla_\mu)^n f(x) \Big|_{x=x_0}. \end{aligned} \tag{3.10}$$

But this sum can exactly be expressed as the exponential

$$\sum_{n=0}^{\infty} \frac{1}{n!}(\epsilon^\mu \nabla_\mu)^n = e^{\epsilon^\mu \nabla_\mu}. \tag{3.11}$$

It is in this sense that we say that $\epsilon^\mu \nabla_\mu$ generates a translation of magnitude $|\epsilon|$ in the ϵ direction. In the same vein, the operator that translates in the direction ϵ^a along the manifold of SU(N_c) is

$$i\nabla^a_{U_R} := [U_R T^a_R]_{ij} \frac{\delta}{\delta U_{Rij}}. \tag{3.12}$$

This is seen if one computes

$$\begin{aligned} e^{-\epsilon^a (i\nabla^a_{U_R})} U_R &= U_R(1 + \epsilon^a T^a_R + \frac{1}{2}(\epsilon^a T^a_R)^2 + ...) \\ &= U_R e^{i\epsilon^a T^a_R}. \end{aligned} \tag{3.13}$$

The term to the right of U is an exponential of Lie algebra generators and is thus an element of SU(N_c). Given that the product of two group elements is itself a group element, we conclude the U has been translated to another position on the group manifold. The object, $i\nabla^a_U$, also satisfies all the conditions required to be a Lie derivative, so we will refer to it as such.

There is an identity that immediately follows from this definition of the Lie derivative:

$$[Ut^a]_{ij}\frac{\delta}{\delta U_{ij}} = [-t^a U^\dagger]_{ij}\frac{\delta}{\delta U^\dagger_{ij}}, \tag{3.14}$$

where we have restricted ourselves to the fundamental representation for convenience's sake. This holds in all representations. To show this, one would need to demonstrate that when either operator in equation (3.14) is applied to an arbitrary Wilson line that they produce the same result.

First we need to write down what the functional derivative of a Wilson line with respect to an anti-Wilson line is. To determine this, consider the following:

$$\frac{\delta}{\delta U^\dagger_{\alpha\beta}}U_{ij}U^\dagger_{jk} = U_{ij}\delta_{\alpha j}\delta_{\beta k} + \frac{\delta U_{ij}}{\delta U^\dagger_{\alpha\beta}}U^\dagger_{jk}. \tag{3.15}$$

We see that the right hand side contains the term we seek. First, notice that the object we are differentiating is actually a Kronecker delta in $SU(N_c)$, as per the property of Hermiticity (3.8). Therefore this derivative is zero. Second, we can remove the factor multiplying the functional derivative we are interested in by multiplying both sides by the appropriate inverse element, U_{kl}. These result in

$$\frac{\delta U_{il}}{\delta U^\dagger_{\alpha\beta}} = -U_{i\alpha}U_{\beta l}. \tag{3.16}$$

Thus we have determined the functional dependence of the anti-Wilson line on its corresponding Wilson line. Armed with this knowledge we can rewrite the functional derivative with respect to a Wilson line in terms of the functional derivative with respect to an anti-Wilson line. In other words, we can come up with some expression in terms of $\frac{\delta}{\delta U^\dagger_{\alpha\beta}}$ that has the same action as the regular functional derivative, i.e. $\frac{\delta}{\delta U_{\alpha\beta}}U_{ij} = \delta_{\alpha i}\delta_{\beta j}$. Staring at equation (3.16), it's not hard to see that this takes the form of

$$\frac{\delta}{\delta U_{\alpha\beta}}U_{ij} = -U^\dagger_{k\alpha}U^\dagger_{\beta m}\frac{\delta}{\delta U^\dagger_{km}}U_{ij} = \delta_{\alpha i}\delta_{\beta j} \tag{3.17}$$

Referring back to equation (3.14), it is now easy to show that this relation is true by rewriting the function derivative:

$$\begin{aligned}[Ut^a]_{ij}\frac{\delta}{\delta U_{ij}} &= -[Ut^a]_{ij}U^\dagger_{jl}U^\dagger_{ki}\frac{\delta}{\delta U^\dagger_{kl}} \\ &= -[t^a U]_{kl}\frac{\delta}{\delta U^\dagger_{kl}},\end{aligned} \tag{3.18}$$

and the identity is proven.

The Lie derivative (3.12) is also known as a left invariant vector field. We can construct

a corresponding right invariant vector field, another Lie derivative as such:

$$i\bar{\nabla}^a_U = -[t^a U]_{ij}\frac{\delta}{\delta U_{ij}} = [U^\dagger t^a]_{ij}\frac{\delta}{\delta U^\dagger_{ij}}, \tag{3.19}$$

where the second equality is proven much the same as for equation (3.14). Throughout this work we won't just be working with single arbitrary elements of $SU(N_c)$. As suggested at the start of the chapter, we will be working with fields. In other words, our Wilson lines possess a coordinate dependence. The implication this has for this discussion on Lie derivatives is that the functional derivative has to hit the coordinate dependence as well.

$$\begin{aligned}\frac{\delta U_{ij,\boldsymbol{x}}}{\delta U_{\alpha\beta,\boldsymbol{y}}} &= \delta_{\alpha i}\delta_{\beta j}\delta^{(2)}(\boldsymbol{x}-\boldsymbol{y}) \\ i\nabla^a_{\boldsymbol{y}} U_{\boldsymbol{x}} &= U_{\boldsymbol{y}} t^a.\end{aligned} \tag{3.20}$$

These left and right invariant vector field have a number of inter-relating properties. They both individually satisfy the commutation relations of $SU(N_c)$. The commutation relations are given by

$$[t^a, t^b] = if^{abc}t^c, \tag{3.21}$$

where f^{abc} is the anti-symmetric colour tensor as discussed later in the section on the adjoint representation 3.3. Consequently, the Lie derivatives satisfy

$$[i\nabla^a_{\boldsymbol{x}}, i\nabla^b_{\boldsymbol{y}}] = if^{abc}i\nabla^c_{\boldsymbol{x}}\delta^{(2)}(\boldsymbol{x}-\boldsymbol{y}); \qquad [i\bar{\nabla}^a_{\boldsymbol{x}}, i\bar{\nabla}^b_{\boldsymbol{y}}] = if^{abc}i\bar{\nabla}^c_{\boldsymbol{x}}\delta^{(2)}(\boldsymbol{x}-\boldsymbol{y}). \tag{3.22}$$

These two Lie derivatives also commute among themselves,

$$[i\nabla^a_{\boldsymbol{x}}, i\bar{\nabla}^b_{\boldsymbol{y}}] = 0. \tag{3.23}$$

The proof for these statements can be found in the appendix D.

3.1.2 As Gauge Links

In order to keep the Lagrangian of partons gauge invariant, i.e. invariant under the group action of colour rotations, the derivative in the kinetic term needs to be promoted to a covariant derivative. This is accomplished with the introduction of a gauge link. The following discussion comes from chapter 15 of [2]. Let's illustrate this with an example by considering the following Lagrangian of Dirac fields

$$\mathcal{L} = -\bar{\psi}(x)(i\partial_\mu - m)\psi(x) \tag{3.24}$$

which consists only of a kinetic and mass term. One of the great benefits of the Lagrangian formalism is the ability make manifest the symmetries of your system within the Lagrangian itself. In other words, we find it useful to construct Lagrangians that are invariant under the gauge transformation

$$\psi(x) \to e^{i\alpha(x)}\psi(x), \tag{3.25}$$

where $\alpha(x)$ is purely real. Then, $\bar{\psi}$, being the conjugate of ψ will have the opposite transformation

$$\bar{\psi}(x) \to e^{-i\alpha(x)}\bar{\psi}(x). \tag{3.26}$$

Clearly, the mass term of (3.24), $m\bar{\psi}\psi$ is invariant under this transformation. The kinetic term is not, however, as we get an extra term arising from the derivative acting on the gauge transformation. To make (3.24) gauge invariant then, our goal is to modify the kinetic term so that it respects this symmetry, i.e. we will promote the partial derivative, ∂_μ to a covariant derivative D_μ which obeys

$$D_\mu e^{i\alpha(x)}\psi(x) = e^{i\alpha(x)}D_\mu\psi(x). \tag{3.27}$$

A covariant derivative instructs one how to make infinitesimal changes to a function whilst remaining on the manifold of interest. The regular derivative treats the manifold as flat space, but we are interested in working on the curved sub-space that obeys symmetries of $SU(N_c)$. How, then, do we construct D_μ? The insight comes from constructing an operator that describes how the gauge transformation acting on the field changes along a path between two points. In other words, we want an operator, $U(y,x)$, to act on the fields in such a way that under the transformation law (3.25), this field transforms as

$$U(y,x)\psi(x) \to e^{-i\alpha(y)}U(y,x)\psi(x). \tag{3.28}$$

We then construct covariant derivative using this operator. But first, lets talk about U for a moment. It is what we call a comparator or a gauge link, as it links a local gauge transformation to applied at two different space time coordinates. Its suggestive labelling implies that we will discover that the Wilson line plays this role when we set our Lagrangian and symmetries to that of QCD, which is indeed the case.

The covariant derivative is then constructed as

$$n^\mu D_\mu\psi(x) = \lim_{\epsilon\to 0}\frac{1}{\epsilon}[\psi(x+\epsilon n) - U(x+\epsilon n, x)\psi(x)]. \tag{3.29}$$

To make this definition more explicit, we can consider the expansion of U to first order.

$$U(x+\epsilon n, x) = 1 - ig\epsilon n^\mu A_\mu(x) + \mathcal{O}(\epsilon^2) \tag{3.30}$$

In the case of QCD, the field $A_\mu(x)$ turns out to be the gluon gauge field. It is the infinitesimal limit of the gauge link, also known as a *connection*. This is the equivalent of the Christoffel symbol used to define the covariant derivative in the context of General Relativity and Differential Geometry.

With this we can explicitly write down the covariant derivative of our Lagrangian as

$$D_\mu\psi(x) = \partial_\mu\psi(x) + igA_\mu\psi(x) \tag{3.31}$$

Under this definition, D_μ satisfies (3.27), so long as the gauge field, A_μ, obeys certain transformation laws that depend on the gauge symmetry we are trying to impose.

Combinations of Wilson lines called correlators may also enter as the gauge-link in other contexts, such as nuclear structure functions [10] or hard processes [11].

3.1.3 As colour transportation operators

In the previous section, we showed that Wilson lines can be used to construct the covariant derivative. We can turn this around and show how the covariant derivative gives rise to Wilson lines. To reiterate what a covariant derivative does, it describes how to perform an infinitesimal translation along a manifold. In flat space, it just reduces to a regular partial derivative. On a more complicated manifold, like a sphere, the ordinary partial derivative would create a "straight-line" translation that takes you off the surface. It is for this reason that an extra term, called the *connection* is introduced that compensates for this effect and keeps the differentiated object on the sphere. This notion also applies to more complicated manifolds, like SU(3), where the connection is the gauge field. This covariant derivative can then be used to define the parallel transport equation, the solution of which will describe how the object we transport changes in color space as we move it through space time. The parallel transport equation is given by

$$\frac{d\gamma^\mu}{ds} D_\mu U_{[\gamma;b,a]} = 0, \tag{3.32}$$

where D_μ is the covariant derivative derived from the relevant symmetry. In the case of QCD, this has the Wilson line solution (3.1).

Here's another, perhaps more intuitive way to think about it. The colour state of a parton can be thought of as a vector in colour space. The basis vectors point in the red, green and blue directions. This vector corresponds to the amplitude of finding the parton in a particular colour state, so the magnitude is constrained to one. Since it is an amplitude, the components are complex and the colour vector is constrained to live on the complex unit sphere.

We expect the partons that are moving through a colourful medium would exchange colour with their surroundings. In other words, their colour vector would rotate to match the amplitude of being in another colour state. Which operator performs rotations in $\mathbb{C}^3$? Elements of $SU(3)$. So Wilson lines describe the colour rotation of a colourful object as it travels along a certain path.

3.1.4 As a Sum of Soft-Collinear Gluons (Eikonal Approximation)

We have stated earlier that, in the Regge limit, gluon emission diagrams have a soft and collinear divergences, necessitating some sort of resummation. In this section we will demonstrate how this divergence arises and, to our great convenience, that a resummation exists and takes the form of a Wilson line. This section closely follows chapter 1.2.3 of [12]

Consider the emission of a gluon by a quark.

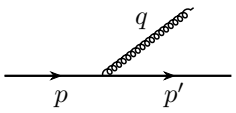

whose amplitude is given by [2]

$$\frac{i(\not{p} - \not{k}) - m}{(p-k)^2 - m^2 + i\epsilon}(-igA^{\mu a}t^a\gamma^\mu)u(p), \tag{3.33}$$

where the first factor is the Dirac propagator for a fermion, the second factor is the gluon vertex joining to the background field A and $u(p)$ is a quark in-state. We note at this point that inherent in the fermion propagator is a soft and collinear divergence. To see this, expand the denominator

$$(p-k)^2 - m^2 = p^2 + k^2 - 2p^\mu k_\mu - m^2 \tag{3.34}$$

The ϵ is neglected as it is just used to determine the integration contour. The four-momentum squared gives the invariant mass squared of the particle. For the quark, $p^2 = m^2$ and, since the gluon is massless, $k^2 = 0$. Then the only term that survives in the denominator is the Minkowski product of p and k

$$(p-k)^2 - m^2 = -2p^0k^0 + 2|p||k|\cos\theta, \tag{3.35}$$

where θ is the angle between the quark and emitted gluon. Clearly this has a soft divergence when $|k| = k^0 \to 0$. To see the collinear divergence, expand $|p|$ in powers of p^0:

$$\begin{aligned} |p| &= \sqrt{(p^0)^2 - m^2} \\ &= p^0\sqrt{1 - \frac{m^2}{(p^0)^2}} \\ &= p^0\left(1 + \mathcal{O}\left(\frac{m^2}{(p^0)^2}\right)\right) \end{aligned} \tag{3.36}$$

So for large p^0, which is what we're working with, $|p|$ is the same size as p^0. Thus when the gluon is collinear, i.e. $\theta = 0$, this denominator vanishes as well. Hence the collinear divergence. This necessitates a re-summing of all such diagrams in the hope of cancelling the divergence.

In the context of the CGC, and thus the eikonal limit, we have $k \ll p$. Since the gluon is massless, we also have that $m = m_q$, the mass of the quark, which will cancel against p^2, which is the invariant mass of the quark, when we expand the denominator. The last consequence of the Regge limit is that $\not{p} - \not{k} \approx \not{p}$. Since we are in the high energy limit, we have that $|p| \gg m$. Applying these simplifications, the amplitude becomes

$$\frac{ip_\nu\gamma^\nu}{-2p\cdot k + i\epsilon}(-igA^{\mu a}t^a\gamma^\mu)u(p), \tag{3.37}$$

where we have resolved $\not{p}$ into $p_\nu\gamma^\nu$. We will now use several properties of the γ-matrices to eliminate them from this expression. To start, note that γ^μ commutes with $A^{\mu a}t^a$:

$$\frac{ip_\nu\gamma^\nu\gamma^\mu}{-2p\cdot k + i\epsilon}(-igA^{\mu a}t^a)u(p). \tag{3.38}$$

Next, we employ the Dirac equation: $p_\nu\gamma^\nu u(p) = 0$ (in the high energy / negligible mass case) to insert a zero in the numerator. We write this zero as $p_\nu\gamma^\mu\gamma^\nu u(p)$ to obtain

$$\frac{ip_\nu(\gamma^\nu\gamma^\mu + \gamma^\mu\gamma^\nu)}{-2p\cdot k + i\epsilon}(-igA^{\mu a}t^a)u(p). \tag{3.39}$$

The γ-matrices may now be eliminated via the identity: $(\gamma^\nu\gamma^\mu + \gamma^\mu\gamma^\nu) = 2g^{\mu\nu}$, where $g^{\mu\nu}$ is the Minkowski metric. Expressing p_ν as the product of a magnitude and unit

vector, $|p|\eta_\nu$, (3.39) can be written as

$$\frac{2i|p|\eta_\nu g^{\mu\nu}}{-2|p|\eta\cdot k+i\epsilon}(-igA^{\mu a}t^a)u(p). \tag{3.40}$$

p may now be cancelled from the equation, given an appropriate rescaling of ϵ to keep it infinitesimal, finally granting us a what is known as the Wilson propagator:

$$\frac{i}{-\eta\cdot k+i\epsilon}(-ig\eta^\mu A^{\mu a}t^a)u(p). \tag{3.41}$$

Let's take a moment to consider (3.41), which describes the amplitude of the Wilson line of a quark emitting a gluon. The first factor is known as the Wilson propagator. The second factor, in brackets, is the (Wilson) gluon vertex joining to the background field, $A^{\mu a}$. Note that the propagator has a soft and collinear divergence: if k is sufficiently small or points in the same direction as the quark, the propagator blows up to infinity. This is why it is insufficient to take the leading order Feynman diagram of gluon exchange to approximate deep inelastic scattering - the result is just unitarity violating. It is for this reason that we need to turn to resumming all such diagrams with n gluon emissions, with the hope that the divergences cancel and we get a finite result. The second half of the section aims to do precisely this.

Without an argument for why any individual Feynman diagram is more important than any other, we are left with no recourse but to sum all of them. A priori, this is a daunting task, considering the increasing complexity of the diagrams when one includes the gluon self-interaction vertices. Fortunately, it can be shown that only terms that are constructed as an ordered product of (3.41) contribute to the eikonal cross-section. This was shown in, for instance, [13, 14].

Generically, we now want to perform the sum over all ordered products of Wilson propagators,

$$\sum_{m=0}^{\infty}(-ig\eta)^m A(k_m)...A(k_1)\prod_{f=1}^{m}\left(\frac{i}{-\eta\sum_{j=1}^{f}k_j+i\epsilon}\right), \tag{3.42}$$

where we have compacted $A=A^at^A$ and it is understood that for each A, there is an η it contracts with. The aim is to show that this gives us a Wilson line. Actually, since Wilson lines live in position space, we need to find the Fourier transform of (3.42). We will consider the mth term of this sum and show that it is equal to the mth term in the Taylor expansion of the path-ordered exponential that is the Wilson line.

The Fourier transform of the mth term of (3.42) is

$$(-ig\eta)^m\int\frac{d^4k_1...d^4k_m}{(4\pi)^{2m}}A(k_m)...A(k_1)\prod_{f=1}^{m}\left(\frac{i}{-\eta\sum_{j=1}^{f}k_j+i\epsilon}e^{-i\tau_m\eta\cdot k_f}\right). \tag{3.43}$$

Consider the product in (3.43). If we evaluate it in the $m = 1$ case we find that it is the Fourier transform of a Heaviside step function:

$$\frac{i}{-\eta k_1 + i\epsilon} e^{-i\tau_2 \eta\cdot k_f} = \int_{-\infty}^{\infty} d\tau_1 \; \theta(\tau_2 - \tau_1) e^{-\tau_1 \eta\cdot k_1} = \int_{-\infty}^{\tau_2} d\tau_1 \; e^{-\tau_1 \eta\cdot k_1}, \tag{3.44}$$

although this requires a relabeling of $\tau_m \to \tau_{m+1}$ to read more easily. The mth term case reads similarly:

$$\prod_{f=1}^{m} \left(\frac{i}{-\eta \sum_{j=1}^{f} k_j + i\epsilon} e^{-i\tau_m \eta\cdot k_f} \right) = \int_{-\infty}^{\infty} d\tau_m ... \int_{-\infty}^{\tau_3} d\tau_2 \int_{-\infty}^{\tau_2} d\tau_1 \; e^{-i\eta\cdot \sum_{j=1}^{m} t_j k_j}. \tag{3.45}$$

Next we look at the parts that depend on k_i, namely the gauge fields, A, and the exponential terms. Straight forwardly this is the Fourier transform of the gauge field:

$$\int \frac{d^4k}{(4\pi)^2} e^{-i\tau\eta\cdot k} A_\mu(k) = A_\mu(\tau\eta^\nu). \tag{3.46}$$

Putting all of this together, the mth term of (3.42) now looks like

$$(-ig\eta)^m \int_{-\infty}^{\infty} d\tau_m ... \int_{-\infty}^{\tau_3} d\tau_2 \int_{-\infty}^{\tau_2} d\tau_1 \prod_{j=1}^{m} A_\mu(\tau_j \eta^\nu), \tag{3.47}$$

which is precisely the mth term of the Taylor expansion of the path-ordered exponential

$$\mathcal{P}\exp\left[-ig \int_{-\infty}^{\infty} \eta \cdot A(\tau\eta) \right]. \tag{3.48}$$

Thus we have shown that a Wilson line can be interpreted as the sum of all diagrams with an eikonal line emitting any number of gluons, vis-a-vis

$$\sum_{n=1}^{\infty} \tag{3.49}$$

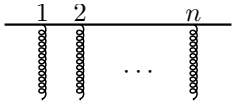

3.2 Wilson Line Derivatives

The derivative of a Wilson line with respect to its transverse coordinates is complicated by the path ordering. This is a non-trivial result that we will make use of, so we present the result and proof here. We don't get a contribution from the exponent dropping to the left or the right of the exponential, instead the contribution drops in the middle of the path:

$$\partial_i U(v) = ig \int_{-\infty}^{\infty} dv^- U[\infty, v^-; \boldsymbol{v}] t^c \left(\partial_i A_c^+(v^-, \boldsymbol{v}) \right) U[v^-, -\infty; \boldsymbol{v}], \tag{3.50}$$

where $U[b,a;v] = P\text{exp}\left\{ig\int_a^b dz^- t^c A_c^+(z^-,\boldsymbol{v})\right\}$ and $U(v) = U[\infty,-\infty,\boldsymbol{v}]$. The partial derivative ∂_i is with respect to the transverse coordinates, i. We show that equation (3.50) is true up to second order and then to all orders by expanding the Wilson lines in terms of their Dyson series (see Peskin and Schroeder chapter 4 for an overview). Dyson series encode path ordering in the limits of a series of integrals. Consider the the derivative of the Dyson series of the Wilson line ($A(x) := t^c A_c^+(x,\boldsymbol{v})$ for brevity):

$$\begin{aligned}
\partial_i U(x) =&\partial_i \left(\mathbb{1} + ig\int_{-\infty}^{\infty} dx_1 A(x_1) + (ig)^2 \int_{-\infty}^{\infty} dx_1 \int_{-\infty}^{x_1} dx_2 A(x_1)A(x_2) + \dots \right) \\
=&ig\int_{-\infty}^{\infty} dx_1 \partial_i A(x_1) \\
&+ \underbrace{(ig)^2 \int_{-\infty}^{\infty} dx_1 \int_{-\infty}^{x_1} dx_2 \partial_i A(x_1)A(x_2)}_{(1)} + \underbrace{(igs)^2 \int_{-\infty}^{\infty} dx_1 \int_{-\infty}^{x_1} dx_2 A(x_1)\partial_i A(x_2)}_{(2)} \\
&+ \dots
\end{aligned} \tag{3.51}$$

From the other side, let's insert the Dyson series into equation (3.50) and show they are equal (up to second order).

$$\begin{aligned}
\partial_i U(x) =&ig\int_{-\infty}^{\infty} dx\, U[\infty,x;\boldsymbol{v}] \left(\partial_i A^-(x,\boldsymbol{v})\right) U[x,-\infty;\boldsymbol{v}] \\
=&ig\int_{-\infty}^{\infty} dx \left[\mathbb{1} + ig\int_x^{\infty} dx_1\, A(x_1) + \dots\right] (\partial_i A(x)) \times \left[\mathbb{1} + igs\int_{-\infty}^{x} dx_1\, A(x_1) + \dots\right] \\
=&ig\int_{-\infty}^{\infty} dx\, \partial_i A(x) \\
&+ \underbrace{(ig)^2 \int_{-\infty}^{\infty} dx \int_{-\infty}^{x} dx_1 \partial_i A(x)A(x_1)}_{(1)} + \underbrace{(ig)^2 \int_{-\infty}^{\infty} dx \int_{x}^{\infty} dx_1\, A(x_1)\partial_i A(x)}_{(2)} \\
&+ \dots
\end{aligned} \tag{3.52}$$

Comparing equations (3.51) and (3.52), the terms labelled (1) are already equal and the terms labelled (2) are equivalent under the use of corollary 3.2 and exchange of variables $x \leftrightarrow x_1$. Hence, the two equations are equal up to second order. It remains to be shown that they are equal to all orders. The nth order in g term in the expansion

(3.51) is given by

$$\partial_i U(v) \overset{\text{nth order}}{=} \sum_{k=1}^{n} \int_{-\infty}^{\infty} dx_1 \int_{-\infty}^{x_1} dx_2 ... \int_{-\infty}^{x_{n-1}} dx_n A(x_1)...A(x_{k-1})\partial_i A(x_k)A(x_{k+1})...A(x_n). \tag{3.53}$$

The nth term in (3.52) is given by

$$\begin{aligned} & ig \int_{-\infty}^{\infty} dx U[\infty, x] \left(\partial_i A^-(x)\right) U[x, -\infty]] \\ \overset{\text{nth order}}{=} & \sum_{k=1}^{n} (ig)^n \int_{-\infty}^{\infty} dx \int_{x}^{\infty} dx_1 \int_{x}^{x_1} dx_2 ... \int_{x}^{x_{k-2}} dx_{k-1} \int_{-\infty}^{x} dx_{k+1} \int_{-\infty}^{x_{k+1}} dx_{k+2} ... \int_{-\infty}^{x_{n-1}} dx_n \\ & \times A(x_1)...A(x_{k-1})\partial_i A(x_k)A(x_{k+1})...A(x_n). \end{aligned} \tag{3.54}$$

We will show that these two expression are equivalent and thus that the derivative of a Wilson line is as proposed. The trick is much the same as for the 2nd order case, we employ (3.57) repeatedly until (3.54) looks like (3.53). The first exchange of integrals goes like

$$\int_{-\infty}^{\infty} dx \int_{x}^{\infty} dx_1 = \int_{-\infty}^{\infty} dx_1 \int_{x}^{x_1} dx. \tag{3.55}$$

The second exchange is

$$\int_{-\infty}^{x_1} dx \int_{x}^{x_1} dx_2 = \int_{-\infty}^{x_1} dx_2 \int_{-\infty}^{x_2} dx \tag{3.56}$$

This should be repeated $k-1$ times and then x should be relabelled x_k, then the two nth-order terms will be precisely the same.

Corollary: Integrating the lower right half-plane

The following two integrals are equivalent, because they both integrate over the same region, the triangle in figure 3.2.

$$\int_{-\infty}^{c} dx \int_{-\infty}^{x} dy\ f(x,y) = \int_{y}^{c} dx \int_{-\infty}^{c} dy\ f(x,y) \tag{3.57}$$

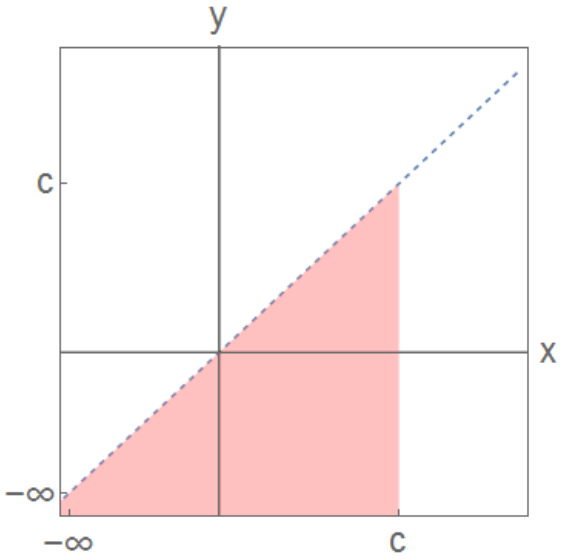

FIGURE 3.1: Triangle whose vertices are given by $(-\infty, -\infty), (c, -\infty), (c, c)$.

3.3 The adjoint representation of $su(N_c)$

When discussing the Lie algebra, $su(N_c)$, one cannot avoid talking about the adjoint representation. While the fundamental representation is chosen by convention, the adjoint representation can be constructed out of any representation and is thus more inherent to any Lie algebra. But critical for our purposes is that Wilson lines in the adjoint representation correspond not to quarks or anti-quarks, but to gluons.

A Wilson line in a given representation, R, is generically given by (suppressing notions of path-ordering for now) the exponential of Lie algebra elements in that representation

$$U_R(s) = e^{sX^a iT_R^a}, \tag{3.58}$$

where, s parametrizes some path on the group that goes through the unit element. For simplicity's sake, we will restrict ourselves to the fundamental representation, $U := U_{R=F}$, $t := T_F$. Given that the action of a group element on a Lie-algebra element in the adjoint representation is defined to be

$$U_A^{ab} t^b = Adj(U) t^a = U t^a U^\dagger, \tag{3.59}$$

we show, in the adjoint representation $R = A$, that

$$U_A^{ab} = 2\text{tr}\left(t^a U t^b U^\dagger\right). \tag{3.60}$$

To prove this we make use of the fact that, for $su(N_c)$, we have the following inner product

$$2\text{tr}\left(t^a t^b\right), \tag{3.61}$$

with the following normalization condition for generators

$$\text{tr}(t^a t^b) = \frac{1}{2}\delta^{ab}. \tag{3.62}$$

Equation (3.60) then follows as the projection of the adjoint action (3.59) onto the fundamental generators using (3.61) as the inner product.

This representation can be constructed using any choice of generators, t^a. This makes the adjoint representation unique in this respect. However, we would like to be able to construct Wilson lines in the adjoint representation using their own generators. To do this we construct the generators and then prove that they generate the adjoint Wilson lines. The adjoint generators are given by the commutation relations of the generators of $su(N_c)$ in any representation

$$[t^a, t^b] = if^{abc}t^c, \tag{3.63}$$

where if^{abc}, including the factor of i, is the generator of the adjoint representation and is anti-symmetric in its colour indices. To prove they are the generators, we need to demonstrate that

$$U_A^{ab}(s) = e^{sX^c i(if^{abc})}, \tag{3.64}$$

with the initial condition $U_A(0) = \mathbb{1}$. We make use of equation (3.60), substituting the exponential forms of the Wilson lines.

$$2\text{tr}\left[t^a e^{sX^c it^c} t^b e^{-sX^c it^c}\right] \stackrel{!}{=} e^{-sX^c f^{abc}}. \tag{3.65}$$

Next, we differentiate both sides with respect s and set s to zero:

$$\begin{aligned}
\frac{d}{ds}\Big|_{s=0}: \quad 2\text{tr}\left(t^a X^c it^c t^b - t^a t^b X^c it^c\right) &\stackrel{!}{=} -X^c f^{abc} \\
2\text{tr}\left(t^a X^c i[t^c, t^b]\right) &\stackrel{!}{=} -X^c f^{abc} \\
2\text{tr}\left(t^a X^c (i)^2 f^{cbj} t^j\right) &\stackrel{!}{=} -X^c f^{abc} \\
-X^c f^{cbj} 2\text{tr}\left(t^a t^j\right) &\stackrel{!}{=} -X^c f^{abc} \\
-X^c f^{cbj}\delta^{aj} &\stackrel{!}{=} -X^c f^{abc} \\
-X^c f^{cba} &\stackrel{!}{=} -X^c f^{abc}.
\end{aligned} \tag{3.66}$$

When one use the cyclicity of f ($f^{cba} = f^{abc}$) one obtains equality and we have proved what we set out to do.

Adjoint Wilson lines carry the interpretation of a gluon and the colour rotation thereof. To see why this is the case, one can repeat the argument of 3.1.4, replacing the fundamental generators with adjoint ones.

A consequence of using if^{abc} as the generator for Wilson lines is that the resulting Wilson line is purely real and the Hermitian conjugate of an adjoint Wilson line results in the same Wilson line. This matches with the intuition of how an adjoint Wilson line

should behave if it were to carry the interpretation of a gluon, since anti-gluons themselves are just gluons.

Throughout the rest of this work, rather than leaving the representation unspecified we use

$$U := U_{R=F} \tag{3.67}$$

for fundamental Wilson lines and

$$\widetilde{U} := U_{R=A} \tag{3.68}$$

for adjoint Wilson lines.

Chapter 4

JIMWLK

Having motivated that Wilson lines are the relevant degrees of freedom in the low-Bjorken x regime, we need to now try and determine a precise expression for them for use in the computation of observables. The most precise method to date for computing Wilson line correlators is the Jalilian-Marian+Iancu+McLerran+Weigert+Leonidov+Kovner equation. Shortened to JIMWLK (pronounced "gym-walk") in all texts.

JIMWLK is a renormalization group flow equation, a differential equation that determines the evolution of all Wilson line correlators as the rapidity is changed. This is an evolution equation that, given some initial condition, lets one calculate the precise numerical value of Wilson line correlators for all energies.

Here we will give a broad-strokes strategy to deriving JIMWLK to leading order in rapidity and in the subsequent subsections provide more calculation details. The fastest route to finding the evolution equation for all Wilson line correlators is the method suggested in [4], that is to find the evolution for their generating functional (GF):

$$\mathcal{Z}[J^\dagger, J] = \langle e^{\mathcal{S}^{q\bar{q}}_{\text{ext}}[b, J^\dagger, J]} \rangle_b, \tag{4.1}$$

where the action is given by

$$\mathcal{S}^{q\bar{q}}_{\text{ext}}[b, J^\dagger, J] = \int d^2z \, \left\{ [J^\dagger_{\boldsymbol{z}}]_{ij} [U_{\boldsymbol{z}}[b]]_{ij} + [J_{\boldsymbol{z}}]_{ij} [U^\dagger_{\boldsymbol{z}}[b]]_{ij} \right\}, \tag{4.2}$$

and b is the background field of the target proton. Bold coordinates represent transverse coordinates. The averaging procedure, $\langle ... \rangle_b$ is given by

$$\langle ... \rangle_b := \int \mathcal{D}[b] ... e^{S_{QCD}[b]}, \tag{4.3}$$

where S_{QCD} is the QCD action and contains all the information about the possible field configurations. A difficulty that arises here is that we don't know what the background field configuration, b, is. Therefore, we cannot actually compute this average naïvely. The crux of JIMWLK is getting around this problem by computing the Wilson line correlators directly without knowledge of the background field, except for the following two assumptions: First, due to the large rapidity separation between the projectile and target proton, from the perspective of the projectile, the proton is an incredibly Lorentz contracted gluon field. In other words, this background field has a delta-like support in the x^- direction

$$b^+(x) = \delta(x^-)\beta(\boldsymbol{x}) \tag{4.4}$$

where β contains the unconstrained, transverse distribution of the background field. Second, again because of the Lorentz contraction, the projectile interacts with target only for an instant. Basically, the target proton looks frozen to the projectile and we can treat it as time independent. One immediate consequence of this is that we can simplify the path of our Wilson lines. We define our coordinate system such that (in light cone coordinates) the target proton is moving in the x^+ direction and the eikonal quarks and gluons move in the x^- direction, interacting with the target only instantaneously at $x^- = 0$. The start and end of the Wilson line path is inconsequential, so we set them to $-\infty$ and ∞ respectively:

$$U(\boldsymbol{x}) := U(\boldsymbol{x})_{[\infty,-\infty]} = \mathcal{P}\exp\left[ig\int_{-\infty}^{\infty} dx^-\, b^{+a}(x^-,\boldsymbol{x})t^a\right]. \tag{4.5}$$

Wilson line correlators are then generated in the usual way by taking functional derivatives with respect to J and $J^\dagger$ in the GF and setting them to zero.

$$\begin{aligned}\frac{\delta}{\delta J^\dagger}e^{\mathcal{S}^{q\bar{q}}_{\text{ext}}[b,J^\dagger,J]}\bigg|_{J=J^\dagger=0} &= Ue^{\mathcal{S}^{q\bar{q}}_{\text{ext}}[b,J^\dagger,J]}\bigg|_{J=J^\dagger=0}\\ &= U\end{aligned}$$

$$\begin{aligned}\frac{\delta}{\delta J}e^{\mathcal{S}^{q\bar{q}}_{\text{ext}}[b,J^\dagger,J]}\bigg|_{J=J^\dagger=0} &= U^\dagger e^{\mathcal{S}^{q\bar{q}}_{\text{ext}}[b,J^\dagger,J]}\bigg|_{J=J^\dagger=0}\\ &= U^\dagger.\end{aligned} \tag{4.6}$$

More generally, any correlator can by generated by taking successive functional derivatives:

$$\frac{\delta}{\delta J_1}\cdots\frac{\delta}{\delta J_n}\frac{\delta}{\delta J_1^\dagger}\cdots\frac{\delta}{\delta J_m^\dagger}\mathcal{Z}[J^\dagger,J]\bigg|_{J=J^\dagger=0} = \langle U_1^\dagger\otimes\cdots\otimes U_n^\dagger U_1\otimes\cdots\otimes U_m\rangle_b. \tag{4.7}$$

In order to find how this GF evolves, we form a finite difference equation, considering the GF at two different rapidities.

$$\frac{d}{dY}\langle e^{\mathcal{S}^{q\bar{q}}_{\text{ext}}[b,J^\dagger,J]}\rangle_b = \lim_{\Delta Y\to 0}\frac{\langle e^{\mathcal{S}^{q\bar{q}}_{\text{ext}}[b+\delta A,J^\dagger,J]}\rangle_{b,\delta A} - \langle e^{\mathcal{S}^{q\bar{q}}_{\text{ext}}[b,J^\dagger,J]}\rangle_b}{\Delta Y} \tag{4.8}$$

The ΔY dependence of the numerator sits in δA, which is a small fluctuation about the background field. This evolution equation describing the rapidity evolution of the Wilson line correlator GF is what we call the JIMWLK equation. To compute this finite difference - and calculate JIMWLK to leading order, we need to expand the GF in δA to second order. Second order, because the first order term is zero, as we will prove in the next subsections. We can express this expansion diagrammatically and what we obtain is two terms: one representing the exchange of a gluon between pairs of partons that pierce the medium and one representing the self interaction of a parton emitting and

absorbing a gluon.

$$\langle e^{\mathcal{S}^{q\bar{q}}_{\rm ext}[b+\delta A,J^\dagger,J]}\rangle_{b,\delta A} \approx \langle e^{\mathcal{S}^{q\bar{q}}_{\rm ext}[b,J^\dagger,J]}\rangle_b$$

$$+(J^\dagger_x, J_x)$$

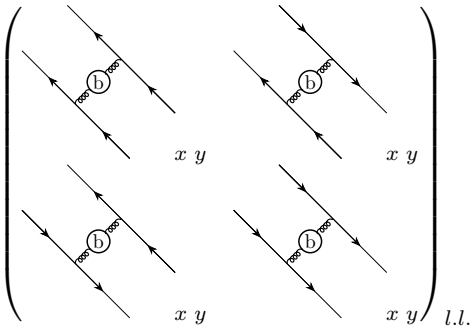

$$l.l.$$

$$\begin{pmatrix} J^\dagger_y \\ J_y \end{pmatrix}$$

$$+(J^\dagger_x, J_x)$$

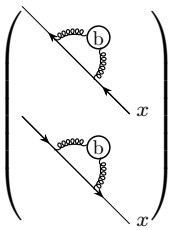

$$l.l. \quad , \tag{4.9}$$

where $l.l.$ stands for leading $\ln(1/x_{bj})$ contribution. The diagrams here indicate a gluon exchange between quarks (positive x^-, y^- light cone direction) and anti-quarks (negative x^-, y^- light cone direction) where the gluon interacts with the background field, b. We see that the effect of rapidity evolution of the target, and thus the averaging procedure, in the projectile frame is that incoming partons are endowed with an extra gluon. In terms of correlators, this means the rapidity evolution of any correlator involves the presence of said correlator with an adjoint-Wilson line inserted. In other words, the evolution of an n-point correlator is inexorably linked to the evolution of the n+1-point correlator. Consequently, the evolution of the n+1-point correlator is linked to the evolution of the n+2 correlator. This leads to an infinite tower of differential equations - it does not terminate - known as the Balitsky hierarchy. The purpose of this thesis is to explore one strategy of extracting useful information from this hierarchy in the face of not being able to solve it exactly.

In the next few subsections we go over the above calculation with much more rigour and at the end of this chapter will go over an example of the evolution of the 2-point Wilson line correlator.

4.1 Expanding the Generating Functional

Expand to second order so that we may form a finite difference equation.

$$
\begin{aligned}
&\langle e^{\mathcal{S}^{q\bar{q}}_{\text{ext}}[b+\delta A, J^\dagger, J]}\rangle_{b,\delta A} = \\
&= \langle \left(1 + \delta A^a_x \frac{\delta}{\delta b^a_x} + \frac{1}{2}\delta A^a_x \frac{\delta}{\delta b^a_x}\delta A^b_y \frac{\delta}{\delta b^b_y} + \mathcal{O}(\delta A^3)\right) e^{\mathcal{S}^{q\bar{q}}_{\text{ext}}[b, J^\dagger, J]}\rangle_{b,\delta A} \\
&= \langle e^{\mathcal{S}^{q\bar{q}}_{\text{ext}}[b, J^\dagger, J]}\rangle_b + \frac{1}{2}\langle \delta A^a_x \frac{\delta}{\delta b^a_x}\delta A^b_y \frac{\delta}{\delta b^b_y} e^{\mathcal{S}^{q\bar{q}}_{\text{ext}}[b, J^\dagger, J]}\rangle_{b,\delta A} + \dots \\
&= \langle e^{\mathcal{S}^{q\bar{q}}_{\text{ext}}[b, J^\dagger, J]}\rangle_b + \langle \langle \delta A^a_x\rangle_{\delta A} \ \frac{\delta}{\delta b^a_x} e^{\mathcal{S}^{q\bar{q}}_{\text{ext}}[b, J^\dagger, J]}\rangle_b \\
&\quad + \frac{1}{2}\langle \langle \delta A^a_x \delta A^b_y\rangle_{\delta A}[b] \Bigg(\underbrace{\left(\frac{\delta}{\delta b^a_x}\mathcal{S}^{q\bar{q}}_{\text{ext}}[b, J^\dagger, J]\right)\left(\frac{\delta}{\delta b^b_y}\mathcal{S}^{q\bar{q}}_{\text{ext}}[b, J^\dagger, J]\right)}_{\text{(i)}} + \underbrace{\frac{\delta}{\delta b^a_x}\frac{\delta}{\delta b^b_y}\mathcal{S}^{q\bar{q}}_{\text{ext}}[b, J^\dagger, J]}_{\text{(ii)}} \Bigg) \\
&\quad \times e^{\mathcal{S}^{q\bar{q}}_{\text{ext}}[b, J^\dagger, J]}\rangle_b + \dots \ .
\end{aligned}
\tag{4.10}
$$

We make use of implicit Einstein summation convention, where x and y are integrated over. The first term cancels against the un-Taylored term of (4.8), as expected. Take heed that the linear term in δA vanishes for reasons explained in Appendix A

$$\langle \delta A\rangle_{\delta A} = 0 \tag{4.11}$$

Thus the evolution is driven by terms quadratic in δA. Said quadratic term, $\langle \delta A_x \delta A_y\rangle$, is the propagator in the presence of a strong background field , whose expression is derived in Appendix B. We want to evaluate terms (i) and (ii) by executing the functional derivatives. The functional derivative of the Wilson line with respect to its gauge field is complicated by the path ordering. We will get a generator inserted along the path at the point of the derivative. A detailed derivation can be found in section (3.50).

$$
\begin{aligned}
\frac{\delta}{\delta b^{a+}_x} U_{\boldsymbol{z}}[b] &= -\, ig\delta_{x^+0}\delta_{\boldsymbol{xz}} \int dz^- \delta_{x^- z^-} U_{\boldsymbol{z};\infty,z^-} t^a U_{\boldsymbol{z};z^-,-\infty} \\
&= -\, ig\delta_{x^+0}\delta_{\boldsymbol{xz}} U_{\boldsymbol{z};\infty,x^-} t^a U_{\boldsymbol{z};x^-,-\infty}
\end{aligned}
\tag{4.12}
$$

It is handy for future calculations to divorce the x^- dependence from the inside of the Wilson line. This can be done through the use of Heaviside functions:

$$\frac{\delta}{\delta b^{a+}_x} U_{\boldsymbol{z}}[b] = -ig\delta_{x^+0}\delta_{\boldsymbol{xz}} \left[\theta(x^-) t^a U_{\boldsymbol{z}}[b] + \theta(-x^-) U_{\boldsymbol{z}}[b] t^a\right] . \tag{4.13}$$

This is true only with our choice of gauge field. The Dirac delta in 4.4 is only triggered if the limits of the integral lie on either side of zero. Hence, the left Wilson line is different from identity only if $x^- < 0$ and the right Wilson line only if $x^- > 0$. Similarly, the

derivative of an anti-Wilson line is

$$\frac{\delta}{\delta b_x^{a+}} U_{\boldsymbol{z}}^\dagger[b] = ig\delta_{x^+0}\delta_{\boldsymbol{xz}} \left[\theta(x^-)U_{\boldsymbol{z}}^\dagger[b]t^a + \theta(-x^-)t^a U_{\boldsymbol{z}}^\dagger[b]\right] \tag{4.14}$$

Thus the derivative of our action is

$$\begin{aligned}\frac{\delta S[...]}{\delta b_x^{a+}} = & \int d^2z \left(J_{\boldsymbol{z}}^\dagger \frac{\delta}{\delta b_x^{a+}} U_{\boldsymbol{z}} + J_{\boldsymbol{z}} \frac{\delta}{\delta b_x^{a+}} U_{\boldsymbol{z}}^\dagger\right) \\ = & -ig\delta_{x^+0}\Big(J_{\boldsymbol{x}}^\dagger \left[\theta(x^-)t^a U_{\boldsymbol{x}} + \theta(-x^-)U_{\boldsymbol{x}}t^a\right] \\ & -J_{\boldsymbol{x}} \left[\theta(x^-)U_{\boldsymbol{x}}^\dagger t^a + \theta(-x^-)t^a U_{\boldsymbol{x}}^\dagger\right]\Big)\end{aligned} \tag{4.15}$$

Getting back to the expressions in (4.10) we respectively obtain

$$\begin{aligned}\textcircled{i} = & (-ig)^2\delta_{x^+0}\delta_{y^+0} \\ & \times\Big\{ J_{\boldsymbol{x}}^\dagger \left[\theta(x^-)t^a U_{\boldsymbol{z}} + \theta(-x^-)U_{\boldsymbol{x}}t^a\right] - J_{\boldsymbol{x}} \left[\theta(x^-)U_{\boldsymbol{x}}^\dagger t^a + \theta(-x^-)t^a U_{\boldsymbol{x}}^\dagger\right] \Big\} \\ & \times\Big\{ J_{\boldsymbol{y}}^\dagger \left[\theta(y^-)t^a U_{\boldsymbol{y}} + \theta(-y^-)U_{\boldsymbol{y}}t^a\right] - J_{\boldsymbol{y}} \left[\theta(y^-)U_{\boldsymbol{y}}^\dagger t^a + \theta(-y^-)t^a U_{\boldsymbol{y}}^\dagger\right] \Big\}\end{aligned} \tag{4.16}$$

To calculate the second term, we need to compute the double functional derivative of a Wilson lines. Verily, it is

$$\begin{aligned}\frac{\delta}{\delta b_y^{b+}}\frac{\delta}{\delta b_x^{a+}} U_{\boldsymbol{z}}[b] = & (-ig)^2\delta_{y^+0}\delta_{\boldsymbol{yz}}\delta_{x^+0}\delta_{\boldsymbol{xz}} \\ & \times \{\theta(y^- - x^-)U_{\boldsymbol{z};\infty,y^-}t^b U_{\boldsymbol{z};y^-,x^-}t^a U_{\boldsymbol{z};x^-,-\infty} \\ & + \theta(x^- - y^-)U_{\boldsymbol{z};\infty,x^-}t^a U_{\boldsymbol{z};x^-,y^-}t^b U_{\boldsymbol{z};y^-,-\infty}\}.\end{aligned} \tag{4.17}$$

We can then do the same trick as in (4.13) to remove the x^- and y^- dependence from the Wilson lines themselves to make future evaluation of integrals easier.

$$\begin{aligned}\frac{\delta}{\delta b_y^{b+}}\frac{\delta}{\delta b_x^{a+}} U_{\boldsymbol{z}}[b] = & (-ig)^2\delta_{y^+0}\delta_{\boldsymbol{yz}}\delta_{x^+0}\delta_{\boldsymbol{xz}} \\ & \times\Big\{\theta(x^-)\theta(y^-)\left(\theta(x^- - y^-)t^a t^b + \theta(y^- - x^-)t^b t^a\right)U \\ & +\theta(-x^-)\theta(-y^-)U\left(\theta(x^- - y^-)t^a t^b + \theta(y^- - x^-)t^b t^a\right) \\ & +\theta(-x^-)\theta(y^-)t^b U t^a + \theta(x^-)\theta(-y^-)t^a U t^b\Big\}\end{aligned} \tag{4.18}$$

For the corresponding anti-Wilson line, it is simply the Hermitian conjugate of (4.18), granting us

$$\begin{aligned}
\text{(ii)} = \quad & (-ig)^2\delta_{y^+0}\delta_{x^+0}\delta_{\boldsymbol{xy}} \\
& \times\Big[J^\dagger_{\boldsymbol{x}}\Big\{\theta(x^-)\theta(y^-)\left(\theta(x^- - y^-)t^at^b + \theta(y^- - x^-)t^bt^a\right)U \\
& +\theta(-x^-)\theta(-y^-)U\left(\theta(x^- - y^-)t^at^b + \theta(y^- - x^-)t^bt^a\right) \\
& +\theta(-x^-)\theta(y^-)t^bUt^a + \theta(x^-)\theta(-y^-)t^aUt^b\Big\} \\
& +J_{\boldsymbol{x}}\Big\{\theta(x^-)\theta(y^-)\left(\theta(x^- - y^-)t^bt^a + \theta(y^- - x^-)t^at^b\right)U^\dagger \\
& +\theta(-x^-)\theta(-y^-)U^\dagger\left(\theta(x^- - y^-)t^bt^a + \theta(y^- - x^-)t^at^b\right) \\
& +\theta(-x^-)\theta(y^-)t^aU^\dagger t^b + \theta(x^-)\theta(-y^-)t^bU^\dagger t^a\Big\}\Big].
\end{aligned} \tag{4.19}$$

In order to arrive at the JIMWLK equation, we now have to evaluate the convolution of the propagator against these Wilson lines. The propagator has the following form:

$$\begin{aligned}
\left\langle \delta A^{a+}_x \delta A^{b+}_y \right\rangle =& \partial_{\boldsymbol{x}}\partial_{\boldsymbol{y}} \int \frac{dp^-}{4\pi(p^-)^3}\frac{d^2q_\perp}{(2\pi)^2}\frac{d^2k_\perp}{(2\pi)^2}[\theta(x^- - y^-)\theta(p^-) - \theta(y^- - x^-)\theta(-p^-)] \\
& \times e^{-i(q.x-k.y)}\int d^2\boldsymbol{z}\; e^{-i(q_\perp - k_\perp).\boldsymbol{z}}\widetilde{U}_{\boldsymbol{z};x^-,y^-},
\end{aligned} \tag{4.20}$$

where $p^- = q^- = k^-$, $p^+ = \frac{p_\perp^2 - i\epsilon}{2p^-}$, $q^+ = \frac{q_\perp^2 + i\epsilon}{2q^-}$ and $k^+ = \frac{k_\perp^2}{2k^-}$. They are on-shell momenta and follow the Feynman prescription. We can rewrite the adjoint Wilson line in a manor that extracts its x^- and y^- dependence using the same trick as above to obtain

$$\begin{aligned}
\widetilde{U}^{ab}_{x^-,y^-} = \quad & \theta(-x^-)\theta(-y^-)\delta^{ab} + \theta(x^-)\theta(y^-)\delta^{ab} \\
+ \quad & \theta(-x^-)\theta(y^-)\widetilde{U}^{ab\dagger}_{\boldsymbol{z}} + \theta(x^-)\theta(-y^-)\widetilde{U}^{ab}_{\boldsymbol{z}}
\end{aligned} \tag{4.21}$$

The products of all these sums of Wilson lines gives us many terms to calculate, but the underlying mechanic of JIMWLK should soon present itself. Let us write down explicitly all the terms arising from (i) and calculate the first few. We will then do the same for (ii). Take note that for the product of Heaviside theta functions, $\theta(x)\theta(-x) = 0$ and $\theta(x)^2 = \theta(x)$ under the integral sign.

4.2 Gluon exchange terms

We evaluate the terms in (i), revealing them to behave like gluon exchange terms.

$$\begin{aligned}
&\left\langle \delta A_x^{a+} \delta A_y^{b+} \right\rangle \left(\frac{\delta}{\delta b_x} \mathcal{S}_{\text{ext}}^{q\bar{q}}[b, J^\dagger, J] \right) \left(\frac{\delta}{\delta b_y} \mathcal{S}_{\text{ext}}^{q\bar{q}}[b, J^\dagger, J] \right) \qquad (4.22)\\
= &\int d^4x d^4y \, \partial_{\boldsymbol{x}} \partial_{\boldsymbol{y}} \int \frac{dp^-}{4\pi (p^-)^3} \frac{d^2q_\perp}{(2\pi)^2} \frac{d^2k_\perp}{(2\pi)^2} [\theta(x^- - y^-)\theta(p^-) - \theta(y^- - x^-)\theta(-p^-)] \\
&\times e^{-i(q.x - k.y)} \int d^2\boldsymbol{z} \, e^{-i(q_\perp - k_\perp).\boldsymbol{z}} (-ig)^2 \delta_{x^+0} \delta_{y^+0} \\
&\times \Big(\theta(-x^-)\theta(-y^-)\delta^{ab} + \theta(x^-)\theta(y^-)\delta^{ab} + \theta(-x^-)\theta(y^-)\widetilde{U}_{\boldsymbol{z}}^{ab\dagger} + \theta(x^-)\theta(-y^-)\widetilde{U}_{\boldsymbol{z}}^{ab} \Big) \\
&\times \Big\{ J_{\boldsymbol{x}}^\dagger \left[\theta(x^-) t^a U_{\boldsymbol{x}} + \theta(-x^-) U_{\boldsymbol{x}} t^a \right] - J_{\boldsymbol{x}} \left[\theta(x^-) U_{\boldsymbol{x}}^\dagger t^a + \theta(-x^-) t^a U_{\boldsymbol{x}}^\dagger \right] \Big\} \\
&\times \Big\{ J_{\boldsymbol{y}}^\dagger \left[\theta(y^-) t^b U_{\boldsymbol{y}} + \theta(-y^-) U_{\boldsymbol{y}} t^b \right] - J_{\boldsymbol{y}} \left[\theta(y^-) U_{\boldsymbol{y}}^\dagger t^b + \theta(-y^-) t^b U_{\boldsymbol{y}}^\dagger \right] \Big\}
\end{aligned}$$

Next we multiply out the Wilson line terms. Also, we can simplify the preamble by evaluating the x^+ and y^+ integrals. The Dirac deltas just set them to zero, simplifying the p^- dependence of the equation. Now a change of variables, $p^- \to -p^-$, can be performed on the term containing $\theta(-p^-)$, resulting in following simplification:

$$\begin{aligned}
&\frac{1}{(p^-)^3} \theta(x^- - y^-)\theta(p^-) - \theta(y^- - x^-)\theta(-p^-) \\
\to &\frac{1}{(p^-)^3} \theta(x^- - y^-)\theta(p^-) + \theta(y^- - x^-)\theta(p^-) \\
= &\frac{1}{(p^-)^3} \theta(p^-)
\end{aligned}$$

Implementing this, we get

$$
\begin{aligned}
& \left\langle \delta A_x^{a+} \delta A_y^{b+} \right\rangle \left(\frac{\delta}{\delta b_x} \mathcal{S}_{\text{ext}}^{q\bar{q}}[b, J^\dagger, J] \right) \left(\frac{\delta}{\delta b_y} \mathcal{S}_{\text{ext}}^{q\bar{q}}[b, J^\dagger, J] \right) \\
= \quad & \int d^3x d^3y \, \partial_{\boldsymbol{x}} \partial_{\boldsymbol{y}} \int \frac{dp^-}{4\pi (p^-)^3} \frac{d^2q_\perp}{(2\pi)^2} \frac{d^2k_\perp}{(2\pi)^2} \theta(p^-) \\
& \times e^{-i(q_\perp . \boldsymbol{x} - k_\perp . \boldsymbol{y})} e^{\frac{-i(q_\perp^2 - i\epsilon)}{2p^-} x^- + \frac{i(k_\perp^2 + i\epsilon)}{2p^-} y^-} \int d^2\boldsymbol{z} \, e^{-i(q_\perp - k_\perp).\boldsymbol{z}} (-ig)^2 \\
\times \Big\{ \quad & \theta(x^-)\theta(y^-) \Big(- \underbrace{J_{\boldsymbol{x}}^\dagger J_{\boldsymbol{y}} t^a U_{\boldsymbol{x}} U_{\boldsymbol{y}}^\dagger t^a}_{(1)} + \cdots \Big) \\
+ \quad & \theta(-x^-)\theta(-y^-) \Big(- \underbrace{J_{\boldsymbol{x}}^\dagger J_{\boldsymbol{y}} U_{\boldsymbol{x}} t^a t^a U_{\boldsymbol{y}}^\dagger}_{(2)} + \cdots \Big) \\
+ \quad & \theta(-x^-)\theta(y^-) \widetilde{U}_{\boldsymbol{z}}^{ab\dagger} \Big(- \underbrace{J_{\boldsymbol{x}}^\dagger J_{\boldsymbol{y}} U_{\boldsymbol{x}} t^a U_{\boldsymbol{y}}^\dagger t^b}_{(3)} + \cdots \Big) \\
+ \quad & \theta(x^-)\theta(-y^-) \widetilde{U}_{\boldsymbol{z}}^{ab} \Big(- \underbrace{J_{\boldsymbol{x}}^\dagger J_{\boldsymbol{y}} t^a U_{\boldsymbol{x}} t^b U_{\boldsymbol{y}}}_{(4)} + \cdots \Big) \Big\}.
\end{aligned}
\tag{4.23}
$$

For each pair of theta functions, we have chosen a representative term to perform the full calculation on. The mathematics for the remaining terms proceeds exactly as they do for those terms. We will actually leave the $\boldsymbol{x}$, $\boldsymbol{y}$ and $\boldsymbol{z}$ integrals unevaluated, leaving our calculation dependant only on the theta functions and not the accompanying Wilson lines. Take note that the partial derivatives with respect to transverse coordinates only act on terms coming from the propagator - they do not hit the Wilson lines or source currents, J. The space-time integrals over x and y, apply to all terms.

Since the structure of the Wilson lines does not change in the rest of the calculation, one can look at their diagrammatic representation.

Let's start with the term simplest to compute: (1). We first perform the x^- and y^- integrals. The part of the calculation dependant on these terms comprises of the theta function and the complex Gaussians in momenta. The particular epsilon prescription present lets these integrals converge without hassle.

$$
\begin{aligned}
& \int dx^- dy^- \, e^{\frac{-i(q_\perp^2 - i\epsilon)}{2p^-} x^- + \frac{i(k_\perp^2 + i\epsilon)}{2p^-} y^-} \theta(x^-)\theta(y^-) \\
= \quad & \int_0^\infty \int_0^\infty dx^- dy^- \, e^{\frac{-i(q_\perp^2 - i\epsilon)}{2p^-} x^- + \frac{i(k_\perp^2 + i\epsilon)}{2p^-} y^-} \\
= \quad & \left(-\frac{2ip^-}{q_\perp^2} \right) \left(-\frac{-2ip^-}{k_\perp^2} \right) \\
= \quad & \frac{4(p^-)^2}{q_\perp^2 k_\perp^2}
\end{aligned}
\tag{4.24}
$$

The next step is to perform the integrals in the transverse momenta, $q_\perp$ and $k_\perp$. This integral looks tricky, but is actually standard. It is the Greens function to the two dimensional Laplace operator, whose solution is known to take the form of a log:

$$\begin{aligned} & \int \frac{dq_\perp^2}{(2\pi)^2}\frac{1}{q_\perp^2}e^{iq_\perp\cdot(\boldsymbol{x}-\boldsymbol{z})}\int \frac{dk_\perp^2}{(2\pi)^2}\frac{1}{k_\perp^2}e^{ik_\perp\cdot(\boldsymbol{z}-\boldsymbol{y})} \\ = \quad & \frac{-1}{4\pi}\ln((\boldsymbol{x}-\boldsymbol{z})^2/\mu)\frac{-1}{4\pi}\ln((\boldsymbol{z}-\boldsymbol{y})^2/\mu). \end{aligned} \tag{4.25}$$

The μ is an artefact of regularization that will fall away in the next step. In order to get JIMWLK in its canonical form, we now apply the latent derivatives on the transverse coordinates. Let us not forget that the derivatives only hit terms arising from the propagator and don't interact with the Wilson lines that are being multiplied in.

$$\partial_{\boldsymbol{x}}\partial_{\boldsymbol{y}}\ln((\boldsymbol{x}-\boldsymbol{z})^2/\mu)\ln((\boldsymbol{z}-\boldsymbol{y})^2/\mu) = -4\mathcal{K}_{\boldsymbol{xyz}}, \tag{4.26}$$

where $\mathcal{K}$ is the JIMWLK integral kernel, defined as

$$\mathcal{K}_{\boldsymbol{xyz}} := \frac{(\boldsymbol{x}-\boldsymbol{z})\cdot(\boldsymbol{z}-\boldsymbol{y})}{(\boldsymbol{x}-\boldsymbol{z})^2(\boldsymbol{z}-\boldsymbol{y})^2}, \tag{4.27}$$

leaving the integral over transverse coordinates alone, the last remaining integral is over p^-. This integral is divergent, so we employ a cut-off that forms the basis of the RG equation.

$$\int \frac{dp^-}{(p^-)^3}(p^-)^2 = \ln(1/x_{bj}). \tag{4.28}$$

This is indeed Bjorken-x, x_{bj}, what we use to define the Regge limit. Altogether, ① can now be expressed as

$$① = \frac{g^2}{\pi}\frac{4}{(4\pi)^2}\ln(1/x_{bj})\int d^2\boldsymbol{x}d^2\boldsymbol{y}d^2\boldsymbol{z}\mathcal{K}_{\boldsymbol{xyz}}J^\dagger_{\boldsymbol{x}}J_{\boldsymbol{y}}t^aU_{\boldsymbol{x}}U^\dagger_{\boldsymbol{y}}t^a \tag{4.29}$$

All the terms will have this generic structure of the convolution of the integral with two fundamental Wilson lines and an adjoint Wilson line joining them, the adjoint Wilson line here being the identity. See (4.41) for a visual representation of this term.

Calculation of term ② proceeds similarly, the only difference arises from the step equivalent to (4.24). Term ② has precisely the epsilon prescription and theta function structure so that the x^- and y^- integrals diverge. These divergences can be dealt with. We isolate the diverging part and show that it falls away when acted upon by the transverse derivatives. Consider the part of term ② that only depends on x^-. We add zero to it by adding and subtracting the integral over the other half of x^-,

$$\begin{aligned} \int dx^- e^{\frac{-i(q_\perp^2-i\epsilon)}{2p^-}x^-}\theta(-x^-) \quad &= \quad \int dx^- e^{\frac{-i(q_\perp^2-i\epsilon)}{2p^-}x^-}[\theta(-x^-)+\theta(x^-)-\theta(x^-)] \\ &= \quad \int dx^- e^{\frac{-i(q_\perp^2-i\epsilon)}{2p^-}x^-} - \int dx^- e^{\frac{-i(q_\perp^2-i\epsilon)}{2p^-}x^-}\theta(x^-). \end{aligned} \tag{4.30}$$

The second term is just the negative of the term obtained in (4.24) and enters the rest of the calculation as in term (1). The same thing happens with the y^- integral, contributing another minus sign, which cancels with the first one. This leaves us with a contribution that looks the same as term (1), just with a different order of Wilson lines and generators. The first term, however, is a Dirac delta and the diverging part of this integral, which we will now show doesn't contribute to the overall calculation.

Evaluating the x^- integral in this term gives the following Dirac delta:

$$\int dx^- e^{\frac{-i(q_\perp^2 - i\epsilon)}{2p^-}x^-} = \delta\left(\frac{q_\perp^2}{2p^-}\right). \tag{4.31}$$

We will show that this Dirac delta removes the $\boldsymbol{x}$ dependence in its associated term. Inserting this into the integral in $q_\perp$, we then change to polar coordinates, followed by employing the generalized scaling property of the delta to see how it triggers under the integral:

$$\begin{aligned}
\partial_{\boldsymbol{x}} \int d^2q_\perp e^{iq_\perp\cdot\boldsymbol{x}}\delta\left(\frac{q_\perp^2}{2p^-}\right) &= \partial_{\boldsymbol{x}} \int d|q_\perp| d\theta |q_\perp| e^{i|q_\perp||\boldsymbol{x}|\cos\theta}\delta\left(\frac{|q_\perp|^2}{2p^-}\right). \\
&= \partial_{\boldsymbol{x}} \int d|q_\perp| d\theta |q_\perp| e^{i|q_\perp||\boldsymbol{x}|\cos\theta}\delta(|q_\perp|)\frac{p^-}{|q_\perp|} \\
&= \partial_{\boldsymbol{x}} \int d\theta p^- \\
&= 0.
\end{aligned} \tag{4.32}$$

Thus the divergent part of the x^- integral does not contribute, leaving only with the converging part. The same result would be found for the y^- integral. The rest of the calculation follows identically and we find that

$$(2) = \frac{1}{\pi^2}\frac{g^2}{4\pi}\ln(1/x_{bj})\int d^2\boldsymbol{x}d^2\boldsymbol{y}d^2\boldsymbol{z}\mathcal{K}_{\boldsymbol{xyz}}J^\dagger_{\boldsymbol{x}}J_{\boldsymbol{y}}U_{\boldsymbol{x}}t^a t^a U^\dagger_{\boldsymbol{y}}. \tag{4.33}$$

The calculation of terms (3) and (4) follow the same way. The only difference is they only have a single diverging integral, so there will be a relative minus sign, and they contain non-trivial adjoint Wilson lines. So we obtain

$$(3) = -\frac{1}{\pi^2}\frac{g^2}{4\pi}\ln(1/x_{bj})\int d^2\boldsymbol{x}d^2\boldsymbol{y}d^2\boldsymbol{z}\mathcal{K}_{\boldsymbol{xyz}}J^\dagger_{\boldsymbol{x}}J_{\boldsymbol{y}}\widetilde{U}^{ab\dagger}_{\boldsymbol{z}}U_{\boldsymbol{x}}t^a U^\dagger_{\boldsymbol{y}}t^b \tag{4.34}$$

and

$$(4) = -\frac{1}{\pi^2}\frac{g^2}{4\pi}\ln(1/x_{bj})\int d^2\boldsymbol{x}d^2\boldsymbol{y}d^2\boldsymbol{z}\mathcal{K}_{\boldsymbol{xyz}}J^\dagger_{\boldsymbol{x}}J_{\boldsymbol{y}}\widetilde{U}^{ab}_{\boldsymbol{z}}t^a U_{\boldsymbol{x}}t^b U^\dagger_{\boldsymbol{y}}. \tag{4.35}$$

These four terms carry the interpretation of gluon exchanges between two Wilson lines. This will be made more clear when we represent things diagrammatically (4.41).

4.3 Self interaction terms

The calculation of (ii) follows the same path. Let's write the full expression down and see what simplifications can be made.

$$
\begin{aligned}
&\left\langle \delta A_x^{a+} \delta A_y^{b+} \right\rangle \frac{\delta}{\delta b_x} \frac{\delta}{\delta b_y} \mathcal{S}_{\text{ext}}^{q\bar{q}}[b, J^\dagger, J] \\
= &\int d^4x d^4y \, \partial_{\boldsymbol{x}} \partial_{\boldsymbol{y}} \int \frac{dp^-}{4\pi (p^-)^3} \frac{d^2q_\perp}{(2\pi)^2} \frac{d^2k_\perp}{(2\pi)^2} [\theta(x^- - y^-)\theta(p^-) - \theta(y^- - x^-)\theta(-p^-)] \\
&\times e^{-i(q.x - k.y)} \int d^2\boldsymbol{z} e^{-i(q_\perp - k_\perp).\boldsymbol{z}} (-ig)^2 \delta_{x^+0} \delta_{y^+0} \delta_{\boldsymbol{xy}} \\
&\times \Big(\theta(-x^-)\theta(-y^-)\delta^{ab} + \theta(x^-)\theta(y^-)\delta^{ab} + \theta(-x^-)\theta(y^-)\widetilde{U}_{\boldsymbol{z}}^{ab\dagger} + \theta(x^-)\theta(-y^-)\widetilde{U}_{\boldsymbol{z}}^{ab} \Big) \\
&\times \Big\{ J_{\boldsymbol{x}}^\dagger \big[\theta(x^-)\theta(y^-) \left(\theta(x^- - y^-) t^a t^b + \theta(y^- - x^-) t^b t^a \right) U \\
&+ \theta(-x^-)\theta(-y^-) U \left(\theta(x^- - y^-) t^a t^b + \theta(y^- - x^-) t^b t^a \right) \\
&+ \theta(-x^-)\theta(y^-) t^b U t^a + \theta(x^-)\theta(-y^-) t^a U t^b \big] + J_{\boldsymbol{x}} [c.c.] \Big\},
\end{aligned}
\tag{4.36}
$$

where $c.c.$ stands for the complex conjugate of the terms multiplying $J_{\boldsymbol{x}}^\dagger$. Again, this simplifies into the four quadrants of the $x^- y^-$ plane, but the Kronecker delta simplifies the additional theta functions even further. We also take advantage of the fact that adjoint Wilson lines are real, hence daggering merely transposes them.

$$
\begin{aligned}
&\left\langle \delta A_x^{a+} \delta A_y^{b+} \right\rangle \frac{\delta}{\delta b_x} \frac{\delta}{\delta b_y} \mathcal{S}_{\text{ext}}^{q\bar{q}}[b, J^\dagger, J] \\
= &\int d^3x d^3y \, \partial_{\boldsymbol{x}} \partial_{\boldsymbol{y}} \int \frac{dp^-}{4\pi (p^-)^3} \frac{d^2q_\perp}{(2\pi)^2} \frac{d^2k_\perp}{(2\pi)^2} \theta(p^-) \\
&\times e^{-i(q.x - k.y)} \int d^2\boldsymbol{z} e^{-i(q_\perp - k_\perp).\boldsymbol{z}} (-ig)^2 \delta_{\boldsymbol{xy}} \\
&\times \Big\{ J_{\boldsymbol{x}}^\dagger \Big(\underbrace{\theta(x^-)\theta(y^-) t^a t^a U}_{(5)} + \underbrace{\theta(-x^-)\theta(-y^-) U t^a t^a}_{(6)} \\
&+ \underbrace{\big[\theta(-x^-)\theta(y^-) + \theta(x^-)\theta(-y^-) \big] \widetilde{U}_{\boldsymbol{z}}^{ab} t^a U t^b}_{(7)} \Big) \\
&+ J_{\boldsymbol{x}} (c.c.) \Big\}.
\end{aligned}
\tag{4.37}
$$

We neglect writing the complex conjugated terms as their calculation proceeds exactly the same. The calculation for terms (5) – (7) proceed very similarly as the do for the first four. The difference in calculation comes from the fact that the $\boldsymbol{y}$ integral is now easily performable due to the presence of an extra Dirac delta. Otherwise the calculation proceeds the same as that of (1)-(4). Care must be taken with minus signs: (6) picks up two factors of a minus sign and the two theta terms of (7) each pick up

one minus sign. All in all, we obtain

$$\textcircled{5} = \frac{1}{\pi}\frac{g^2}{4\pi^2}\ln(1/x_{bj})\int d^2\boldsymbol{x}d^2\boldsymbol{z}\mathcal{K}_{\boldsymbol{xxz}}J^\dagger_{\boldsymbol{x}}t^at^aU_{\boldsymbol{x}} \tag{4.38}$$

$$\textcircled{6} = \frac{1}{\pi}\frac{g^2}{4\pi^2}\ln(1/x_{bj})\int d^2\boldsymbol{x}d^2\boldsymbol{z}\mathcal{K}_{\boldsymbol{xxz}}J^\dagger_{\boldsymbol{x}}U_{\boldsymbol{x}}t^at^a \tag{4.39}$$

$$\textcircled{7} = -2\frac{1}{\pi}\frac{g^2}{4\pi^2}\ln(1/x_{bj})\int d^2\boldsymbol{x}d^2\boldsymbol{z}\mathcal{K}_{\boldsymbol{xxz}}J^\dagger_{\boldsymbol{x}}\widetilde{U}^{ab}_{\boldsymbol{z}}t^aU_{\boldsymbol{x}}t^b. \tag{4.40}$$

4.4 Diagramatic representation

Equations (4.29), (4.33), (4.34), (4.35), (4.38), (4.39) and (4.40) can be expressed diagrammatically. Each Wilson line is the path-ordered colour rotation of a quark moving in the x^- direction, piercing the CGC that is moving in the x^+ direction. The generators, t^a and t^b, are drawn as the emission of a gluon from the quark and the gluon propagator is represented by the joining of the gluons. Whether the gluon is emitted when x^- is positive or negative is granted by the theta prescriptions given in (4.16) and (4.19), consequently, an adjoint Wilson line is only accrued when the gluon pierces the medium as well. These rules are used to draw the following diagrams even though we have

integrated out the theta functions and gluon propagator by now.

$$\ln(1/x_{bj}) \int_{\boldsymbol{z}} \mathcal{K}_{\boldsymbol{xxz}} \quad t^a U_{\boldsymbol{x}} U^\dagger_{\boldsymbol{y}} t^a = \tag{4.41a}$$

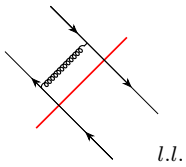

$$\ln(1/x_{bj}) \int_{\boldsymbol{z}} \mathcal{K}_{\boldsymbol{xxz}} \quad \tilde{U}^{ab\dagger}_{\boldsymbol{z}} U_{\boldsymbol{x}} t^a U^\dagger_{\boldsymbol{y}} t^b = \tag{4.41b}$$

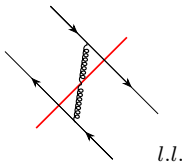

$$\ln(1/x_{bj}) \int_{\boldsymbol{z}} \mathcal{K}_{\boldsymbol{xxz}} \quad \tilde{U}^{ab}_{\boldsymbol{z}} t^a U_{\boldsymbol{x}} t^b U^\dagger_{\boldsymbol{y}} = \tag{4.41c}$$

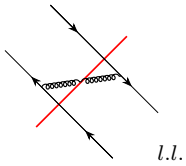

$$\ln(1/x_{bj}) \int_{\boldsymbol{z}} \mathcal{K}_{\boldsymbol{xxz}} \quad U_{\boldsymbol{x}} t^a t^a U^\dagger_{\boldsymbol{y}} = \tag{4.41d}$$

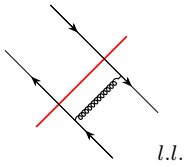

$$\ln(1/x_{bj}) \int_{\boldsymbol{z}} \mathcal{K}_{\boldsymbol{xxz}} \quad t^a t^a U_{\boldsymbol{x}} = \tag{4.41e}$$

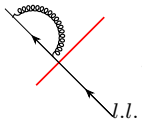

$$\ln(1/x_{bj}) \int_{\boldsymbol{z}} \mathcal{K}_{\boldsymbol{xxz}} \quad U_{\boldsymbol{x}} t^a t^a = \tag{4.41f}$$

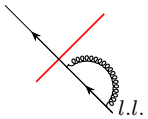

$$\ln(1/x_{bj}) \int_{\boldsymbol{z}} \mathcal{K}_{\boldsymbol{xxz}} \quad \tilde{U}^{ab}_{\boldsymbol{z}} t^a U_{\boldsymbol{x}} t^b = \tag{4.41g}$$

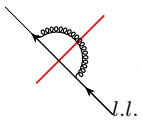

where $l.l.$ stands for leading $\ln(1/x_{bj})$ contribution. These can be neatly categorized as gluon exchange diagrams or self interaction diagrams:

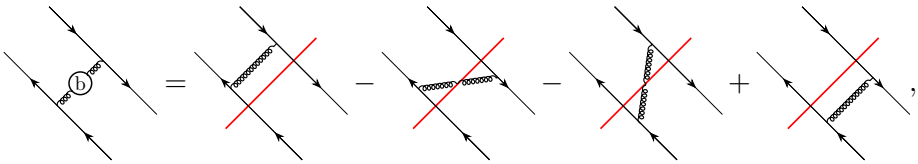

(4.42)

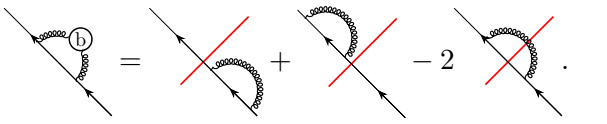

(4.43)

There are also contributions arising from $q\bar{q}$, $\bar{q}q$ and $\bar{q}\bar{q}$ pairs, where the arrows on the diagram of an anti-quark point the other direction. Putting them all together we can

finally reconstruct (i) and (ii) diagrammatically.

$$\text{(i)} = (J_x^\dagger, J_x)$$ 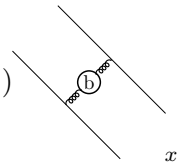 $$\begin{pmatrix} J_y^\dagger \\ J_y \end{pmatrix} := (J_x^\dagger, J_x)$$ 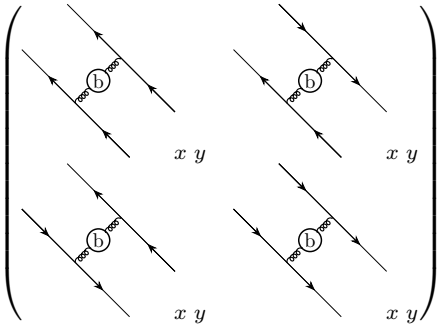 $$\begin{pmatrix} J_y^\dagger \\ J_y \end{pmatrix},$$ (4.44)

$$\text{(ii)} = (J_x^\dagger, J_x)$$ 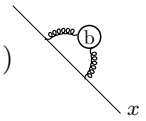 $$:= (J_x^\dagger, J_x)$$ 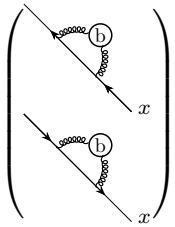 . (4.45)

4.5 Completing the finite difference equation

Having computed all the relevant components, we may return to equation (4.10). We remain cognisant of the following facts: $\langle \delta A \rangle = 0$, we may express (i) and (ii) in terms of equation (4.44) and equation (4.45), and of our evaluation of the gluon propagator as per equations (4.29), (4.33), (4.34), (4.35), (4.38), (4.39) and (4.40). The expansion of the generating functional then becomes

$$\left\langle e^{S_{ext}^{g\bar{q}}[b+\delta A, J^\dagger, J]} \right\rangle_{b,\delta A} = \left\langle e^{S_{ext}^{g\bar{q}}[b, J^\dagger, J]} \right\rangle_b$$

$$-\frac{1}{2}\frac{1}{\pi^2}\frac{g^2}{4\pi}\langle \int_{\boldsymbol{xy}} \left((J_x^\dagger, J_x) \right.$$ 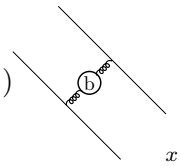 $$\left. \begin{pmatrix} J_y^\dagger \\ J_y \end{pmatrix} + (J_x^\dagger, J_x) \right.$$ 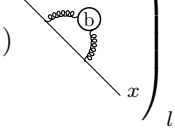 $$\left. \right)_{l.l.} e^{S_{ext}^{g\bar{q}}[b, J^\dagger, J]} \rangle_b .$$ (4.46)

We can now finally complete the finite difference equation in rapidity that constitutes leading-order JIMWLK. Recall that rapidity sits in the field fluctuation δA and that $\Delta Y = \ln(1/x_{bj})$. Then

$$\frac{d}{dY}\left\langle e^{S_{ext}^{g\bar{q}}[b+\delta A, J^\dagger, J]} \right\rangle_{b,\delta A} \approx \frac{\left\langle e^{S_{ext}^{g\bar{q}}[b+\delta A, J^\dagger, J]} \right\rangle_{b,\delta A} - \left\langle e^{S_{ext}^{g\bar{q}}[b, J^\dagger, J]} \right\rangle_b}{\Delta Y}$$

$$= -\frac{\alpha_s}{2\pi^2}\frac{1}{\ln(1/x_{bj})}\langle \int_{\boldsymbol{xy}} \left((J_x^\dagger, J_x) \right.$$ 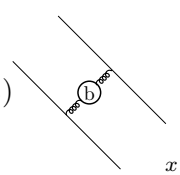 $$\left. \begin{pmatrix} J_y^\dagger \\ J_y \end{pmatrix} + (J_x^\dagger, J_x) \right.$$ 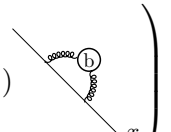 $$\left. \right)_{l.l.} e^{S_{ext}^{g\bar{q}}[b, J^\dagger, J]} \rangle_b ,$$ (4.47)

where $\alpha_s = \frac{g^2}{4\pi}$ is the strong coupling constant. With this equation fully realized, one must marvel at the fact that JIMWLK maps correlators of Wilson lines onto correlators of Wilson lines. It is this reason why the consideration of coincident limits of Wilson lines are so important. They remain valid all through rapidity evolution and give us an analytic benchmark for determining whether our numerical methods are valid or not. Rapidity evolution being an endomorphism on the space of Wilson line correlators also suggest that we might be able to rewrite JIMWLK in terms of operators that naturally perform this endomorphism. This will be done in the next subsection.

We must also note that the insertion of additional gluons means this differential equation is non-linear. The evolution of any n-point correlator depends on the evolution of a higher n-point correlator. This is the cause of the infinite tower that is known as the Balitsky hierarchy [15].

A property of JIMWLK evolution that can be immediately derived is that it evolves the symmetric and anti-symmetric parts of a Wilson line correlator separately. This is an almost trivial consequence of the linearity of the background field averaging procedure. Let some Wilson line correlator, $\langle A \rangle$, be decomposed into the sum of its symmetric ($\langle A_s \rangle$), and anti-symmetric ($\langle A_a \rangle$) parts. Then the evolution of $\langle A \rangle$ is given by

$$\frac{d}{dY}\langle A \rangle = \frac{d}{dY}\left(\langle A_s \rangle + \langle A_a \rangle\right) = -\left(\langle H_{JIMWLK} A_s \rangle + \langle H_{JIMWLK} A_a \rangle\right) \tag{4.48}$$

and the evolution of its transpose, $\langle A^T \rangle$, is given by

$$\frac{d}{dY}\langle A^T \rangle = \frac{d}{dY}\left(\langle A_s \rangle - \langle A_a \rangle\right) = -\left(\langle H_{JIMWLK} A_s \rangle - \langle H_{JIMWLK} A_a \rangle\right). \tag{4.49}$$

If we add or subtract equations (4.48) and (4.49) we get that JIMWLK mus evolve them separately:

$$\begin{aligned} \frac{d}{dY}\langle A_s \rangle &= -\langle H_{JIMWLK} A_s \rangle \\ \frac{d}{dY}\langle A_a \rangle &= -\langle H_{JIMWLK} A_a \rangle \end{aligned} \tag{4.50}$$

4.6 Rewriting the JIMWLK Hamiltonian

The JIMWLK Hamiltonian can be written in a much more compact format. Cognisant of the fact that JIMWLK acting on Wilson line correlators results in Wilson line correlators, one might be inspired[4, 16] to rewrite things in terms of the Lie derivatives (3.12)

$$H_{JIMWLK} := -\frac{\alpha_s^2}{2\pi^2}\int d^2\boldsymbol{z}[(1 - U^\dagger_{\boldsymbol{x}} U_{\boldsymbol{z}})(1 - U^\dagger_{\boldsymbol{z}} U_{\boldsymbol{y}})]^{ab} i\nabla^a_{\boldsymbol{x}} i\nabla^b_{\boldsymbol{y}}. \tag{4.51}$$

This is equivalent to the result we obtained.

4.7 Worked example: the Dipole (2-point) correlator

It is pedagogically useful to see how the JIMWLK Hamiltonian behaves in practice. The simplest example one could look at is that of the dipole (2-point) correlator of Wilson lines:

$$\mathrm{tr}(U_{\boldsymbol{x}}U^{\dagger}_{\boldsymbol{y}}) \tag{4.52}$$

The details of the calculation using the JIMWLK Hamiltonian (4.51) are given in appendix one of [17]. Here, we will derive it using the diagrammatic evolution of the generating functional. The dipole is formed by taking two functional derivatives of the generating functional. Simply enough, the evolution will be be determined by two functional derivatives of the evolution equation:

$$\begin{aligned}
&\frac{d}{dY}\left\langle \mathrm{tr}(U_{\boldsymbol{x}}U^{\dagger}_{\boldsymbol{y}})\right\rangle_Y \\
= \;& -\mathrm{tr}\left(\frac{\delta}{\delta J^{\dagger}_{\boldsymbol{x}}}\frac{\delta}{\delta J_{\boldsymbol{y}}}\right)\frac{\alpha_s}{2\pi^2}\frac{1}{\ln 1/x_{bj}}\times \\
&\langle\int_{\boldsymbol{xy}}\Bigg((J^{\dagger}_x,J_x)\quad \begin{matrix}\\ \\ \\ x\;y\end{matrix}\quad \begin{pmatrix}J^{\dagger}_y\\ J_y\end{pmatrix} + (J^{\dagger}_x,J_x)\quad \begin{matrix}\\ \\ x\end{matrix}\Bigg)_{l.l.} e^{S^{q\bar{q}}_{ext}[b,J^{\dagger},J]}\rangle_b\Big|_{J=J^{\dagger}=0}
\end{aligned} \tag{4.53}$$

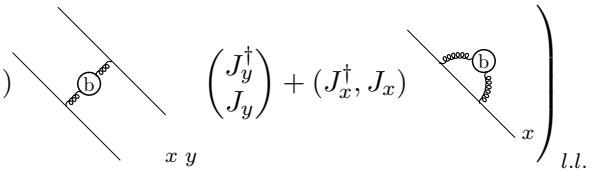

Where terms that go to zero when $J = J^{\dagger} = 0$, diagrams not corresponding to a $q\bar{q}$ pair, have be repressed. Evaluating this gives one instance of the exchange diagrams and one instance of the self energy diagrams with a $U^{\dagger}$ insertion.

$$\begin{aligned}
(4.53) \;&=\; \frac{\alpha_s}{2\pi^2}\mathrm{tr}\Bigg(\quad \begin{matrix}\\ \\ \boldsymbol{xy}\end{matrix}\quad + U^{\dagger}_{\boldsymbol{y}}\quad \begin{matrix}\\ \\ \boldsymbol{x}\end{matrix}\Bigg)_{l.l.} \\
&=\; \frac{\alpha_s}{2\pi^2}\int d^2\boldsymbol{z}\mathcal{K}_{\boldsymbol{xyz}}\left(\left\langle \tilde{U}^{ab}_{\boldsymbol{z}}\mathrm{tr}(t^aU_{\boldsymbol{x}}t^bU^{\dagger}_{\boldsymbol{y}})\right\rangle_Y - C_f\left\langle U_{\boldsymbol{x}}U^{\dagger}_{\boldsymbol{y}}\right\rangle_Y\right)
\end{aligned} \tag{4.54}$$

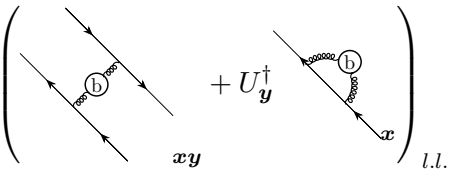

Where $C_f = t^at^a = \frac{N_c^2-1}{2N_c}$. This is indeed the result expected from [17] and, faithfully, the right-hand-side contains a correlator with an attached adjoint Wilson line - a 3-point correlator - to juxtapose against the 2-point correlator on the left. This is but the first rung of the Balitsky hierarchy.

One strategy for overcoming this infinite tower of integro-differential equations is the large N_c limit.

4.8 Approximating JIMWLK - BK and the large N_c limit

The inherent difficulty in solving (4.54) is the non-linearity arising from the gluon insertion. For this equation to be easy to solve, one would hope that the three-point correlator could somehow be expressed entirely in terms two-point correlators so that this system of equation closes and can be solved directly. This leads one to try and

re-express the 3-point correlator. Using identities (3.60) and (D.13) one obtains

$$\left\langle \tilde{U}_{\boldsymbol{z}}^{ab}\mathrm{tr}(t^a U_{\boldsymbol{x}} t^b U_{\boldsymbol{y}}^\dagger)\right\rangle_Y = \left\langle \mathrm{tr}(U_{\boldsymbol{x}}U_{\boldsymbol{z}}^\dagger)\mathrm{tr}(U_{\boldsymbol{z}}U_{\boldsymbol{y}}^\dagger) - \frac{1}{N_c}\mathrm{tr}(U_{\boldsymbol{x}}U_{\boldsymbol{y}}^\dagger)\right\rangle_Y . \tag{4.55}$$

Naïvely, one might consider (4.55) to be a success in this endeavour, but, because of a subtlety, this is not the case. The problem is that the average of a product is not the product of averages:

$$\left\langle \mathrm{tr}(U_{\boldsymbol{x}}U_{\boldsymbol{z}}^\dagger)\mathrm{tr}(U_{\boldsymbol{z}}U_{\boldsymbol{y}}^\dagger)\right\rangle \neq \left\langle \mathrm{tr}(U_{\boldsymbol{x}}U_{\boldsymbol{z}}^\dagger)\right\rangle \left\langle \mathrm{tr}(U_{\boldsymbol{z}}U_{\boldsymbol{y}}^\dagger)\right\rangle . \tag{4.56}$$

For it is the right-hand expression that we would require in order to claim that JIMWLK evolution is closed for the dipole. This is where we introduce the Balitsky-Kovchegov (BK) or the large N_c approximation.

The basic premise is that we neglect terms in JIMWLK evolution that are of order $\frac{1}{N_c^2}$. Ostensibly, this is merely at the cost of introducing a $\frac{1}{N_c} \underset{N_c\to 3}{\to} \frac{1}{9} \approx 10\%$ error in our calculations. What Kovchegov et al. argued in [5] is that

$$\left\langle \mathrm{tr}(U_{\boldsymbol{x}}U_{\boldsymbol{z}}^\dagger)\mathrm{tr}(U_{\boldsymbol{z}}U_{\boldsymbol{y}}^\dagger)\right\rangle = \left\langle \mathrm{tr}(U_{\boldsymbol{x}}U_{\boldsymbol{z}}^\dagger)\right\rangle \left\langle \mathrm{tr}(U_{\boldsymbol{z}}U_{\boldsymbol{y}}^\dagger)\right\rangle + \mathcal{O}\left(\frac{1}{N_c^2}\right). \tag{4.57}$$

Making this substitution into (4.54) and neglecting the $\mathcal{O}\left(\frac{1}{N_c^2}\right)$ terms is what is known as the BK approximation.

Claiming that this procedure requires only a 10% correction from the above argument is a bit disingenuous. This is a 10% correction in the *evolution equation* and not in the expression for the dipole itself. That being said, the final error compared full JIMWLK simulations for the dipole appears be about 0.1% [5], a surprisingly small amount indeed. While this result is amazing, the BK approximation is still lacking in two fundamental ways. The BK approximation fails to preserve coincident limits of Wilson line correlators to all orders and thus violates gauge invariance. Secondly, the BK approximation cannot be used to probe higher n-point correlators.

Some authors have attempted to apply BK factorization to more complicated correlators in order more easily calculate them. However, it is not clear that this factorization is valid for any correlators besides the 3-point correlator above. And even if it were, this factorization necessarily neglects some N_c suppressed correlators, such as those in the off-diagonal of (7.6), so we still don't even get access to all correlators.

What we desire is a different technique for approximating JIMWLK evolution: one that preserves coincidence limits, better approximates the dipole and can be used to access all correlators. Enter the Gaussian truncation.

Chapter 5

Gaussian Truncation

At the end of chapter 4 we discussed the BK approximation, a method for approximating JIMWLK to more easily calculate the behaviour of the dipole operator, and its limitations. In this chapter we will construct a technique for approximating JIMWLK that goes beyond the BK approximation. We will start off by framing an approximation in terms of the Lie derivatives of $su(N_c)$. As discussed in section 3.1.1, the Lie derivative translates along the group manifold of $SU(N_c)$. Thus any approximation expressed purely in terms of these operators will give a result that still lives in $SU(N_c)$. This will solve the issue of the BK approximation violating the coincident limit structure that arises from Wilson lines being elements of $SU(N_c)$.

The approximation that we construct in terms of Lie derivatives is known as the Gaussian truncation. Reframing the approximation in this way will also give us room to naturally extend the approximation to calculating any Wilson line correlator, solving the second major issue with the BK approximation. The Guassian Truncation is a special case of a more generic truncation of the JIMWLK hierarchy that preserves gauge invariance. Just how good an approximation this is, is still under investigation with properties being explored in, [18, 19, 12], but none-the-less it has advantages not afforded by more common truncations and so is worth testing numerically to see how it holds up.

5.1 An Exponential Solution to JIMWLK

Given that Lie derivatives naturally enter as exponentials in order to generator translations along $SU(N_c)$, we try to re-express the JIMWLK evolution in a manner that has an exponential solution in order to take advantage of this fact. The first step in performing the Gaussian truncation, then, is by reparametrizing the rapidity dependence of the Wilson Line correlator into an operator that acts on an initial condition. Naïvely, we can begin by considering the rapidity evolution of an arbitrary Wilson Line correlator and rewriting this in manner that permits an exponential solution

$$\begin{aligned}\frac{d}{dY}\langle A\rangle_Y =& -\langle H_{JIMWLK}A\rangle_Y \\ =&\frac{d}{dY}\langle A\rangle_Y \cdot 1 \\ =&\underbrace{\left(\frac{d}{dY}\langle A\rangle_Y\right)\langle A\rangle_Y^{-1}}_{-M_Y}\langle A\rangle_Y\end{aligned} \tag{5.1}$$

We are permitted to do this so long as $\langle A\rangle_Y^{-1}$ exists. An outline for showing this is the case is as follows. $\langle A\rangle_Y^{-1}$ exists when none of $\langle A\rangle_Y$'s eigenvalues are zero. If any of them were zero, $\langle A\rangle_Y^{-1}$ would have a corresponding eigenvalue of infinity, and likewise M_Y. However, since M_Y parametrizes JIMWLK evolution, it can only have an infinite eigenvalue if JIMWLK itself diverges. It remains to be shown that JIMWLK always converges for colour singlets, but if this is the case then by contraposition, $\langle A\rangle_Y^{-1}$ must exist. We will assume that this is indeed the case and leave the proof for a future work.

Equation (5.1) permits a trivial exponential solution,

$$\langle A\rangle_Y = Pe^{-\int_{Y_0}^{Y} dY' M(Y')}\langle A\rangle_{Y_0}. \tag{5.2}$$

This has shifted the rapidity dependence onto the *exponentiating matrix*, M. It remains to be seen how we can solve for the rapidity dependence of M, but before we explain how that is done we will discuss a difficulty with this reformulation. The way we have formulated equation (5.1), does not make obvious that the symmetry preserving property of JIMWLK (4.50) is preserved. In order to make this property manifest we will perform this parametrization in a different way, using the intuition we gained here, while trying to make the symmetry preservation obvious. The only change to equation (5.1) that we make is that we write down a symmetric combination of M and $\langle A\rangle$:

$$\frac{d}{dY}\langle A\rangle_Y = \underbrace{\frac{1}{2}\left(\frac{d}{dY}\langle A\rangle_Y\right)\langle A\rangle_Y^{-1}}_{-M_Y}\langle A\rangle_Y + \langle A\rangle_Y \underbrace{\frac{1}{2}\langle A\rangle_Y^{-1}\left(\frac{d}{dY}\langle A\rangle_Y\right)}_{-M_Y^T}. \tag{5.3}$$

Now, with the formulation (5.3), regardless of the structure of M, we can ensure that the symmetric and anti-symmetric parts of $\langle A\rangle$ evolve separately. Just as the JIMWLK equation prescribes.

Equation (5.3) now permits the following exponential solution

$$\langle A\rangle_Y = \mathcal{P}\exp\left[-\int_{Y_0}^{Y} dY'\, M(Y')\right]\langle A\rangle_{Y_0}\left(\mathcal{P}\exp\left[-\int_{Y_0}^{Y} dY'\, M(Y')\right]\right)^T, \tag{5.4}$$

with

$$\left(\mathcal{P}\exp\left[-\int_{Y_0}^{Y} dY'\, M(Y')\right]\right)^T = \overline{\mathcal{P}}\exp\left[-\int_{Y_0}^{Y} dY'\, M^T(Y')\right], \tag{5.5}$$

where $\overline{\mathcal{P}}$ denotes anti-path ordering, as introduced in equation (3.3). If one were to insist on constructing a truncation operator that only acts on the left, instead of the symmetric action of equation (5.3), one could use the following:

$$\tilde{M}_Y\langle A\rangle_Y = (M_Y + \langle A\rangle_Y M_Y^T\langle A\rangle_Y^{-1})\langle A\rangle_Y, \tag{5.6}$$

inserting $\tilde{M}$ in place of M in equation (5.1). This is obtained from factoring out $\langle A\rangle$ to the right of equation (5.3). Let's move on to deriving an explicit expression for M.

5.2 Parametrizing Rapidity Evolution

Since we do not know the exact form of M, we write it in the most generic form we are able to that preserves the structure and properties of the Wilson Line Correlator it acts upon. By structure, we mean that if we consider a family of Wilson Line Correlators that map from singlets of n quarks and n anti-quarks, this operator should be an endomorphism on this set. The most important property that needs to be preserved is that of the coincidence limits. Hence, we introduce the basic building block of such an operator:

$$i\overline{\nabla}^a_x U_y = -\delta^{(2)}_{xy} U_y t^a. \tag{5.7}$$

Indeed this is the Lie derivative, the right invariant vector field introduced in (3.19). This operator can be shown to commute with the Wilson Line correlator and instead act on the gluon distribution through integration by parts,

$$\int D[U](i\overline{\nabla}A)Z_Y[U] = \int D[U]A(i\overline{\nabla}Z_Y[U]). \tag{5.8}$$

It is this property of $i\overline{\nabla}$ that implies that the left hand side of (5.8) must preserve the structure and properties of A, since the only thing that changes in the R.H.S is the distribution we average over. We use this functional derivative to build a generic operator

$$\begin{aligned} &- M_Y\langle A\rangle_{Y_0} =: \\ &\Big\langle \left[\frac{1}{2!}\int_{u_1u_2} G_{Y,u_1u_2} i\overline{\nabla}^a_{u_1} i\overline{\nabla}^a_{u_2} + \right. \\ &\left. \frac{1}{3!}\int_{u_1u_2u_3} G^a_{Y,u_1u_2u_3} K_a^{a_1a_2a_3} i\overline{\nabla}^{a_1}_{u_1} i\overline{\nabla}^{a_2}_{u_2} i\overline{\nabla}^{a_3}_{u_3} + \cdots \right] A\Big\rangle_{Y_0}. \end{aligned} \tag{5.9}$$

This has shifted the rapidity dependence on to the n-point G's, which are defined such that this produces the correct evolution. K stands for the color structure constants. This is why there is no 1-point G. The color structure constant for the 2-point G is given by a Kronecker delta and the 3-point ones by the f^{abc}'s and d^{abc}'s. Finding the colour structures for the higher order terms is still an open problem.

The Gaussian truncation is obtained when one truncates this series to the lowest order in G, which we dub the gluon exchange function since it parametrizes JIMWLK evolution. The different n orders of G encode n-wise interactions, G_{xy} encoding pairwise interactions between particles located at x and y, G_{xyz} encoding 3-body interactions, etc.. Heuristically, it is posed that the leading order interaction takes the form of a pairwise interaction, with higher order interactions being suppressed. One can also look at higher n-body interactions as only becoming relevant when there are n bodies. This would imply that truncating to $G_{(n)}$ would serve as a good approximation when dealing with n-point Wilson line correlators. Regardless, all correlators can be accessed by any level of the truncation, which is what makes this strategy so useful. Given all these considerations, we will look at the 2-point correlator, the dipole, and beyond with the lowest order truncation, the Gaussian truncation.

Applying the Gaussian truncation to the $q\bar{q}$ dipole correlator, one obtains

$$\langle \mathrm{tr}(U_{\boldsymbol{x}} U^\dagger_{\boldsymbol{y}})\rangle_Y = N_c e^{-C_f \mathcal{G}_{Y,\boldsymbol{xy}}}, \tag{5.10}$$

where $C_f := t^a t^a$ is the quadratic Casimir of the fundamental representation and

$$\mathcal{G}_{Y,\boldsymbol{xy}} := \int^Y dY' \left(G_{Y',\boldsymbol{xy}} - \frac{1}{2}(G_{Y',\boldsymbol{xx}} + G_{Y',\boldsymbol{yy}}) \right). \tag{5.11}$$

The proof, to lowest order in G:

$$\begin{aligned} \frac{d}{dY}\left\langle \mathrm{tr}(U_{\boldsymbol{x}}U_{\boldsymbol{y}}^\dagger)\right\rangle_Y &\approx \frac{1}{2!}\int_{u_1u_2} G_{Y,u_1u_2}\left(\frac{1}{2}i\overline{\nabla}^c_{u_1}i\overline{\nabla}^c_{u_2} + \frac{1}{2}i\nabla^c_{u_1}i\nabla^c_{u_2}\right)\left\langle \mathrm{tr}(U_{\boldsymbol{x}}U_{\boldsymbol{y}}^\dagger)\right\rangle_Y \\ &= \frac{1}{2!}\int_{u_1u_2} G_{Y,u_1u_2}(\delta_{\boldsymbol{y}u_1}-\delta_{\boldsymbol{x}u_1})(\delta_{\boldsymbol{y}u_2}-\delta_{\boldsymbol{x}u_2})\left\langle \mathrm{tr}(U_{\boldsymbol{x}}t^at^aU_{\boldsymbol{y}}^\dagger)\right\rangle \\ &= -C_f(G_{Y,\boldsymbol{xy}} - \frac{1}{2}(G_{Y,\boldsymbol{xx}}+G_{Y,\boldsymbol{yy}}))\left\langle \mathrm{tr}(U_{\boldsymbol{x}}U_{\boldsymbol{y}}^\dagger)\right\rangle, \end{aligned} \tag{5.12}$$

which has the exponential solution as claimed. The factor of N_c is obtained from the normalization condition $\langle \mathrm{tr}(U_{\boldsymbol{x}}U_{\boldsymbol{y}}^\dagger)\rangle_{Y_0} \overset{\boldsymbol{x}\to\boldsymbol{y}}{=} N_c$. Note that the right hand side is not the solution to the left hand side. This is not an evolution equation, this is a *re-parametrization* of the rapidity dependence.

We see that the coincident limit is manifest. As $\boldsymbol{x} \to \boldsymbol{y}$ the G's cancel in (5.12). Therefore we find it prudent to define $G_{Y,\boldsymbol{xx}}$ to be zero. This will not affect the above calculation and will be more convenient to work with. Furthermore, we get that

$$\mathcal{G}_{Y,\boldsymbol{xy}} = \int_{Y_0}^{Y} dY' G_{Y',\boldsymbol{xy}} + \mathcal{G}_{Y_0,\boldsymbol{xy}}, \tag{5.13}$$

where $\mathcal{G}_{Y_0,\boldsymbol{xy}}$ is the initial condition of $\mathcal{G}_{Y,\boldsymbol{xy}}$ at $Y = Y_0$. Just like the dipole correlator, $\mathcal{G}$ and G, are invariant under a total translation. Therefore they can only be functions of the distance between the two coordinates, $|\boldsymbol{x}-\boldsymbol{y}|$. This also automatically means that the gluon exchange functions are symmetric in their transverse coordinate arguments.

We present the result of the Gaussian truncation applied to the $q\bar{q}g$ correlator, followed by the derivation.

$$\langle [\tilde{U}_{\boldsymbol{z}}]^{ab}\mathrm{tr}(t^aU_{\boldsymbol{x}}t^bU_{\boldsymbol{y}}^\dagger)\rangle = C_f d_f e^{-\frac{N_c}{2}(\mathcal{G}_{Y,\boldsymbol{xz}}+\mathcal{G}_{Y,\boldsymbol{zy}}-\mathcal{G}_{Y,\boldsymbol{xy}})-C_f\mathcal{G}_{Y,\boldsymbol{xy}}}, \tag{5.14}$$

where C_f is the quadratic Casimir of the fundamental representation and d_f is the dimension of the fundamental representation. They are necessary for the normalization to work out.

Proof:

To lowest order in G, imposing the constraint that G's with repeated coordinates are

zero.

$$\begin{aligned}
&\frac{d}{dY}\langle[\tilde{U}]^{ab}\mathrm{tr}(t^a U_{\boldsymbol{x}} t^b U_{\boldsymbol{y}}^\dagger)\rangle \\
=&\frac{1}{2!}\int_{u_1u_2} G_{Y,u_1u_2}\frac{\delta}{\delta A^{c+}_{u_1,Y}}\frac{\delta}{\delta A^{c+}_{u_2,Y}}\langle 2\mathrm{tr}(t^a U_{\boldsymbol{z}} t^b U_{\boldsymbol{z}}^\dagger)\mathrm{tr}(t^a U_{\boldsymbol{x}} t^b U_{\boldsymbol{y}}^\dagger)\rangle \\
=&\quad G_{Y,\boldsymbol{xz}}\langle 2\mathrm{tr}(t^a U_{\boldsymbol{z}} t^c t^b U_{\boldsymbol{z}}^\dagger)\mathrm{tr}(t^a U_{\boldsymbol{x}} t^c t^b U_{\boldsymbol{y}}^\dagger)\rangle - G_{Y,\boldsymbol{xz}}\langle 2\mathrm{tr}(t^a U_{\boldsymbol{z}} t^b t^c U_{\boldsymbol{z}}^\dagger)\mathrm{tr}(t^a U_{\boldsymbol{x}} t^c t^b U_{\boldsymbol{y}}^\dagger)\rangle \\
&- G_{Y,\boldsymbol{yz}}\langle 2\mathrm{tr}(t^a U_{\boldsymbol{z}} t^c t^b U_{\boldsymbol{z}}^\dagger)\mathrm{tr}(t^a U_{\boldsymbol{x}} t^b t^c U_{\boldsymbol{y}}^\dagger)\rangle + G_{Y,\boldsymbol{yz}}\langle 2\mathrm{tr}(t^a U_{\boldsymbol{z}} t^b t^c U_{\boldsymbol{z}}^\dagger)\mathrm{tr}(t^a U_{\boldsymbol{x}} t^b t^c U_{\boldsymbol{y}}^\dagger)\rangle \\
&- G_{Y,\boldsymbol{xy}}\langle 2\mathrm{tr}(t^a U_{\boldsymbol{z}} t^b U_{\boldsymbol{z}}^\dagger)\mathrm{tr}(t^a U_{\boldsymbol{x}} t^c t^b t^c U_{\boldsymbol{y}}^\dagger)\rangle
\end{aligned} \tag{5.15}$$

In order to make the solution to this differential equation obvious, we employ some identities to simplify this expression. We simplify the first four terms by noticing the presence of the commutator: $t^c t^b - t^b t^c = i f^{cbd} t^d$,

$$\begin{aligned}
(5.15) = &\quad G_{Y,\boldsymbol{xz}}\langle 2\mathrm{tr}(t^a U_{\boldsymbol{z}} i f^{cbd} t^d U_{\boldsymbol{z}}^\dagger)\mathrm{tr}(t^a U_{\boldsymbol{x}} t^c t^b U_{\boldsymbol{y}}^\dagger)\rangle \\
&- G_{Y,\boldsymbol{yz}}\langle 2\mathrm{tr}(t^a U_{\boldsymbol{z}} i f^{cbd} t^d U_{\boldsymbol{z}}^\dagger)\mathrm{tr}(t^a U_{\boldsymbol{x}} t^b t^c U_{\boldsymbol{y}}^\dagger)\rangle \\
&- G_{Y,\boldsymbol{xy}}\langle 2\mathrm{tr}(t^a U_{\boldsymbol{z}} t^b U_{\boldsymbol{z}}^\dagger)\mathrm{tr}(t^a U_{\boldsymbol{x}} t^c t^b t^c U_{\boldsymbol{y}}^\dagger)\rangle.
\end{aligned} \tag{5.16}$$

In order to reveal that this differential equation permits an exponential solution, we exploit the following property of products of generators, (D.11), to rewrite the first two terms and the property (D.7) to rewrite the last term.

$$(5.16) = -\left[\frac{N_c}{2}(G_{Y,\boldsymbol{xz}} + G_{Y,\boldsymbol{zy}}) + G_{Y,\boldsymbol{xy}}\left(C_f - \frac{N_c}{2}\right)\right]\langle[\tilde{U}]^{ab}\mathrm{tr}(t^a U_{\boldsymbol{x}} t^b U_{\boldsymbol{y}})\rangle \tag{5.17}$$

We see that (5.14) must be the correct solution.

This parametrization of Wilson line correlators simply passes the buck one step. How does one obtain an analytic or numeric expression for the gluon exchange functions then? One needs to look no further than the evolution of the dipole, (4.54). When one replaces the correlators in (4.54) with the parametrization obtained from the Gaussian truncation, one finds that the differential equation is now closed. The evolution of the 2-point gluon exchange function, G, does not depend on higher order terms. In other words, we insert the parametrizations of the 2 and 3-point equations into the evolution equation for the dipole to obtain an evolution equation for the gluon exchange function. Therefore, this differential equation can be solved numerically for G. The equation obtained is

$$\frac{d}{dY}\mathcal{G}_{Y,\boldsymbol{xy}} = \frac{\alpha_s}{\pi^2}\int_{\boldsymbol{z}} \mathcal{K}_{\boldsymbol{xyz}}\left(1 - e^{-\frac{N_c}{2}(\mathcal{G}_{Y,\boldsymbol{xz}} + \mathcal{G}_{Y,\boldsymbol{yz}} - \mathcal{G}_{Y,\boldsymbol{xy}})}\right) \tag{5.18}$$

What remains to be determined now is a suitable initial condition. A Gaussian distribution is used and we evolve to the point where we become blind to the initial condition. With all this we can now predict the dipole spectrum. When comparing to full JIMWLK simulations, the Gaussian truncation performs better than the BK approximation [5] as well as when compared to HERA data [20].

It is prudent at this point to mention that these gluon color structure functions are

evolution equation dependent! In other words, if we used a different evolution equation, say the one for the 3-point correlator equation as opposed to that of the dipole, one would obtain a valid but different expression for the G's. Throughout the use of this text the evolution equation from which we divined G is the dipole evolution equation (4.54), resulting in (5.18). A warning is given for those who wish to deviate from this procedure: our results will be difficult to compare.

5.3 Evolution of Non-Trivial Correlators

Before moving on to numerical simulations, we will finsih the discussion of how to apply the Gaussian truncation to higher n-point correlators. When we want to get the evolution of more complicated correlators, it is not sufficient to write down the Gaussian truncation of said correlator and determine the evolution via (5.2), treating A as the correlator of interest. Instead, a matrix of correlators needs to be considered. It is easiest to see why this is the case through the use of Birdtracks. They are a symbolic way of representing Wilson line correlators. An introduction on their use can be found in [21, 12].

To briefly summarize the salient details of bird-tracks, the following diagram corresponds to a $q\bar{q}$ pair

$$\mathrm{tr}(U_{\boldsymbol{x}}U^{\dagger}_{\boldsymbol{y}}) = \tag{5.19}$$

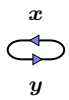

The blue arrows are the Wilson lines. For the $q\bar{q}$ case, the coincident limit $\boldsymbol{x} = \boldsymbol{y}$ implies that the Wilson lines in (5.19) cancel to identity and we are left with the trace of the identity element. This will become important in a moment when we start inserting generators. Diagrammatically, this corresponds to moving the two red arrows on top of each other. When they coincide, the diagram vanishes and we're left with a factor of N_c. When we will normalize the diagram, taking the coincident limit should leave us with a one

The next diagram to consider is the pair of pairs, $q^2\bar{q}^2$:

$$\mathrm{tr}(U_{\boldsymbol{x_1}}U^{\dagger}_{\boldsymbol{y_1}})\mathrm{tr}(U_{\boldsymbol{x_2}}U^{\dagger}_{\boldsymbol{y_2}}) = \tag{5.20}$$

with the coordinates in the brid-track now being implied. We see that a product of two traces is just a "product" of the two bird-tracks, where we draw them vertically. If we take the coincident limit $\boldsymbol{x_2} = \boldsymbol{y_2}$, the second trace turns into a factor of N_c, leaving us only with a single dipole. In bird-tracks, the obvious thing happens and the second loop turns into an N_c, leaving us with just a single loop.

$$\begin{aligned} \mathrm{tr}(U_{\boldsymbol{x_1}}U^{\dagger}_{\boldsymbol{y_1}})\mathrm{tr}(U_{\boldsymbol{x_2}}U^{\dagger}_{\boldsymbol{y_2}}) &\underset{\boldsymbol{x_2}\to\boldsymbol{y_2}}{=} \mathrm{tr}(U_{\boldsymbol{x_1}}U^{\dagger}_{\boldsymbol{y_1}})\mathrm{tr}(\mathbb{1}) \\ &= N_c\,\mathrm{tr}(U_{\boldsymbol{x_1}}U^{\dagger}_{\boldsymbol{y_1}}) \\ &= N_c \end{aligned} \tag{5.21}$$

We observe that contracting a bird track loop results in a factor of N_c. The next thing to consider is when gluon lines attach to the quark lines. Take, for example $q^2\bar{q}^2g$. This

has the effect of inserting a generator into each trace of (5.20) and summing over them. Diagrammatically, this amounts drawing a dashed line joining the two loops

$$\mathrm{tr}(U_{\boldsymbol{x_1}} t^a U^\dagger_{\boldsymbol{y_1}})\mathrm{tr}(U_{\boldsymbol{x_2}} t^a U^\dagger_{\boldsymbol{y_2}}) = \quad , \tag{5.22}$$

with the black arrow representing the generator insertion. It should now be noted that if we consider the coincident limit $\boldsymbol{x_2} = \boldsymbol{y_2}$, we end up taking the trace of a generator. Now we know that the generators of $su(N_c)$ are traceless, meaning this term becomes zero. Diagrammatically, if we shrink a loop that has a single gluon line coming out of it, the entire diagram becomes zero.

$$\begin{aligned} \mathrm{tr}(U_{\boldsymbol{x_1}} t^a U^\dagger_{\boldsymbol{y_1}})\mathrm{tr}(U_{\boldsymbol{x_2}} t^a U^\dagger_{\boldsymbol{y_2}}) &\underset{\boldsymbol{x_2}\to\boldsymbol{y_2}}{=} \mathrm{tr}(U_{\boldsymbol{x_1}} t^a U^\dagger_{\boldsymbol{y_1}})\mathrm{tr}(t^a) \\ &= 0. \end{aligned} \tag{5.23}$$

One can think of this as saying the probability for a gluon to be emitted into the final state is zero as said final state is not a colour singlet. The visualization of this rule is what makes the following argument easier to understand.

It is in our best interest to work with normalized states. Currently, when we make all the coordinates coincident, we end up taking the traces of a number of $N_c \times N_c$ matrices, which results in some N_c dependent factor. The correlators are normalized when, after taking all the coincident limits, the final result is one. Normalized states let us treat these correlators as probability amplitudes. Treating them like amplitudes without normalizing first will lead to a violation of unitarity. To denote normalized correlators, we will use hats for the states that the Wilson lines are sandwiched between. For example, consider the 4-point correlator

$$\quad = \frac{1}{N_c^2}\mathrm{tr}(U_{\boldsymbol{x_1}} U^\dagger_{\boldsymbol{y_1}})\mathrm{tr}(U_{\boldsymbol{x_2}} U^\dagger_{\boldsymbol{y_2}}), \tag{5.24}$$

so that in the limit $y_1 \to y_1$ and $y_2 \to x_2$, this correlator goes to 1.

Consider the set of states that can be constructed out of the following basis states:

where the open dot is given by d^{abc}, the totally symmetric colour tensor and the closed dot is given by f^{abc}, the totally anti-symmetric colour tensor and generator of the adjoint algebra. That is, consider all the correlators than can be constructed by sandwiching 3 Wilson lines and 3 anti-Wilson lines between every combination of these states. We can do this systematically to obtain the following

amplitude matrix (using normalized states)

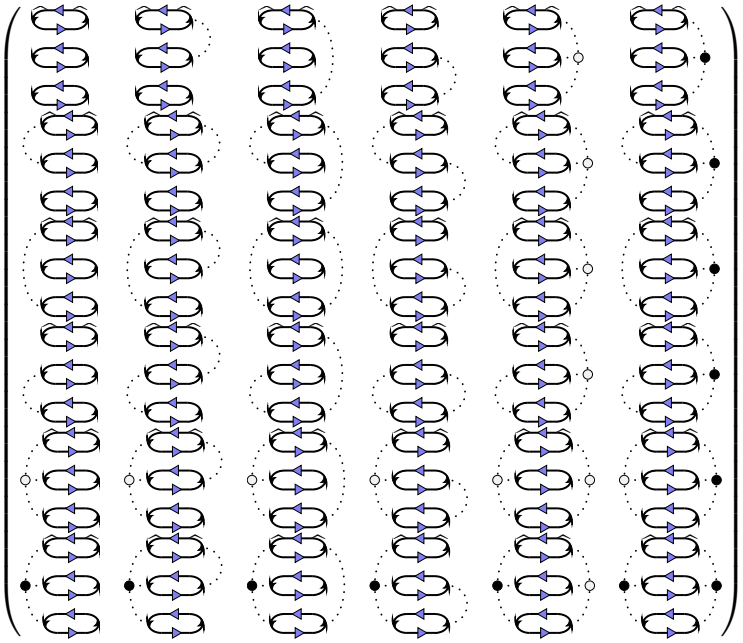

(5.25)

The reason this is called the amplitude matrix is that it represents all the possible correlators that arise from amplitudes that consist of any of the above basis states. Even if only one of the above basis states is present in a calculation, the off-diagonal elements of the amplitude matrix actually give the probability for transitioning to a different basis state. As an example, let's write one of these correlators explicitly to build further intuition for the bird-track notation.

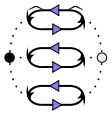

$$= \frac{1}{\sqrt{2N_c(N_c^2-1)}}\sqrt{\frac{N_c}{2(N_c^2-4)(N_c^2-1)}}$$
$$\times f^{def}\,\mathrm{tr}(U^\dagger_{y_1}t^dU_{x_1}t^a)\mathrm{tr}(U^\dagger_{y_2}t^bU_{x_2}t^b)\mathrm{tr}(U^\dagger_{y_3}t^fU_{x_3}t^c)d^{abc}, \tag{5.26}$$

where $x_{1,2,3}$ are the coordinates of the quarks and $y_{1,2,3}$ are the coordinates of the auntiquarks. That factors of N_c in the front are the normalization that ensure, in the coinicident limit $x_{1,2,3} \to y_{1,2,3}$, the diagonal diagrams are equal to 1. Since this is an orthogonal basis, in the full coincident limit off diagonal terms will be equal to zero. More can be said about the normalization of this basis in chapter 5 of [12]. Now, under JIMWLK evolution, all of these correlators are fundamentally inexorable. However, observe what happens when we let the bottom two coordinates be coincident. Consider the top left diagram: by the arguments above it reduces to (5.20).

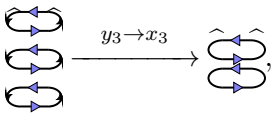

where factors of N_c are implicitly accounted for in the normalization. If we consider the bottom left diagram, making the bottom two coordinates coincident will make this

term zero by the argument presented for (5.23).

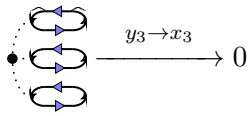

Finally, consider the bottom right term. In this coincident limit we get the trace reduces to a Wilson line in the adjoint representation, a la (3.60). Adjoint Wilson lines can be represented with a dotted line.

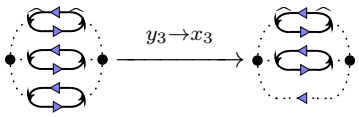

(5.27)

If we apply this reasoning to the entirety of (5.25), we get the following matrix

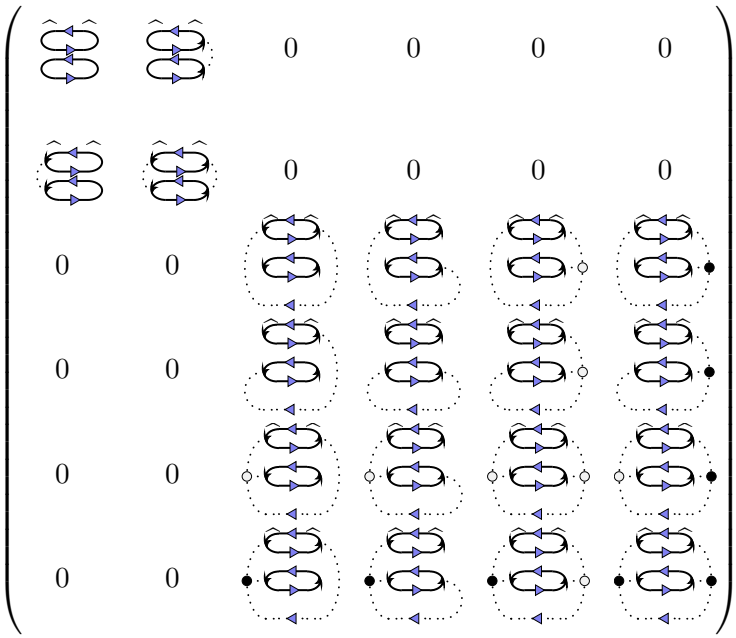

(5.28)

The amplitude matrix has block-diagonalized. There are two important things to note about this. One: JIMWLK still feeds information from the bottom block into the top one. Two: In the parametrization prescribed by (5.1), elements of (5.28), mix only as they would under a matrix exponentiation, i.e. each block only mixes with itself. Considering the first point, does this mean we need to consider all possible correlators when seeking the evolution of just one, as JIMWLK commands? No. We have parametrized JIMWLK evolution by the evolution of the gluon colour structure functions, G.

This is a key statement about the Gaussian truncation - it provides a plausible and systematic method of linearly evolving states. The non-linearity associated with JIMWLK evolution, the feeding of information from higher order blocks, is instead contained within the evolution of the gluon exchange functions. However, one cannot ignore the second point about the parametrization, that the blocks still mix their own terms among themselves in the matrix exponentiation. It is for this reason one must consider

the entire block when seeking the evolution of a higher order correlator.

In the section 7, we will discuss the gritty details of how to implement this procedure numerically.

In summary, we have developed a tool that gives us partial access to all Wilson line correlators while preserving coincident limits.

5.4 Limitations and Open Questions on the Gaussian Truncation

While the Gaussian truncation proposes to perform an amazing feat in granting access to any Wilson line correlator, it is a new tool whose potential is still being explored. We find it prudent to remain cognisant of the limitations and assumptions that go into this truncation.

Given that this is a truncation and not the full evolution, it is obvious that some information is lost, but can we quantify this? The way we have constructed the Gaussian truncation, it can only produce an imitation of JIMWLK that is purely real. In other words, it has no way of accessing the imaginary part of any correlator. In order to access these additional degrees of freedom, one would need to go beyond the Gaussian truncation to higher order gluon exchange functions. The odderon is an example of a contribution to an observable that depends on the imaginary part of the dipole correlator that would require this [22].

If one were to do this, the numeric computation of the G's would be non-trivial. Reference would need to be made to more complicated correlators than the dipole to obtain the evolution equations for each higher order G. What more is that these evolution equations would mix the G's n a non-trivial way to make their evolution numerically costly to compute.

Even if one were to go through the effort of specifying the minimum number G's needed to access every degree of freedom in a given correlator, there is no statement that is yet made about how many more G's are needed to qualify for a good approximation. Another way of saying this is that there is no parameter associated with the gluon exchange functions with which to expand in to put an upper bound on the error. Instead we go by the heuristic argument that higher order G's correspond to additional gluon exchanges that should only enter for more complicated correlators. This doesn't make this truncation worse than the large N_c limit, though, since it is also a heuristic that hasn't been shown to be analytically true beyond the dipole correlator.

All this being said, the Gaussian truncation shows real promise. It's property of gauge invariance preservation is highly desirable and preliminary numerics yield good results. The open problems listed above serve as fertile ground for future research.

Chapter 6

Numerical Implementation of the Gaussian Truncation: the Dipole

Having established the theory behind the Gaussian truncation, we move on to systematizing the process of numerically computing the simplest Wilson line correlator: the dipole. We detail how we use the evolution of this object to obtain the numerical form of the gluon colour structure functions and how to then take these functions to recreate the dipole correlator at different rapidities. We argue for the numerical stability of this algorithm and finally we extract information about the nuclear saturation scale Q_s.

We reiterate the result of 5.18

$$\frac{d}{dY}\mathcal{G}_{Y,\boldsymbol{xy}} = \frac{\alpha_s}{\pi^2}\int_{\boldsymbol{z}} \mathcal{K}_{\boldsymbol{xyz}}\left(1 - e^{-\frac{N_c}{2}\left(\mathcal{G}_{Y,\boldsymbol{xz}}+\mathcal{G}_{Y,\boldsymbol{yz}}-\mathcal{G}_{Y,\boldsymbol{xy}}\right)}\right)$$

which can be easily solved using standard numerical methods to obtain $\mathcal{G}$. A Gaussian initial condition is used, with the notion that $\mathcal{G}$ can evolve until it is "blind" to the initial condition. The constraint imposed on this evolution is that it needs to be able to, at some rapidity, match experimental data. Given the that we are trying to access information concerning Wilson line correlators through a renormalization equation, we are not given an initial condition for free. Hence the need to explore the rapidity evolution of this Gaussian truncated dipole until is best matches the data. Any evolution that we apply after finding this matching condition will serve as a prediction for how the correlator evolves.

We leave comparison to experimental data for another day, and instead focus on the result of numerical evolution. The implementation 5.18 was handled by Javier Albacete [23], who gave us the following result for the Dipole correlator when using (5.10)

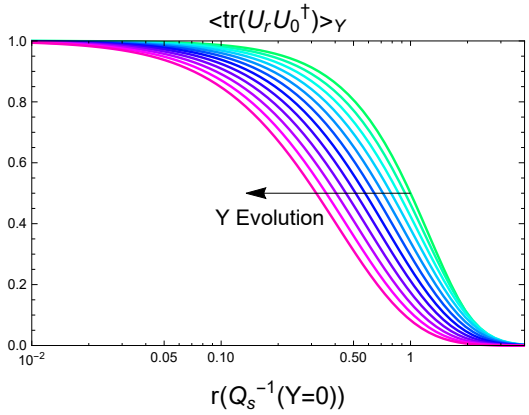

FIGURE 6.1: Plotted is the dipole correlator, $S := \frac{1}{N_c}\left\langle \text{tr}(U_{\mathbf{0}}U^{\dagger}_{\boldsymbol{r}})\right\rangle_Y$, as function of distance, r, over a range of rapidities. The arrow indicates the trend of rapidity evolution to shift the curve to the left. Green is the lowest rapdity, with each line a rapidity of one greater until the magenta line with largest rapidty $Y = 10$.

Despite starting from a fictitious initial condition, this qualitatively matches the shape of the dipole that has been successfully used in comparison to data [20]. We see that the dipole behaves like a sigmoid function. In order to describe the evolution, we find it useful to define the correlation length, r_s and saturation scale, Qs. The correlation length is roughly the distance at which the dipole experiences an inflection, which we take to be when $S = \frac{1}{2}$. The saturation scale is just the energy at which this takes place, so in natural units

$$Q_s = \frac{1}{r_s}(GeV). \tag{6.1}$$

Thus, the statement that the correlation length is decreasing is the statement that the saturation scale increases as we increase rapidity (and Energy). The scale of r is arbitrary, since it comes from an arbitrary (unrelated to physical experiment) initial condition, so we plot in units of $Q_s(Y = 0)$, the point at which the zero rapidity curve has the value of 0.5.

Now that we know this, we can ask a question about the profile of the dipole: Is it just that the curve is moving left with the saturation scale, or is it becoming steeper or shallower? Plotting in units of inverse saturation scale we get

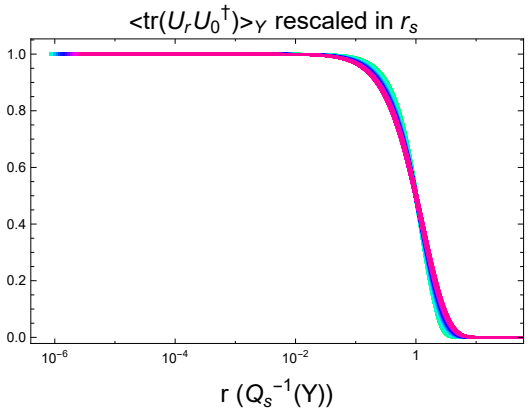

FIGURE 6.2: We plot the dipole, but for each curve the r axis has been rescaled such that r is units of $1/Q_s$. Green is the lowest rapdity, with each line a rapidity of one greater until the magenta line with largest rapidty $Y = 10$.

Now we see that at higher rapidities the dipole becomes more tense, the slope of its inflection point becoming steeper. If the shape of the curve were to remain constant with rapidity evolution, that would imply that we were in the perfect scaling regime. Since the slope is not constant, we know the curve isn't perfectly scaling. We would expect this since the running coupling affects scaling, but whether all of the scaling properties are accounted for by the running coupling is yet to be determined. Thus the change in saturation scale isn't all that is different about the dipole correlator at higher rapidities, but it accounts for most of the difference.

Seeing that we are able to extract the saturation scale for each curve, we can thus numerically infer what the saturation scale is as a function of rapidity. This is done simply by finding at which r is the dipole $S = \frac{1}{2}$, for each rapidity, Y. Then one inverts the r to obtain the saturation scale, Q_s and plots against each corresponding rapidity. Following this procedure we obtain

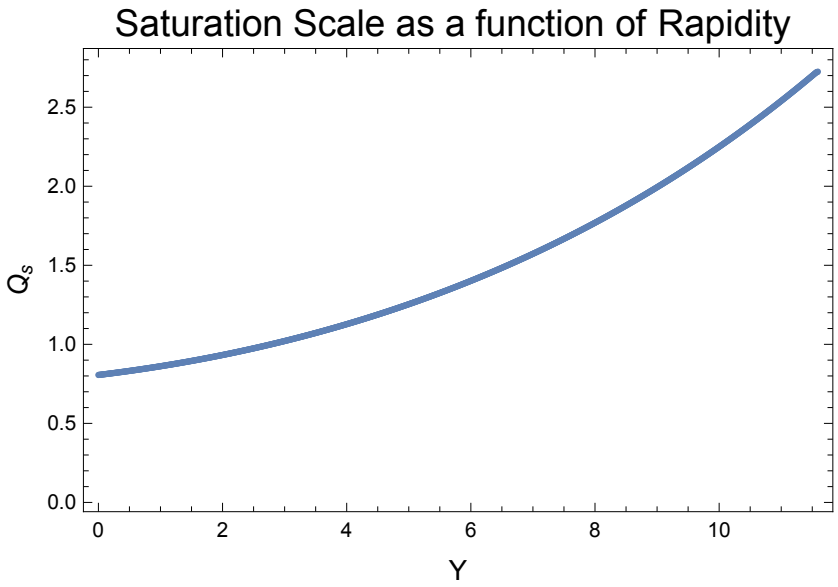

FIGURE 6.3: The saturation scale, Q_s, of the dipole correlator as a function of rapidity, Y.

The units of the saturation scale are arbitrary, since we extract it from a dipole whose initial condition had an arbitrary (unrelated to experiment) spacial dependence. The saturation scale is critical because it determines where the characteristic behavior of Wilson line correlators appears. In scattering experiments that involve a large nucleus as a target, such as lead or gold, the color evolution is treated as multiple successive colour rotations as the projectile parton passes through each successive nucleon. Thus we expect the parton to undergo an effective rapidity increase in excess of that with a single proton target. It was shown in [24] that we can determine the effective saturation scale increase in the presence of a nucleus target. Through the use of (6.3) we can reverse engineer the saturation scale to determine the required rapidity evolution. This procedure grants us the power to make predictions for proton-nucleus with almost no increase in algorithmic complexity. This will be explained in more detail in Appendix C.

Yet more information can be extracted from $\mathcal{G}$. We used the Gaussian truncation for the dipole equation (5.18) to determine $\mathcal{G}$. Let us not forget that this is constructed from a more fundamental element, G, through the integral $\mathcal{G}_Y = \int_{Y_0}^{Y} dY' G_{Y'}$. While it is sufficient for the dipole to compute $\mathcal{G}$, it turns out to be necessary for higher n-point correlators to actually compute G directly. This necessity arises as a consequence of the matrix exponentiation used to parametrize and compute more complicated correlators, as we will demonstrate in the next section. These quantities are related simply: G is merely the derivative of $\mathcal{G}$ with respect to rapidity. Numerically, we extract G through a finite (central) difference equation,

$$G(Y) = \frac{\mathcal{G}(Y + \Delta Y) - \mathcal{G}(Y - \Delta Y)}{2\Delta Y} + \mathcal{O}(\Delta Y^2), \tag{6.2}$$

where we have suppressed position dependencies. To check the validity of this, we can recover $\mathcal{G}$ from G and consequently reconstruct the dipole. We do this and obtain

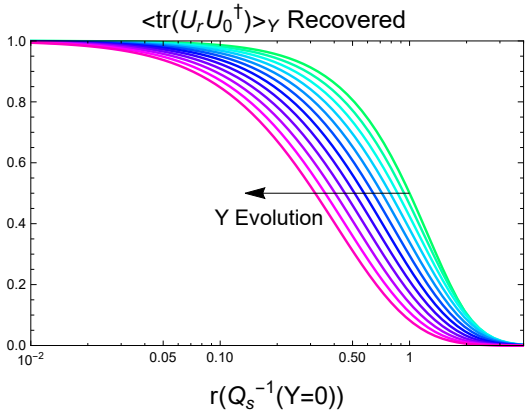

FIGURE 6.4: Reconstruction of the dipole using the extracted G functions. The arrow indicates the trend of rapidity evolution to shift the curve to the left. Green is the lowest rapdity, with each line a rapidity of one greater until the magenta line with largest rapidty $Y = 10$.

Qualitatively, this is figure is what we expected, it matches figure 6.1. This is indistinguishable from 6.1 to the naked eye, so it is more insightful to plot the difference between the original dipole data in 6.1 and the reconstruction in 6.4. We can do this at different resolutions, ΔY.

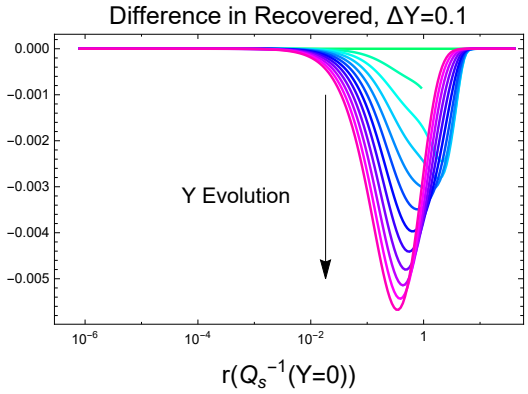

FIGURE 6.5: Plotted is the difference in dipoles between direct evolution using equation (5.18) and the reconstruction using equation (5.18). This is performed at a resolution of $\Delta Y = 0.1$. Green is the lowest rapdity, with each line a rapidity of one greater until the magenta line with largest rapidty $Y = 10$.

If we increase the rapidity resolution by a factor of ten, we then get the following difference

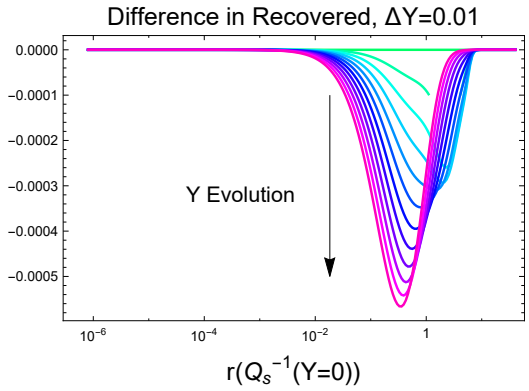

FIGURE 6.6: Compare with figure 6.5. Plotted is the difference in dipoles between direct evolution using equation (5.18) and the reconstruction using equation (5.18). This is performed at a resolution of $\Delta Y = 0.01$. Green is the lowest rapdity, with each line a rapidity of one greater until the magenta line with largest rapidty $Y = 10$.

We see that increasing the resolution by a factor of ten, reduces the error by a factor of ten. This suggests numerical stability in our algorithm.

Having successfully compute the dipole correlator, in the next chapter we will move on to calculating more complicated, 4-point correlators.

Chapter 7

Numerical evolution of higher n-point correlators

We have mentioned before that higher order correlators mix in their evolution. In other words it is a mistake to think that the rapidity dependence of the four point correlator is given by the Gaussian truncation operator acting solely on the correlator in question:

$$\left\langle \mathrm{tr}(U_{\boldsymbol{x_1}}U^\dagger_{\boldsymbol{y_1}})\mathrm{tr}(U_{\boldsymbol{x_2}}U^\dagger_{\boldsymbol{y_2}})\right\rangle_Y \neq \exp^{\frac{1}{2}N_c(1-N_c^2)\left(\mathcal{G}_Y(x_1,y_1)+\mathcal{G}_Y(x_2,y_2)\right)}\left\langle \mathrm{tr}(U_{\boldsymbol{x_1}}U^\dagger_{\boldsymbol{y_1}})\mathrm{tr}(U_{\boldsymbol{x_2}}U^\dagger_{\boldsymbol{y_2}})\right\rangle_{Y_0}. \tag{7.1}$$

Instead we need to consider the simultaneous evolution of all non-equivalent singlet states - and their transition operators - that can be constructed from the basis of $q^n\bar{q}^n$. In this chapter we will go through the details of how to compute these higher n-point correlators numerically. Given that we will be dealing with correlators with a non-trivial evolution and more complicated coordinate dependencies, we shall also explore several coincident limits as means of testing the validity of this process. Beyond that we shall implement the infamous large N_c limit and compare the predictions made between these two methods.

Granted some amplitude matrix $\langle A\rangle$, we use the Gaussian truncation to compute the exponentiating matrix M. The goal is then to numerically implement (5.4)

$$\langle A\rangle_Y = \mathcal{P}\exp\left[-\int_{Y_0}^{Y} dY'\, M(Y')\right]\langle A\rangle_{Y_0}\left(\mathcal{P}\exp\left[-\int_{Y_0}^{Y} dY'\, M(Y')\right]\right)^T,$$

where in the second exponential, we just write M instead of M^T, since we have constructed it to be symmetric. Path ordering makes things difficult. To ameliorate this we employ a strategy of splitting each path into a discrete number of segments:

$$\mathcal{P}\exp\left[-\int_{Y_0}^{Y_n} dY\, M(Y)\right] =$$
$$\mathcal{P}\left(\exp\left[-\int_{Y_{n-1}}^{Y_n} dY\, M(Y)\right]\exp\left[-\int_{Y_{n-2}}^{Y_{n-1}} dY\, M(Y)\right]...\exp\left[-\int_{Y_0}^{Y_1} dY\, M(Y)\right]\right). \tag{7.2}$$

The utility of splitting is that it actually lets us to (partially) get around path ordering. As we shrink the integral into small enough steps, the degree to which M does not commute with itself also shrinks. This comes from the notion that when the step size is infinitesimal, M at the bounds of the integral doesn't change at all, so must commute with itself. Small perturbations away from this should introduce only small corrections. This lets us ignore the path ordering symbol and compute the matrix exponential directly. To reiterate, we break the path ordered exponential into many small, composed pieces and take advantage of the fact that for small enough pieces, we can ignore path ordering.

$$\begin{aligned} &\mathcal{P}\exp\left[-\int_{Y_0}^{Y_n} dY\ M(Y)\right] \\ \approx\ &\exp\left[-\int_{Y_{n-1}}^{Y_n} dY'\ M(Y')\right]\exp\left[-\int_{Y_{n-2}}^{Y_{n-1}} dY'\ M(Y')\right]...\exp\left[-\int_{Y_0}^{Y_1} dY'\ M(Y')\right]. \end{aligned} \tag{7.3}$$

Equation (5.4) now becomes amenable to numeric computation. We break the integral into discrete chunks, exponentiate them and apply them successively to an initial condition to obtain our amplitude of correlators at an evolved rapidity. The segments of non-path ordered exponentials we will call *rigid exponentials* and will be discussed more in section 7.5.

What, then, do we use for an initial condition? We simply apply the Gaussian truncation to $\langle A\rangle$ and set $Y = Y_0$. I.e. we let

$$\langle A\rangle_{Y_0} = \exp\left[-M(Y_0)\right], \tag{7.4}$$

where it is understood that $M(Y_0) = \frac{1}{2}\int_{u_1u_2}\mathcal{G}_{Y_0,u_1u_2}i\overline{\nabla}^a_{u1}i\overline{\nabla}^a_{u_2}\langle A\rangle$ and $\mathcal{G}_{Y_0}$ is the rapidity integral of the gluon exchange function, $\int_{Y_0}^{Y} dY'\ G(Y')$ evaluated at $Y = Y_0$. We make note that, while this choice of initial condition is a guess, it does satisfy coincidence limit and symmetry properties we expect the full solution to maintain. So our full algorithm is now:

$$\langle A\rangle_{Y_{n+1}} = \exp\left[-\int_{Y_n}^{Y_{n+1}} dY' M(Y')\right]\langle A\rangle_{Y_n}\exp\left[-\int_{Y_n}^{Y_{n+1}} dY' M(Y')\right], \tag{7.5}$$

which is iterated until the desired rapidity is reached. Now that we have our algorithm, we can start computing correlators. For simplicity's sake, this chapter will focus on the singlets of 2 quarks and 2 anti-quarks, but this work is easily extended to more complicated correlators only at the cost of requiring more computational power.

A normalized basis for $q^2\bar{q}^2$ is given by $\frac{1}{N_c}$  , $\frac{1}{N_c\sqrt{N_c^2-1}}$  . The basis is not unique, but we find this basis most convenient as it makes inherently obvious which correlators go to 1 in the coincident limit of a quark and anti-quark. If one desired to make manifest

the behaviour of quark-quark and anti-quark-anti-quark coincident limits, one would use a different basis instead [18]. The obtained amplitude matrix is then given by:

$$\langle A\rangle_Y = \left\langle \begin{pmatrix} \frac{1}{N_c^2}\mathrm{tr}(U_{x_1}U_{y_1}^\dagger)\mathrm{tr}(U_{x_2}U_{y_2}^\dagger) & \frac{1}{N_c^2\sqrt{N_c^2-1}}\mathrm{tr}(U_{x_1}U_{y_1}^\dagger t^b)\mathrm{tr}(U_{x_2}U_{y_2}^\dagger t^b) \\ \frac{1}{N_c^2\sqrt{N_c^2-1}}\mathrm{tr}(U_{x_1}t^aU_{y_1}^\dagger)\mathrm{tr}(U_{x_2}t^aU_{y_2}^\dagger) & \frac{1}{N_c^2(N_c^2-1)}\mathrm{tr}(U_{x_1}t^aU_{y_1}^\dagger t^b)\mathrm{tr}(U_{x_2}t^aU_{y_2}^\dagger t^b) \end{pmatrix} \right\rangle_Y \tag{7.6}$$

Or, more compactly, with birdtracks:

$$\langle A\rangle_Y = \left\langle \right\rangle_Y \quad , \tag{7.7}$$

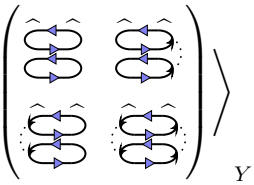

where we use blue arrows for the Wilson lines to indicate implicitly that we are using normalized states. Applying the Gaussian truncation to this provides the following exponentiating matrix

$$\frac{d}{dY}\langle A\rangle = M(Y)\langle A\rangle = \left\langle \frac{1}{2}\int_{u_1u_2} G_{Y,u_1u_2}\, i\overline{\nabla}^a_{u_1} i\overline{\nabla}^a_{u_2} A \right\rangle, \tag{7.8}$$

in which we find

$$M^{11} = \frac{\left(N_c^2-1\right)\left(G\left(x_1,y_1\right)+G\left(x_2,y_2\right)\right)}{2N_c}, \tag{7.9a}$$

$$M^{12} = \frac{\sqrt{N_c^2-1}\left(-G\left(x_1,x_2\right)+G\left(x_1,y_2\right)+G\left(x_2,y_1\right)-G\left(y_1,y_2\right)\right)}{2N_c}, \tag{7.9b}$$

$$M^{21} = \frac{\sqrt{N_c^2-1}\left(-G\left(x_1,x_2\right)+G\left(x_1,y_2\right)+G\left(x_2,y_1\right)-G\left(y_1,y_2\right)\right)}{2N_c}, \tag{7.9c}$$

$$\begin{aligned} M^{22} = \frac{1}{2N_c}\big(&N_c^2G\left(x_1,y_2\right)+N_c^2G\left(x_2,y_1\right)+2G\left(x_1,x_2\right)-G\left(x_1,y_1\right) \\ &-2G\left(x_1,y_2\right)-2G\left(x_2,y_1\right)-G\left(x_2,y_2\right)+2G\left(y_1,y_2\right)\big), \end{aligned} \tag{7.9d}$$

where M is symmetric, as expected by our construction of it. Applying (7.5) to this, we can finally explore the outcomes of the Gaussian truncation. Briefly, we will discuss how we will represent the output of this result. These correlators depend on four coordinates and rapidity, so in order to bypass the use of six dimensional plots we do two things: we represent calculations of different rapidities with differently coloured curves and we parametrize the coordinate dependencies with a single path dependence. To explain this second point we introduce diagrams that visually convey the physical set up of the transverse positions of the two quarks and anti-quarks.

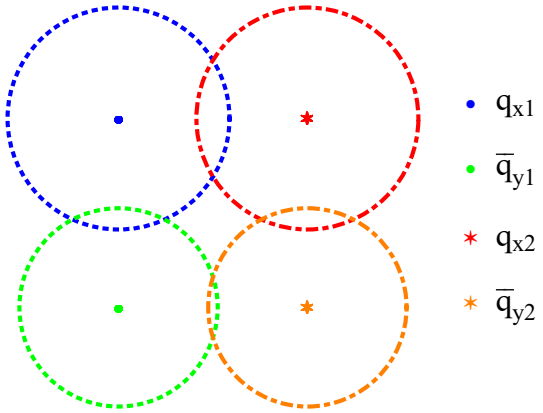

FIGURE 7.1: Two quarks (coordinates x_1 and x_2) and two anti-quarks (coordinates y_1 and y_2) arranged in a square.

Figure 7.1 shows two quarks and anti quarks arranged in a square. The circles surrounding each particle are of radius $\frac{1}{Q_s}$, the correlation length. We draw these in because we expect the behaviour of the Wilson line correlators to change dramatically when the quarks move from inside one another's circle of influence to the outside. We also expect particular behaviour in the coincident limit of two particles. Consider placing a quark on top of an anti-quark.

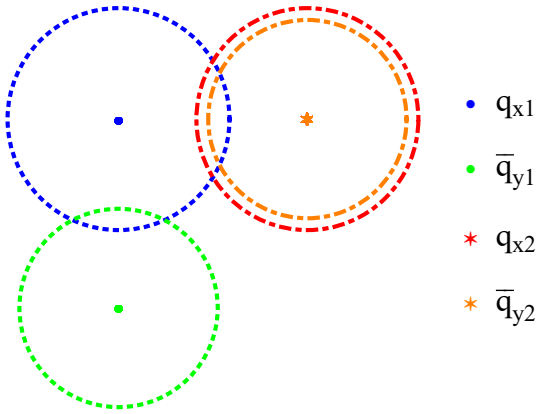

FIGURE 7.2: Two quarks (coordinates x_1 and x_2) and two anti-quarks (coordinates y_1 and y_2) in the coincident limit $x_2 = y_2$.

Figure 7.2 represents the same configuration as before, except we have taken the coincident limit $x_2 = y_2$. Also, the differences in correlation lengths are exaggerated so that q_{x2} and $\bar{q}_{y2}$ may be distinguished. In actuality they possess the same correlation length. Now what interests us is being able to see how the correlators change as we pull away this coincident anti-quark. In figure 7.3 we illustrate $\bar{q}_{y2}$ in different positions, starting at coincidence with q_{x2} and ending outside its range of influence.

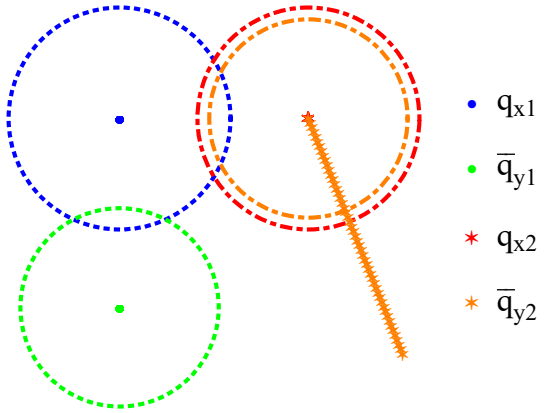

FIGURE 7.3: Two quarks (coordinates x_1 and x_2) and two anti-quarks (coordinates y_1 and y_2) with $\bar{q}_{y2}$ moving along the orange path.

The orange dotted line corresponds to a series of different quark configurations, where the orange particle ($\bar{q}_{y2}$) is at a different point on the orange line in each configuration. This quark is **not moving**. In a given projectile-target interaction, the quark pierces the target at only a single point. We are exploring different quark configurations with three of the coordinates fixed and the fourth coordinate is evaluated at different points along the orange dotted line.

The circles of influence are only drawn around the starting positions of the particles to reduce clutter. They also serve as a means of locating a particle that is coincident with another, in this case the red particle (q_{x2}) is under the starting position of the orange. This is the simplification that allows us to explore the behaviour of $\langle A \rangle_Y$. Instead of tracking the coordinates of all the particles, we may specify the initial configuration and plot how the correlators evolve as the anti-quark is considered to be in different configurations parametrized by this path. We are not limited to moving just this particle, or even just one particle at a time. Figure 7.11 demonstrates the correlator behaviour as we separate two dipoles from each other.

7.1 A Simple Correlator

As the first example, let us plot the following arrangements of two quarks, with transverse coordinates $x_{1,2}$ and anti-quarks, $y_{1,2}$. Let $x_1 = (0, 0)$, $y_1 = (0.5, 0)$, $x_2 = (1, 0)$ and $y_2 = (1 + r, 0)$, with $0 \leq r \leq 2$. This lets us explore the coincident limit $y_2 \to x_2$. What do we predict in this situation? In this limit our amplitude matrix takes the form

$$\langle A \rangle_Y = \left\langle \begin{pmatrix} \text{  } & 0 \\ 0 & \text{  } \end{pmatrix} \right\rangle_Y . \tag{7.10}$$

In other words, the off diagonal terms are zero, as we are taking the trace of a generator. Let's see if the numerics are in agreement with this. We are able to plot figure 7.4.

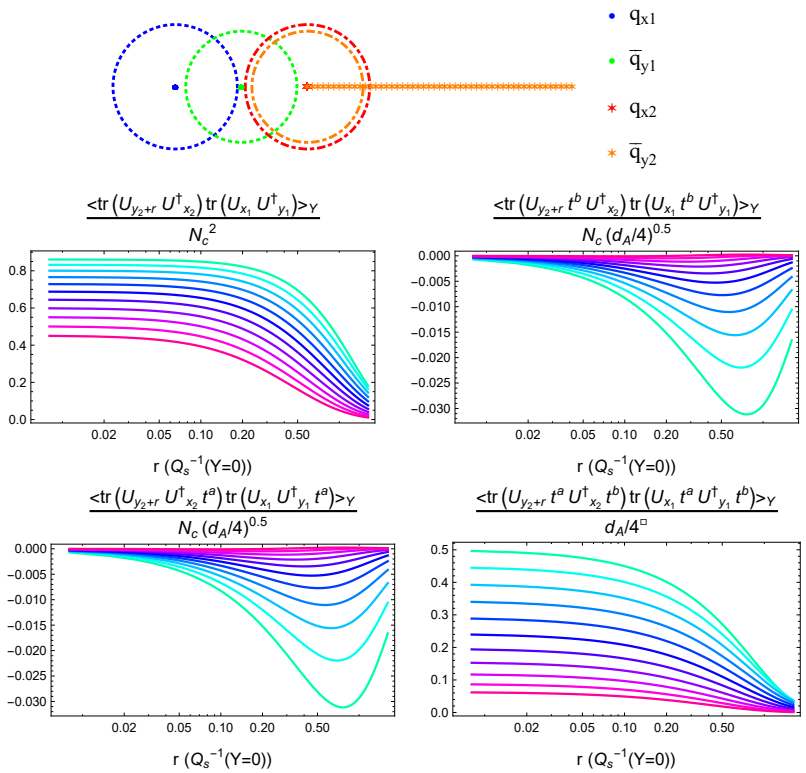

FIGURE 7.4: The top diagram illustrates the position of the quarks, $x_{1,2}$ and anti-quarks $y_{1,2}$ in the transverse plane. The circles are of radius $\frac{1}{Q_s}$ and indicate the sphere of influence of each particle. In this instance, the quark, x_2, and anti-quark, y_2, are coincident and we are plotting the amplitude matrix $\langle A \rangle_Y$ as y_2 is dragged away from the system. The four graphs plot the correlators corresponding to $\langle A \rangle_Y$ at different rapidities. Green is the lowest rapdity, with each line a rapidity of one greater until the magenta line with largest rapidty $Y = 10$.

An important caveat to mention when interpreting these plots, in particular the transverse diagram at the top, is that the circles of influence are drawn using the saturation scale set by the largest rapidity. For lower rapidities the circles would be bigger and thus characteristic behaviour governed by crossing this influence boundary will happen at different transverse distances for different rapidities. We then find it informative to again rescale the figure in Q_s for each curve. This makes it such that Q_s dependant behaviour will visually happen at the same transverse distance. Doing so we obtain

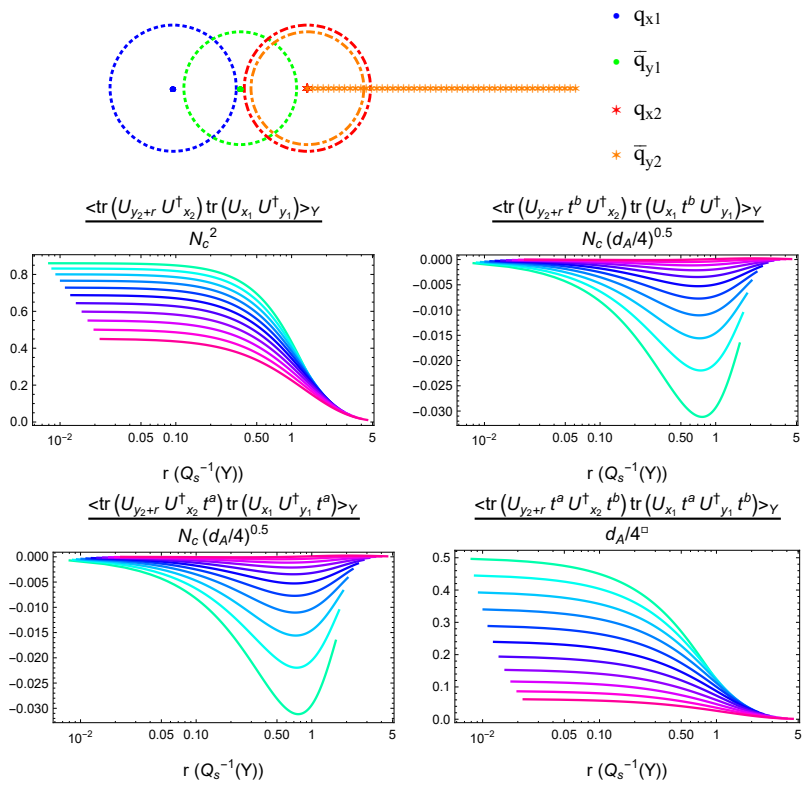

FIGURE 7.5: As 7.4, but these graphs are also scaled in Q_s such that the correlation length is 1 GeV^{-1}, $r_s = 1 = \frac{1}{Q_s}$ for each individual curve. The quark, x_2, and anti-quark, y_2, are coincident and we are plotting the amplitude matrix $\langle A \rangle_Y$ as y_2 is dragged away from the system. The four graphs plot the correlators corresponding to $\langle A \rangle_Y$ at different rapidities. Green is the lowest rapdity, with each line a rapidity of one greater until the magenta line with largest rapidty $Y = 10$.

It is confirmed that the off-diagonal terms are indeed zero when $r = 0$. The next thing we notice is that there is indeed structure related to the saturation scale. The turning point of the off-diagonal terms occur at almost the same transverse position when rescaled, up until the largest rapidities. At which point something strange happens. Lets plot just the largest rapidity curve.

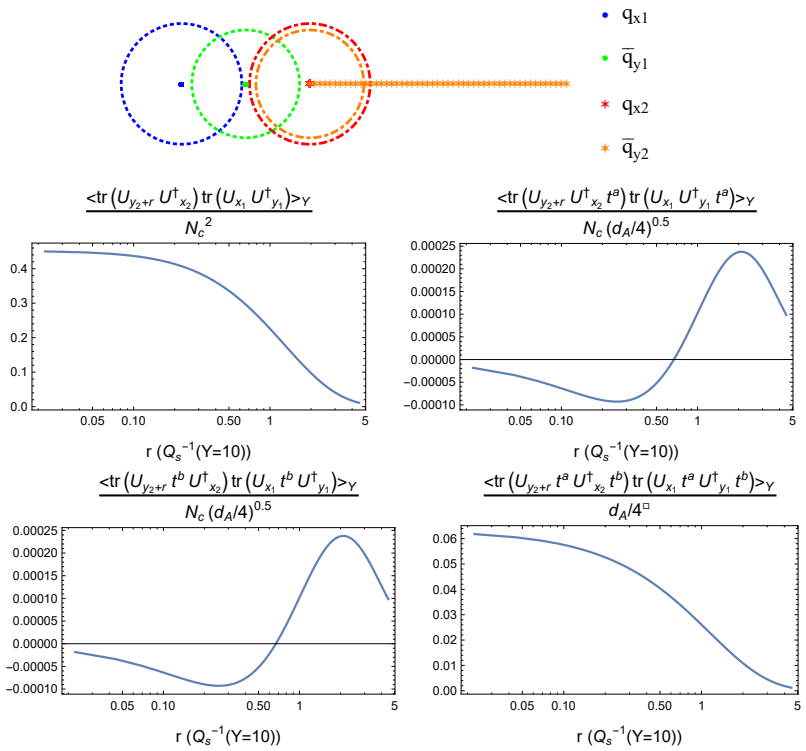

FIGURE 7.6: As 7.5, showing only the curve with the largest rapidity evolution, $Y = 10$.

The off-diagonal terms actually experience a sign change! This behaviour was never actually prohibited. Through the use of identity D.13, we can decompose this correlator into the difference of two correlators:

$$\mathrm{tr}(U_{x_1} t^a U^\dagger_{y_1})\mathrm{tr}(U_{x_2} t^a U^\dagger_{y_2}) = \frac{1}{2}\mathrm{tr}\left(U^\dagger_{y_1} U_{x_1} U^\dagger_{y_2} U_{x_2}\right) - \frac{1}{2N_c}\mathrm{tr}\left(U_{x_1} U^\dagger_{y_1}\right)\mathrm{tr}\left(U_{x_2} U^\dagger_{y_2}\right). \tag{7.11}$$

We see that this correlator can be broken up into the difference of two correlators. In principle the relative size of these two correlators can change, which allows for the sign change in figure 7.6. But even beyond this we cannot say that, necessarily, these correlators are strictly positive. There is no restriction preventing these constituent correlators from being negative. This point is discussed more in section 7.5.

For now, let's investigate other configurations.

7.2 The Gluon-Gluon Dipole Limit

Consider placing two dipoles near each other and explore what happens when we pull the anti-quarks away from the quarks, as in figure 7.7.

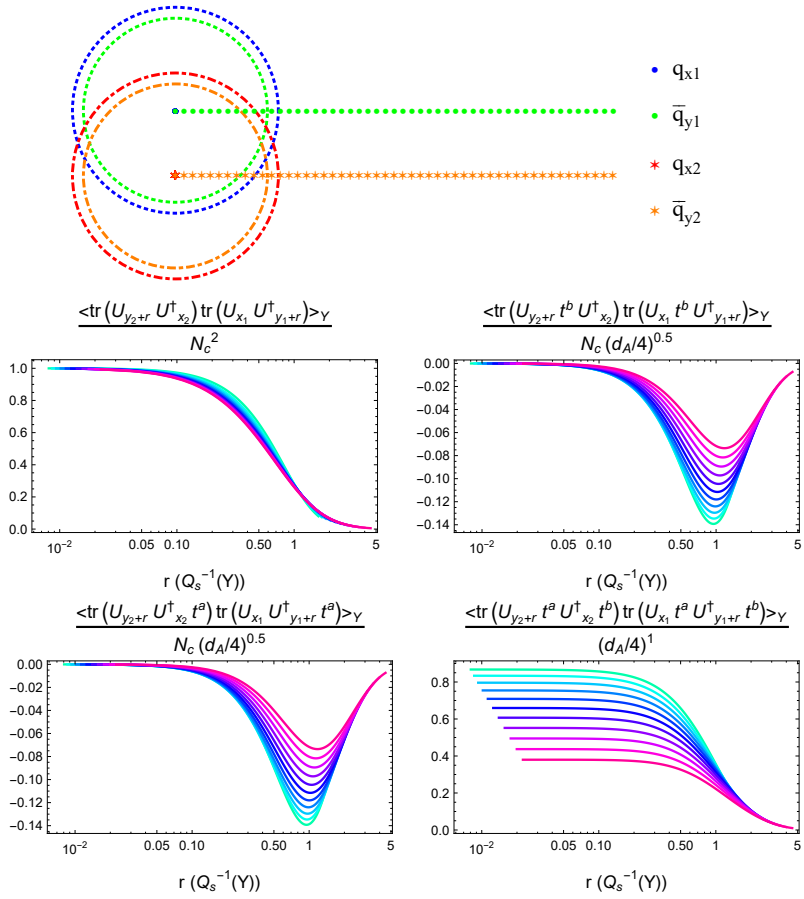

FIGURE 7.7: Particles arranged such that $x_1 = (0,1)$, $y_1 = (r,1)$, $x_2 = (0,0.7)$ and $y_2 = (r,0.7)$, in units of GeV^{-1}. Green is the lowest rapdity, with each line a rapidity of one greater until the magenta line with largest rapidty $Y = 10$. Scaled in Q_s.

Now let's investigate how the correlator behaviour changes as we pull the two dipoles apart.

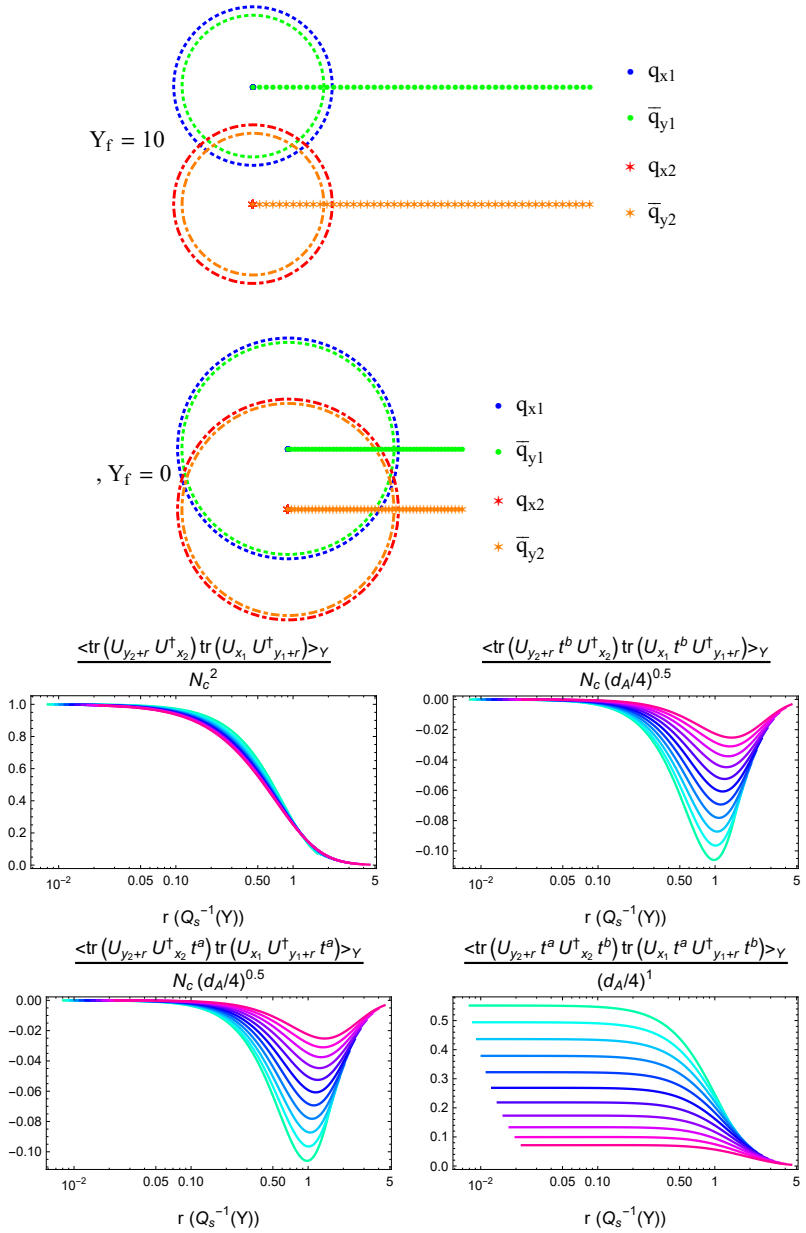

FIGURE 7.8: Particles arranged such that $x_1 = (0,1)$, $y_1 = (r,1)$, $x_2 = (0,0.3)$ and $y_2 = (r,0.3)$, in units of GeV^{-1}. Green is the lowest rapdity, with each line a rapidity of one greater until the magenta line with largest rapidty $Y = 10$. Scaled in Q_s.

In figure 7.8 we have included the circles of influence for the low rapidity particles as well to demonstrate the particles shouldn't be quite decorrelated yet at most rapidities. Since increasing rapidity increases the saturation scale, $Q_s = \frac{1}{r_s}$, then the correlation length decreases. We can pull them even further apart so that the two dipoles are definitely outside each others correlation lengths at all rapidities. The result is figure 7.9.

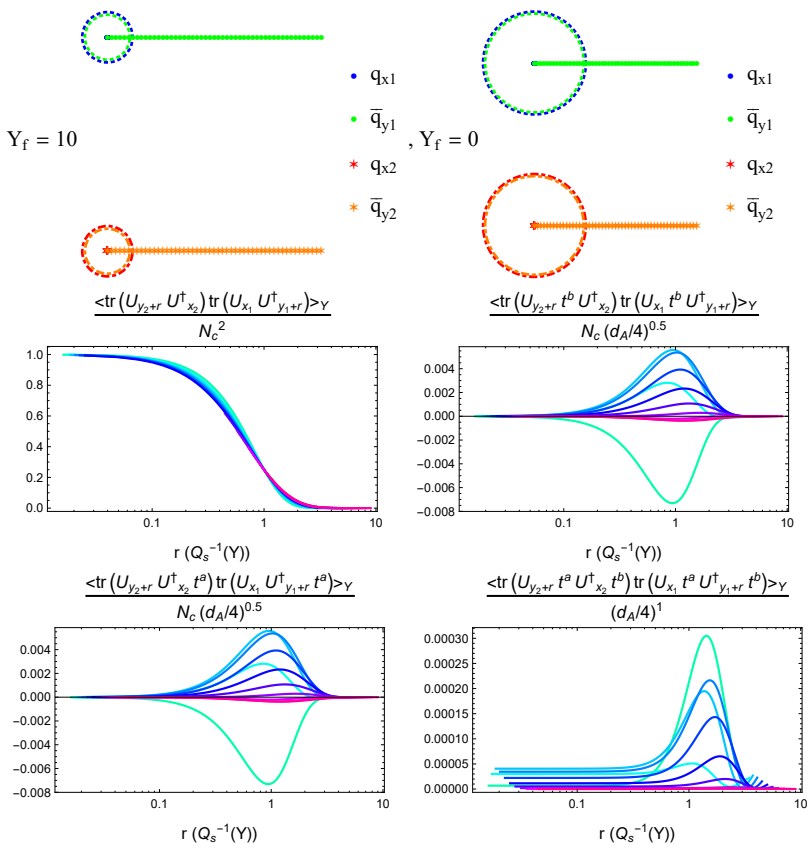

FIGURE 7.9: Particles arranged such that $x_1 = (0,1)$, $y_1 = (r,1)$, $x_2 = (0,-3)$ and $y_2 = (r,-3)$, in units of GeV^{-1}. Green is the lowest rapdity, with each line a rapidity of one greater until the magenta line with largest rapidty $Y = 10$. Scaled in Q_s.

There is non-trivial behaviour in bottom-right and off-diagonal correlators! To see how this behaviour arises, we need to examine its corresponding correlator and how it relates to the gluon-gluon dipole.

In this section we will justify the behaviour of the bottom right component of equation (7.7), $\frac{1}{N_c(N_c^2-1)}$  , that appears in figures 7.8 and 7.9. The four particles are arranged in two dipole pairs where the intra-dipole distance, r, increased. This situation is then compared with one where the inter-dipole distance, which we label l, is increased. Diagrammatically:

$$\left\langle \mathrm{tr}(U_{x_2+r} t^a U^\dagger_{x_2} t^b)\mathrm{tr}(U_{x_1} t^a U^\dagger_{x_1+r} t^b) \right\rangle = \frac{1}{N_c(N_c^2-1)} \quad r \; l \; r \,, \tag{7.12}$$

with $x_2 = x_1 + l$. This correlator has different behaviours as we change the size of r and l in relation to each other and in relation to the correlation length, $r_s = \frac{1}{Q_s}$. The behaviour can be summarized as follows:

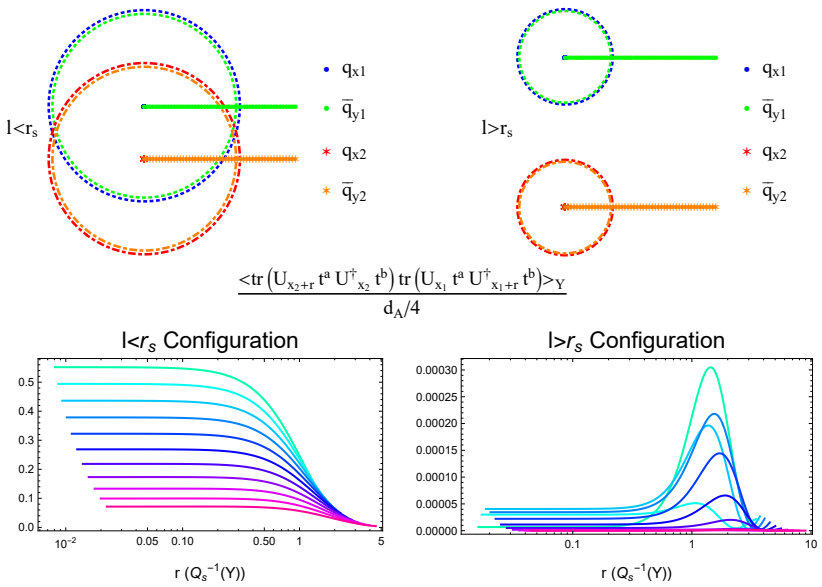

FIGURE 7.10: Two different configurations of $q\bar{q}$ dipoles, with the intra-dipole distance, r, increasing. The first configuration, as figure 7.8, with the inter-dipole distance $l < r_s$ and the second configuration, as figure 7.9, with $l > r_s$. Green is the lowest rapdity, with each line a rapidity of one greater until the magenta line with largest rapidty $Y = 10$. Scaled in Q_s.

One can recognize that the behaviour of this correlator arises from a transition from the $r \ll l$ regime to the $r \approx l$ regime and then to the $r > r_s$ regime. These transitions also happen under the consideration of whether $l < r_s$ or $l > r_s$.

When $r \ll l$, we can apply the definition of the adjoint representation (3.60) to rewrite this four-point correlator as a gluon-gluon dipole correlator with separation l:

$$\left\langle \mathrm{tr}(U_{x_1+l} t^a U^\dagger_{x_1+l} t^b) \mathrm{tr}(U_{x_1} t^a U^\dagger_{x_1} t^b) \right\rangle = 4 \left\langle \widetilde{U}^{ab}_{x_1} \widetilde{U}^{\dagger\, ba}_{x_1+l} \right\rangle , \tag{7.13}$$

or, diagrammatically,

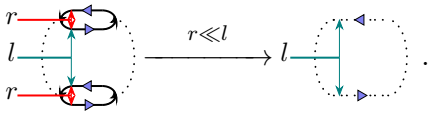

. (7.14)

This explains the small r behaviour of figure 7.10. In this domain the correlator behaves like a gg-dipole. Thus when l is smaller than r_s we expect $\mathcal{O}(0.1)$ behaviour. But when $l > r_s$, we expect the gg-dipole to vanish.

On the other end, when r is much larger than r_s, each of the $q\bar{q}$ dipoles, instead of approximating adjoint Wilson lines, want to vanish. This explains the large r behaviour of  , as it vanishes for large r

In the intermediate range, where r is $\mathcal{O}(r_s)$, the two $q\bar{q}$ dipoles turn on and we have non-trivial behaviour. For large l, the gluon exchange component of the correlator is negligible, but the $q\bar{q}$ dipole component is not. This is why, in the $l > r_s$ configuration we see the correlator suddenly turn on before shrinking back to zero again. Paying

attention to the size of this non-trivial behaviour, we see that largest this correlator can be is for the lowest rapidity curve, and even then it reaches a maximum of 3×10^{-4}. In this regime, this is large compared to the gluon dipole, as said dipole vanishes here. However, in the $l < r_s$, the gg-dipole is much larger than this, of size 5×10^{-1}. Therefore the effects of the $q\bar{q}$ dipoles would be invisible in comparison. Instead we observe a smooth transition from the $r \ll l$ region to the $r > r_s$ boundary without any apparent turning points.

7.3 Isolating the Dipoles

We can also consider situation where we pull the two dipoles apart from each other.

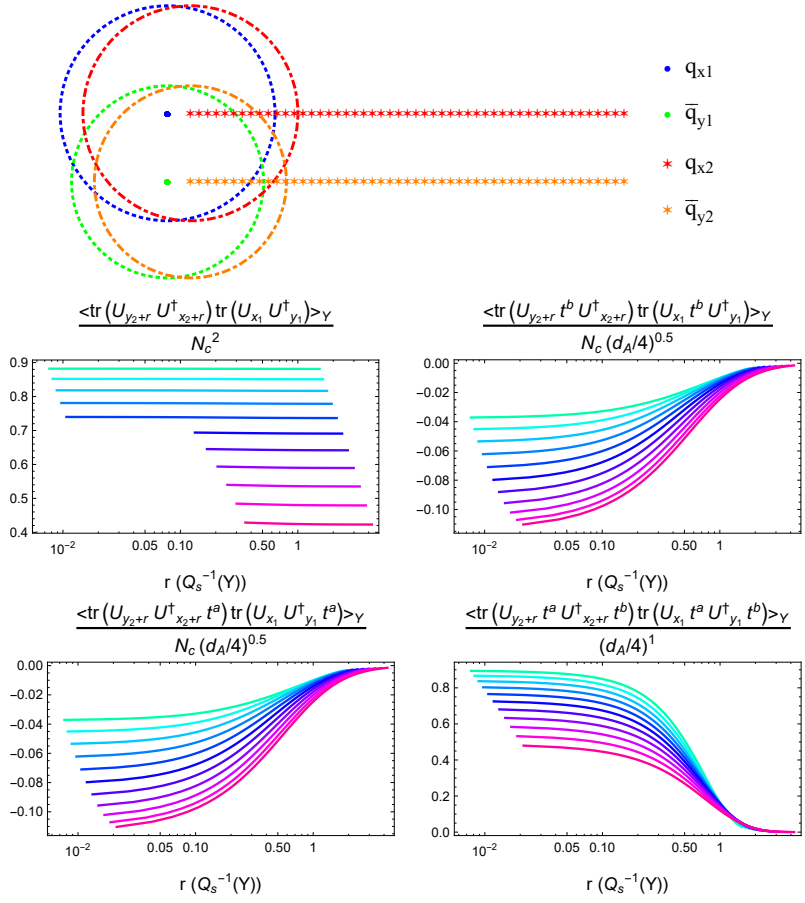

FIGURE 7.11: Particles arranged such that $x_1 = (0, 0.3)$, $y_1 = (0, 0)$, $x_2 = (0.1 + r, 0.3)$ and $y_2 = (0.1 + r, 0)$, in units of GeV^{-1}. Green is the lowest rapdity, with each line a rapidity of one greater until the magenta line with largest rapidty $Y = 10$. Scaled in Q_s.

Of note, the top left correlator seems to stay roughly constant for each rapidity. This is because the correlator corresponds to the product of two dipoles. Now these dipoles are not communicating with each other via the exchange of a gluon or anything like that. Therefore the two dipoles have no way to communicate their inter-dipole distance and the correlator should be independent of r. We can also observe what happens when

we increase the intra-dipole distance. We can illustrate this as

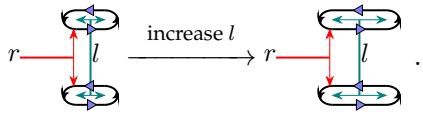

(7.15)

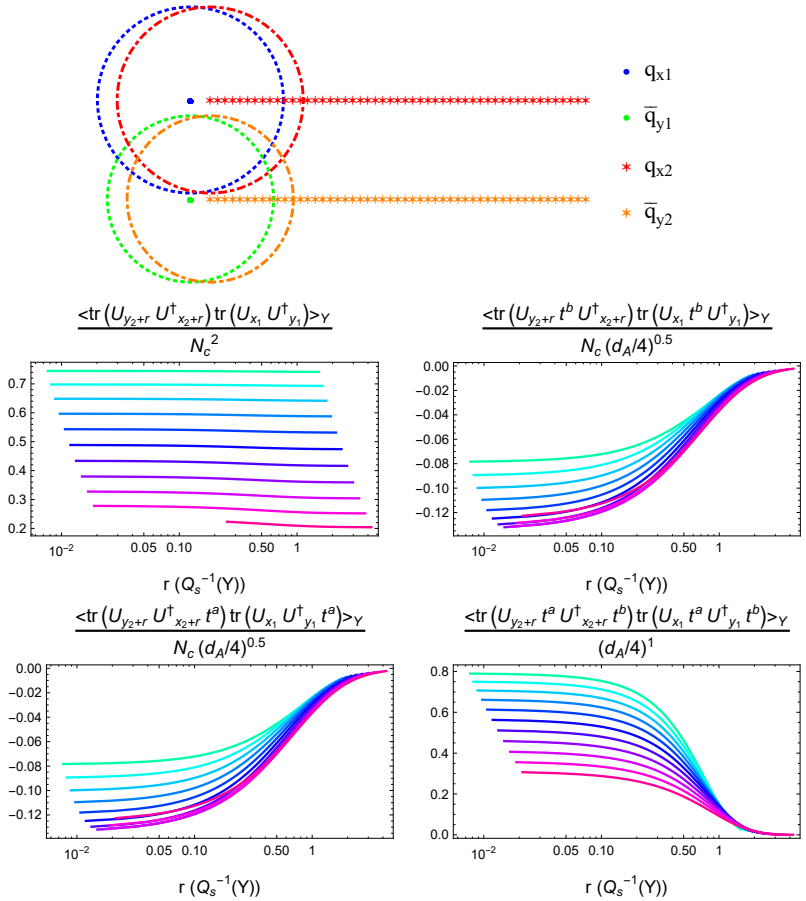

FIGURE 7.12: Particles arranged such that $x_1 = (0, 0.3)$, $y_1 = (0, -0.2)$, $x_2 = (0.1 + r, 0.3)$ and $y_2 = (0.1 + r, -0.2)$, in units of GeV^{-1}. Green is the lowest rapdity, with each line a rapidity of one greater until the magenta line with largest rapidty $Y = 10$. Scaled in Q_s.

Figure 7.12 shows what happens when the intra-dipole distance is on the cusp of the correlation length. We see peculiar behaviour in the largest rapidities. As the rapidity increases from the initial condition in the off-diagonal terms, the curves are depressed, until a turning point is reached at the largest rapidities and the curves reverse direction. This makes sense, since the circles of influence are drawn using the correlation length of the largest rapidity. If we show the circle of influence for the low rapidity curves, we will see these circles are much larger, as in 7.13

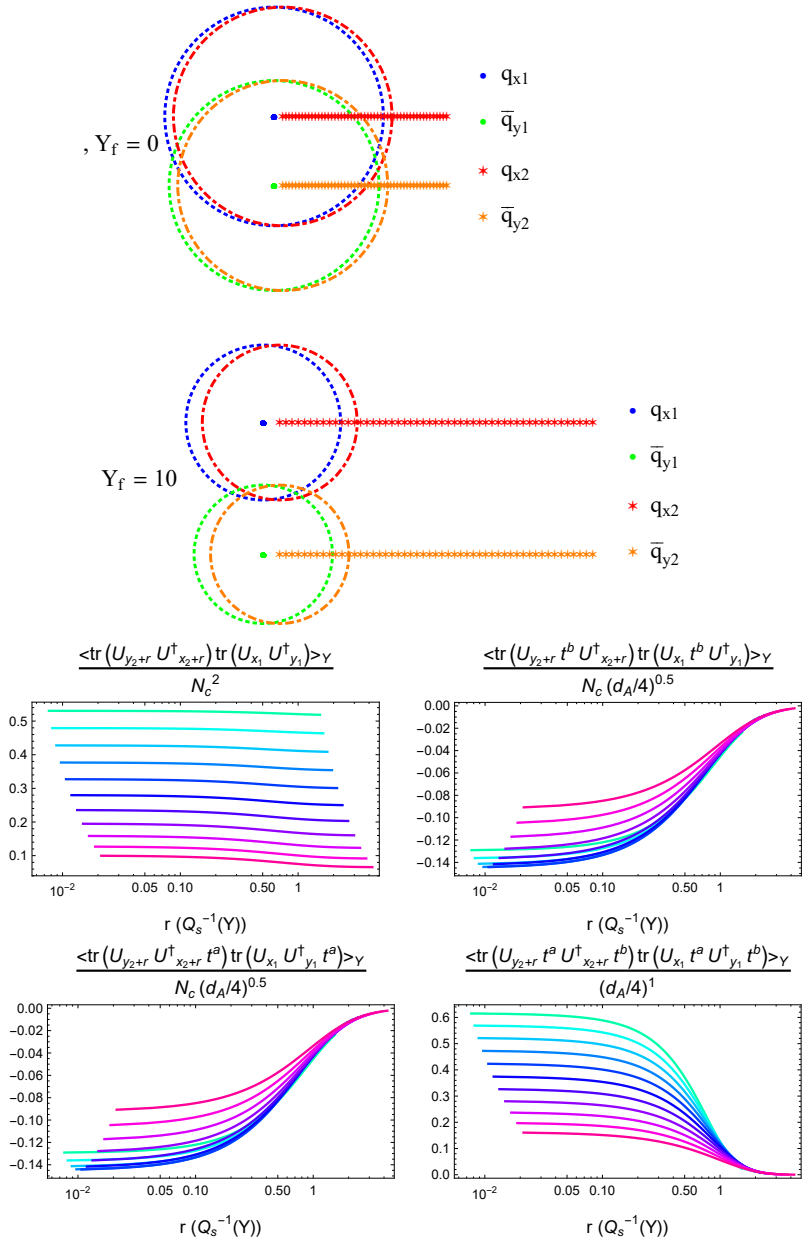

FIGURE 7.13: Particles arranged such that $x_1 = (0, 0.3)$, $y_1 = (0, -0.5)$, $x_2 = (0.1 + r, 0.3)$ and $y_2 = (0.1 + r, -0.5)$, in units of GeV^{-1}. Green is the lowest rapdity, with each line a rapidity of one greater until the magenta line with largest rapidty $Y = 10$. Scaled in Q_s.

In figure 7.13 we see the same off diagonal behaviour as figure 7.12, but even more pronounced, as only the lowest rapidity curves correspond to particles that are within the correlation length of each other.

7.4 Factorization of Correlators

The situation explored in figures 7.7, 7.8 and 7.9 is an excellent opportunity to analyse the degree to which the averaging procedure, $\langle ... \rangle$ factorizes. By factorizing we mean

the degree to which

$$\left\langle \mathrm{tr}(U_{\boldsymbol{x_1}} U^{\dagger}_{\boldsymbol{y_1}}) \right\rangle \left\langle \mathrm{tr}(U_{\boldsymbol{x_2}} U^{\dagger}_{\boldsymbol{y_2}}) \right\rangle \stackrel{?}{=} \left\langle \mathrm{tr}(U_{\boldsymbol{x_1}} U^{\dagger}_{\boldsymbol{y_1}}) \mathrm{tr}(U_{\boldsymbol{x_2}} U^{\dagger}_{\boldsymbol{y_2}}) \right\rangle \tag{7.16}$$

is true. This was discussed in section 4.8, with the result being that factorization is possible for a slightly different correlator and only up to order $\mathcal{O}\frac{1}{N_c^2}$. We have no argument that this procedure generalizes to all correlators, but, regardless, this doesn't stop one from trying and seeing if the result remains reasonable, such as in [25]. Hence we will investigate to what degree factorization is violated in the Gaussian truncation. We compare the particle configurations 7.7 and 7.9. We consider only the correlator constructed out of the average of the product of two dipoles, (7.16), comparing to the product of the averages of two dipoles.

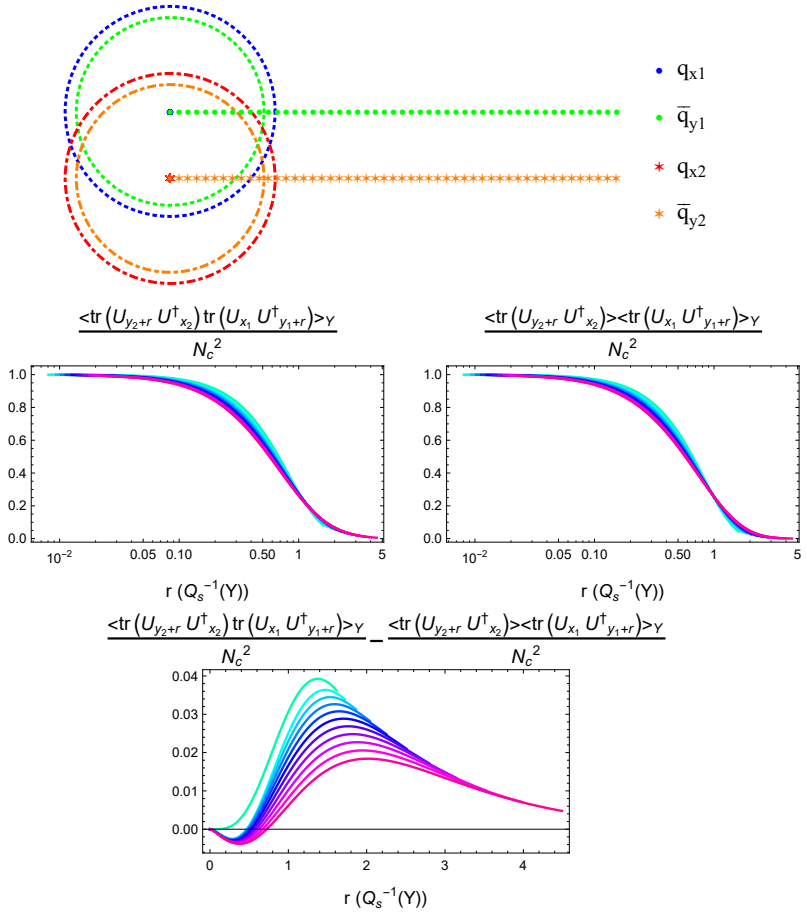

FIGURE 7.14: Particles arranged such that $x_1 = (0,1)$, $y_1 = (r,1)$, $x_2 = (0,0.7)$ and $y_2 = (r,0.7)$, in units of GeV^{-1}. The correlators considered are the average of of the product of two dipoles and the product of the average of two dipoles. The bottom graph is the difference between these two and illustrates the degree to which the factorization is violated. Green is the lowest rapdity, with each line a rapidity of one greater until the magenta line with largest rapidty $Y = 10$. Scaled in Q_s.

Figure 7.14 illustrates the factorization error of two dipoles that are close together. It is unsurprising that, indeed, the correlators fail to full factorize since the two dipoles

should be themselves correlated. In other words, treating the two dipoles as factorizable amounts to treating them as uncorrelated: we simply square a single dipole and ignore information conferred by the presence of a second dipole. What is worth noting is that the coincident limit is satisfied by both expressions and thus they agree at $r = 0$ for all rapidities. It is also unsurprising that they begin to agree at large r, since both dipoles should go to zero in this limit.

Next, let's look at how the factorization error changes when pull the two dipoles far from each other. When the two dipoles are far from each other, they should become decorrelated and factorization should be more valid. Figure 7.15 demonstrates this.

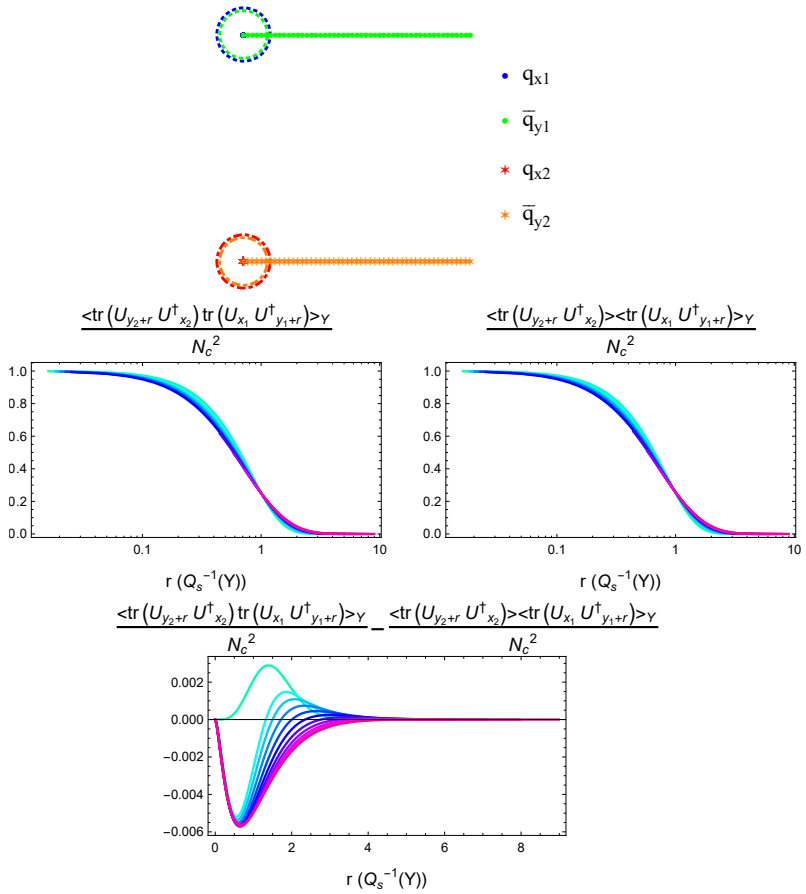

FIGURE 7.15: Particles arranged such that $x_1 = (0, 1)$, $y_1 = (r, 1)$, $x_2 = (0, -3)$ and $y_2 = (r, -3)$, in units of GeV^{-1}. The correlators considered are the average of of the product of two dipoles and the product of the average of two dipoles. The bottom graph is the difference between these two and illustrates the degree to which the factorization is violated. Green is the lowest rapdity, with each line a rapidity of one greater until the magenta line with largest rapidty $Y = 10$. Scaled in Q_s.

Indeed the factorization violation has decreased by an order of magnitude.

7.5 The Importance of Path Dependence: Comparison with the Rigid Exponentiation

An aspect of this field that makes calculating the evolution of these correlators difficult is the path-ordering dependence of the matrix amplitude. It is worth trying to tease out how path ordering affects the evolution by comparing to a numerical simulation where path ordering is neglected. From this comparison one could identify features that are lost or gained through including path-ordering, or whether the evolution is accelerated by its presence. The amplitude matrix where path-ordering is neglected is is called the rigid exponential and was considered in [18], however comparing the numerics of the rigid exponentiation to the full Gaussian truncation hasn't been done before.

To investigate the difference between these two cases, we need some manner of expressing the evolution of $\langle A \rangle$ while dropping path dependence. Dropping path dependence is equivalent to saying that we may integrate M first, then perform the matrix exponential in equation (5.4).

Integration just replaces each G with $\mathcal{G}$, as per equation (5.13). For clarity's sake, let's relabel the components of the integrated M:

$$a_Y := \int_{Y_0}^{Y} dY\ M^{11}(Y) = \frac{\left(N_c^2-1\right)}{2N_c}\left(\mathcal{G}_Y\left(x_1,y_1\right)+\mathcal{G}_Y\left(x_2,y_2\right)\right), \tag{7.17a}$$

$$\begin{aligned} b_Y := \int_{Y_0}^{Y} dY\ M^{22}(Y) =& \frac{1}{2N_c}\left(N_c^2\mathcal{G}_Y\left(x_1,y_2\right)+N_c^2\mathcal{G}_Y\left(x_2,y_1\right)+2\mathcal{G}_Y\left(x_1,x_2\right)-\mathcal{G}_Y\left(x_1,y_1\right)\right. \\ & \left. -2\mathcal{G}_Y\left(x_1,y_2\right)-2\mathcal{G}_Y\left(x_2,y_1\right)-\mathcal{G}_Y\left(x_2,y_2\right)+2\mathcal{G}_Y\left(y_1,y_2\right)\right), \end{aligned} \tag{7.17b}$$

$$\begin{aligned} c_Y := \int_{Y_0}^{Y} dY\ M^{12}(Y) &= \int_{Y_0}^{Y} dY\ M^{21}(Y) \\ &= \frac{\sqrt{N_c^2-1}}{2N_c}\left(-\mathcal{G}_Y\left(x_1,x_2\right)+\mathcal{G}_Y\left(x_1,y_2\right)+\mathcal{G}_Y\left(x_2,y_1\right)-\mathcal{G}_Y\left(y_1,y_2\right)\right). \end{aligned} \tag{7.17c}$$

The matrix exponential of a symmetric matrix is known to be

$$\begin{aligned} \left\langle A^{Rigid}\right\rangle_Y &= \exp\begin{pmatrix} a_Y & c_Y \\ c_Y & b_Y \end{pmatrix} = e^{-\frac{1}{2}(a_Y+b_Y)} \\ &\times \begin{pmatrix} \cosh\left(\frac{1}{2}\sqrt{\Delta_Y}\right)-\frac{a_y-b_Y}{\sqrt{\Delta_Y}}\sinh\left(\frac{1}{2}\sqrt{\Delta_Y}\right) & -2\frac{c_Y}{\sqrt{\Delta_Y}}\sinh\left(\frac{1}{2}\sqrt{\Delta_Y}\right) \\ -2\frac{c_Y}{\sqrt{\Delta_Y}}\sinh\left(\frac{1}{2}\sqrt{\Delta_Y}\right) & \cosh\left(\frac{1}{2}\sqrt{\Delta_Y}\right)+\frac{a_y-b_Y}{\sqrt{\Delta_Y}}\sinh\left(\frac{1}{2}\sqrt{\Delta_Y}\right) \end{pmatrix}, \end{aligned} \tag{7.18}$$

where

$$\Delta_Y := (a_Y-b_Y)^2+4c_Y^2. \tag{7.19}$$

With equation (7.18), we can numerically compute the rigid exponentiation and compare it to the full Gaussian truncation. It is worth noting, before we look at the results, what we might expect about the comparative behaviour. The way we have emulated the path integral in our numerics for the Gaussian truncation is to break the integral into small pieces, where each piece is just the rigid exponentiation. This implies that for low rapidities they should be similar, with the difference growing with rapidity. More importantly the components that encapsulate the coincident limits of the various Wilson line correlators are the gluon exchange functions: $\mathcal{G}, G$. Since the rigid exponentiation unabashedly preserves these terms, we should see the same limiting behaviour when compared to the full Gaussian truncation numerics. The differences, if there are any, should lie between the limiting cases. In figure 7.16 we consider the same quark configuration as 7.6, but compare the Gaussian truncation with the rigid exponentiation.

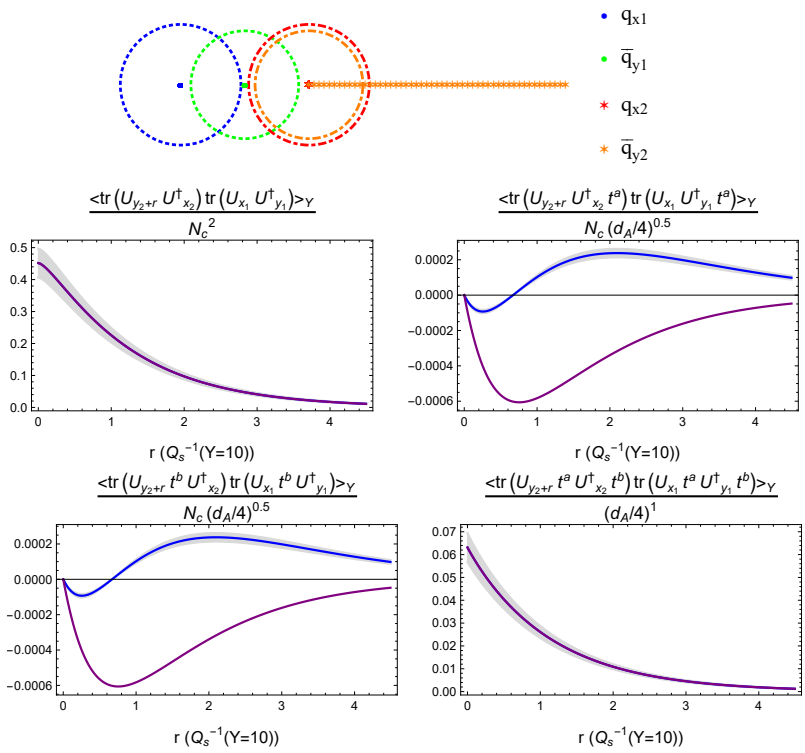

FIGURE 7.16: As 7.6, but with rigid exponentiation comparison comparison. The blue line corresponds to the Gaussian truncation result. The purple line corresponds to the rigid exponentiation. The grey bands are the $\pm 10\%$ intervals of the full Gaussian truncation result.

We see that we obtain the same limiting behaviour as expected, the off-diagonal terms go to zero for $r = 0$ and all the correlators go to zero for large r. Surprisingly, for the diagonal terms, the two curves are nearly indistinguishable. Interestingly, for the off-diagonal terms, the behaviour of the two curves are remarkably different.

The first point about the diagonal terms being unable to distinguish between the the rigid exponentiation and the full Gaussian truncation is explainable by the size of the off diagonal terms. Under path-ordering, what stops the diagonal elements from trivially exponentiating is that information is fed in from the off-diagonal terms. However, since the off-diagonal terms here are three orders of magnitude smaller than the

diagonal terms, this correlator matrix is effectively diagonal and there should be no difference between path-ordering and not. This logic doesn't apply to trying to find the precise value of the off diagonal terms.

For these terms we see that path-ordering makes a critical difference. The rigid exponentiation doesn't even have the same features as the full Gaussian truncation - there isn't a sign change. At equation (7.11), we argued for the allowance of this sign change. Does the rigid exponentiation also allow for this? The only factor in the rigid exponentiation that allows for a sign change in the off-diagonal terms is c_Y. In trying to find quark configurations that introduce a sign change, we find that we need to pull the two $q\bar{q}$ dipoles further apart, as demonstrated in 7.17

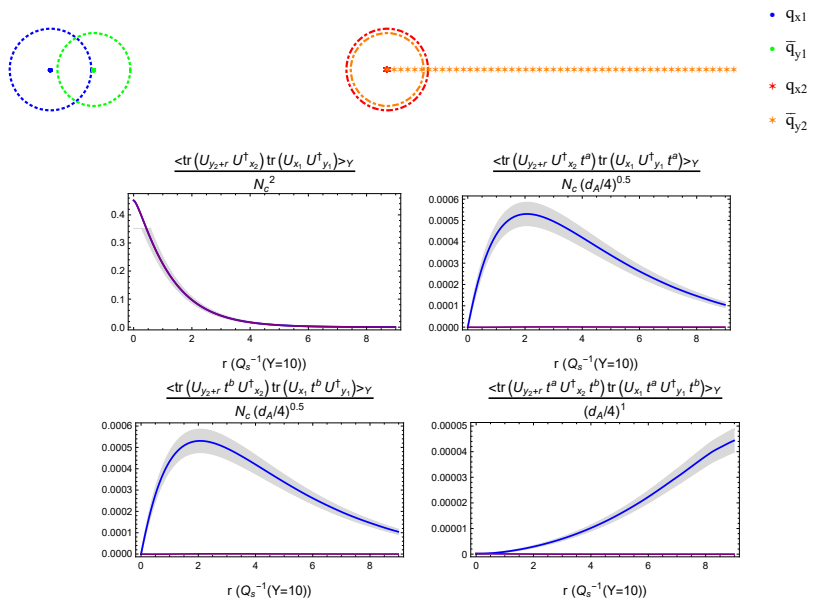

FIGURE 7.17: Two $q\bar{q}$ dipoles seperated by a large distance. The second dipole has its quark and anti-quark coincident and we plot how the correlator changes as these particles are pulled apart. The blue line corresponds to the Gaussian truncation result. The purple line corresponds to the rigid exponentiation. The grey bands are the $\pm 10\%$ intervals of the full Gaussina truncation result.

However, the size of this correlator is negligible compared to the one obtained from the Gaussian truncation, but the sign change is still present. We can plot just the result of the rigid exponentiation to see what's going on better in figure 7.18

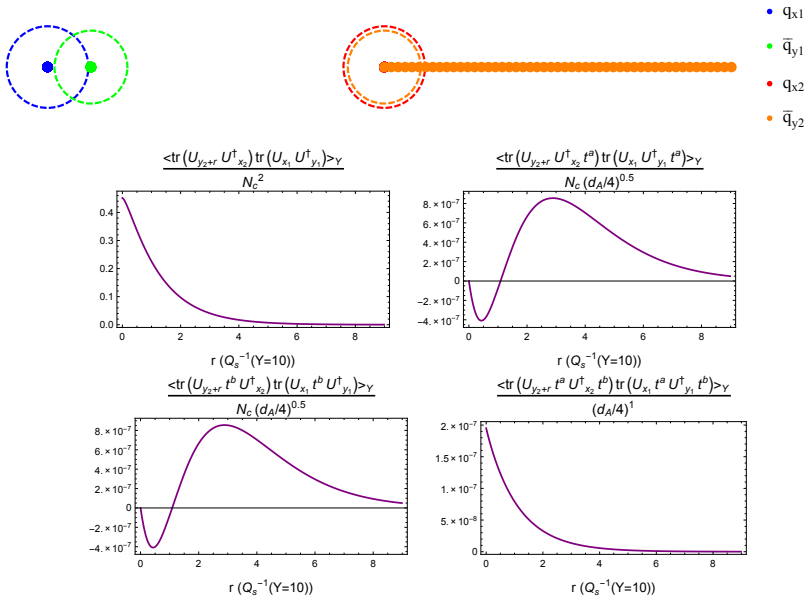

FIGURE 7.18: Two $q\bar{q}$ dipoles seperated by a large distance. The second dipole has its quark and anti-quark coincident and we plot how the correlator changes as these particles are pulled apart. The purple line corresponds to the rigid exponentiation.

Indeed the sign change is present.

7.6 Comparison with the large N_c limit

One of the primary motivations for exploring the Gaussian truncation is to try and go beyond the large N_c limit. In this limit, sub-leading in N_c terms are neglected in order to close the evolution equation of Wilson line correlators. For example, M (7.9) is reduced to

$$M(Y) \xrightarrow{N_c\to\text{large}} \left\langle \begin{pmatrix} -\frac{1}{2}N_c\,(G(x_1,y_1)-G(x_2,y_2)) & 0 \\ 0 & -\frac{1}{2}N_c\,(G(x_1,y_2)-G(x_2,y_1)) \end{pmatrix} \right\rangle \tag{7.20}$$

In particular, the large N_c limit provides no avenue to access the off diagonal terms. In figure [7.11] we compare the Gaussian truncation to the large N_c limit.

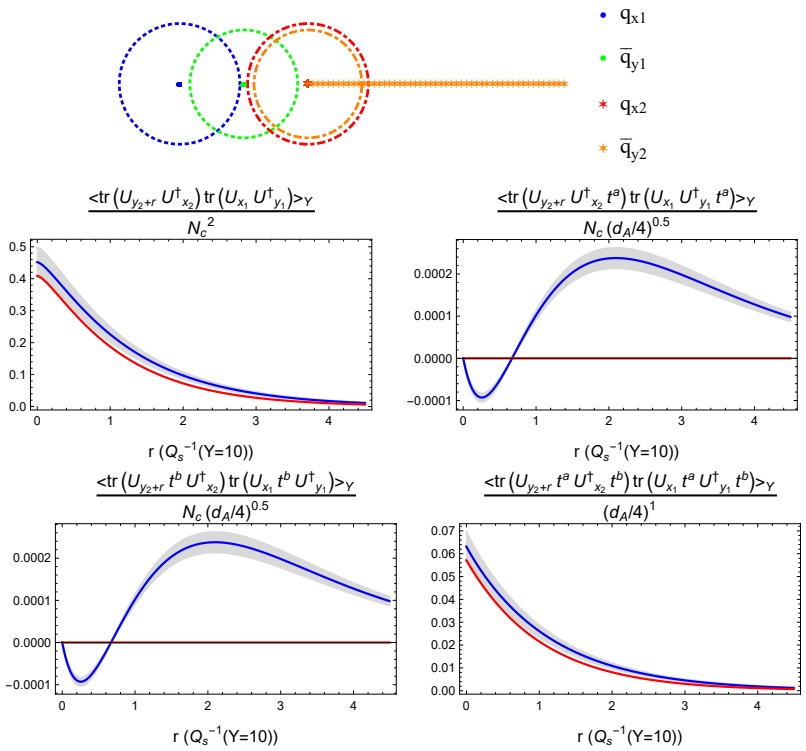

FIGURE 7.19: As 7.6, but with Large N_c limit comparison. The blue line corresponds to the Gaussian truncation result. The red line corresponds to the Gaussian truncation applied to the correlators in the large N_c limit. The grey bands are the $\pm 10\%$ intervals of the full Gaussina truncation result.

We see that the large N_c limit gives a trivial zero result for the off-diagonal terms. For the diagonal terms, we see an order ~10% difference between it and our Gaussian truncation result at larger r.

7.7 Numerical Stability of the Gaussian Truncation

Without any analytical statement about accuracy of the Gaussian truncation, we need some other method to test the validity of our numerical scheme. We can at least check whether our numerical scheme converges, i.e. that decreasing the step-size of the rapidity evolution doesn't radically alter the result of the numerics.

Currently, we are using a rapidity step-size of $\Delta Y = 0.1$. In order to test stability of our numerical method, we can plot one of the quark configurations, evolving to to the same rapidity, but using different resolutions. We can then compare the different curves and infer how changing the resolution changes the behaviour of our correlators. We will do this for the same quark configuration as figure 7.6. The result is figure 7.20.

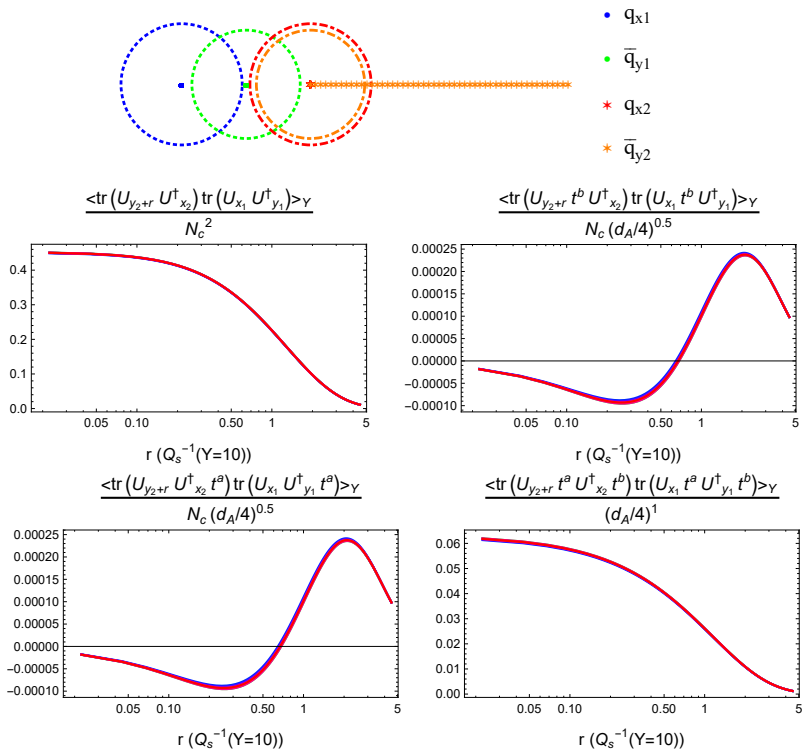

FIGURE 7.20: As 7.6, but with different resolution comparisons. The final rapidity is at $Y = 10$. The orange line corresponds to a rapidity step size of $\Delta Y = 0.1$. The red line corresponds to rapidity step size of $\Delta Y = 0.01$. The colours in between correspond to step sizes of $\Delta Y = 0.09, 0.08, ..., 0.02$.

Numerical stability seems excellent. For the diagonal terms we see hardly any deviation from the highest resolution curve. Remember that we can infer convergence if the deviations from the highest resolution curve by the other high resolution curves is small. For the off diagonal terms there is some deviation between the resolutions, but it is small. Furthermore, the deviations do not have a preferred direction. The highest resolution curve is in between the other curves, suggesting that increasing the resolution endlessly won't continuously push the curve in a particular direction. It seems to have mostly settled.

From this we can conclude that our numerical method appears to be stable.

Chapter 8

Medium-induced gluon radiation: an application of the Gaussian truncation

In [26], the authors present a calculation for the medium-induced gluon radiation in hard forward part scattering in the saturation formalism. They discuss a number of contexts in which this calculation becomes extremely relevant, for example, this induced gluon spectrum can be interpreted as the energy-loss associated with the interaction with cold, nuclear matter. This serves as an important background for studying energy loss in hot nuclear matter, one of the primary probes used to study the quark-gluon-plasma [27].

The relevance of this calculation to this thesis, is that the induced gluon spectrum can be formulated in terms of Wilson lines and is a prime candidate for applying the Gaussian truncation. The authors of [26] do not present any numerical calculations, but show that their analytic calculations reproduce properties that were derived using the opacity expansion. Not only does this give credence to the saturation formalism, but investigating whether these properties can be reproduced would serve as evidence for the success or failure of the Gaussian truncation.

In this section we will re-derive the induced gluon spectrum and demonstrate how one may apply the Gaussian truncation to numerically compute it as well. To start things off, we state the context of the problem. We consider a proton-nucleus (pA) collision, where a parton, a, from the proton scatters off the nucleus target, A, and hadronizes in the forward region, $a(p_0) + \mathrm{A} \to a(p) + \mathrm{X}$. This is in the *forward* and *hard* scattering limit, i.e. where p^+ is arbitrarily large and $|\boldsymbol{p}| \gg Q_s$, the saturation scale.

This is compared to the process where the parton emits a gluon before hadronizing, $a(p_0) + \mathrm{A} \to a(p) + g(p') + \mathrm{X}$. The goal is to compare these to and infer how much of the above cross-section is reduced by the emission of an extra gluon. Considering the *soft* gluon emission limit

$$z := \frac{p'^+}{p_0^+} \ll 1, \tag{8.1}$$

the soft radiation energy spectrum is defined as

$$z\frac{dI_A}{dz} = p'^+\frac{dI_A}{dp'^+} = \frac{\frac{d\sigma(a+\mathrm{A}\to a+g+\mathrm{X})}{dydy'd2\boldsymbol{p}}}{\frac{d\sigma(a+\mathrm{A}\to a+\mathrm{X})}{dyd^2\boldsymbol{p}}} = \frac{\frac{d\sigma(\mathrm{p}+\mathrm{A}\to a+g+\mathrm{X})}{dydy'd2\boldsymbol{p}}}{\frac{d\sigma(\mathrm{p}+\mathrm{A}\to a+\mathrm{X})}{dyd^2\boldsymbol{p}}} \tag{8.2}$$

where $y = \ln(p^+/p)$ is the parton rapidity, and $d\sigma(\text{p+A} \to ...)$ with the distribution of parton a in the proton $f_{a/\text{p}}(x_\text{p}, \mu_F^2)$, with $x_\text{p} = p_0^+/o_\text{p}^+$, p_p is longitudinal momentum of the proton and μ_F the factorization scale. The reduction that arises purely from the presence of the nucleus is the *medium-induced* spectrum, and is calculated from the difference of 8.2 between a nucleus and proton target,

$$z\frac{dI}{dz}\bigg|_{ind} := z\frac{dI_\text{A}}{dz} - z\frac{dI_\text{p}}{dz}. \tag{8.3}$$

It is important to state that the only difference between the pA and pp pictures here, in the saturation regime, is the saturation scale of the target. The way to understand this is to see that a nucleon, in the framework we've been using thus far, merely induces a colour rotation of the projectile parton. Hence the use of Wilson lines. The amount of rotation is dependent on the saturation scale of the nucleon, but adding more nucleons just instigates further colour rotations. This can be emulated performing the calculation for a single nucleon (proton) interaction, but increasing the saturation scale. We will cover this in more detail in the appendix on the nuclear saturation scale, C.

The forward production cross section has been derived for the quark case, $a = q$ [28] and the gluon case, $a = g$ [29]. For simplicity's sake, we will only talk about the quark case. The eikonal part of the cross section can be represented with the following bird-track diagrams

$$\frac{1}{d_f C_f}$$ 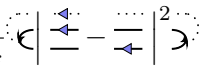 (8.4)

The solid lines correspond to quarks and the dotted line to a gluon. A blue arrow indicates the presence of a Wilson line, while the lack of arrow means a trivial Wilson line, the Kronecker delta. Equation (8.4) is a partonic T-matrix element, where we subtract from the amplitude for an eikonal quark to emit an eikonal gluon the amplitude where an eikonal quark does not emit an eikonal gluon. Let us remember that eikonal partons are what pick up Wilson lines. The gluon line has transverse coordinate $\boldsymbol{x}$ and the top quark has coordinate $\boldsymbol{b}$. By conservation of momentum, the remaining (bottom) quark has coordinate $\boldsymbol{v} = z\boldsymbol{x} + (1-z)\boldsymbol{b}$, where z is the fraction of the momentum carried by the gluon. In the complex conjugate, we use primed coordinates to distinguish between the amplitude and conjugate-amplitude. This distinction will fall away as we trigger Dirac deltas in these coordinate when we perform the full calculation.

The cross section then reads

$$\begin{aligned}
&\frac{d\sigma(\text{pA} \to qg + \text{X})}{dy dy' d^2\boldsymbol{p} d^2\boldsymbol{p}'} = K\frac{\alpha_s}{(2\pi)^6} 4C_f \\
&\times \int_{\boldsymbol{x}}\int_{\boldsymbol{x}'}\int_{\boldsymbol{b}}\int_{\boldsymbol{b}'} e^{-i\boldsymbol{p}\cdot(\boldsymbol{b}-\boldsymbol{b}')-i\boldsymbol{p}'\cdot(\boldsymbol{x}-\boldsymbol{x}')}\frac{(\boldsymbol{x}-\boldsymbol{b})\cdot(\boldsymbol{x}'-\boldsymbol{b}')}{(\boldsymbol{x}-\boldsymbol{b})^2(\boldsymbol{x}'-\boldsymbol{b}')^2} \\
&\times \Big\{S^{(4)}[\boldsymbol{b},\boldsymbol{x},\boldsymbol{b}',\boldsymbol{x}'] + S^{(2)}[\boldsymbol{v},\boldsymbol{v}'] - S^{(3)}[\boldsymbol{b},\boldsymbol{x},\boldsymbol{v}'] - S^{(3)}[\boldsymbol{b}',\boldsymbol{x}',\boldsymbol{v}]^*.\Big\}
\end{aligned} \tag{8.5}$$

K is a prefactor that cancels in the ratio (8.2). The full form of it can be found in [26], equation (2.5).We have also pre-emptively implemented the $z \ll 1$ limit, reducing factors like $(1-z)$ to 1 and such. The four S terms exactly correspond to terms obtained

in the expansion of (8.4). Diagrammatically, they can be written as

$$S^{(4)}[\boldsymbol{b},\boldsymbol{x},\boldsymbol{b}',\boldsymbol{x}'] = \frac{1}{d_f C_f}$$ 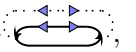 ,

$$S^{(2)}[\boldsymbol{v},\boldsymbol{v}'] = \frac{1}{d_f C_f}$$ 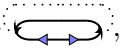 ,

$$S^{(3)}[\boldsymbol{b},\boldsymbol{x},\boldsymbol{v}'] = \frac{1}{d_f C_f}$$ 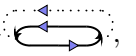 ,

$$S^{(3)}[\boldsymbol{b}',\boldsymbol{x}',\boldsymbol{v}]^* = \frac{1}{d_f C_f}$$ 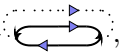 ,

with their full forms given by

$$S^{(4)}[\boldsymbol{b},\boldsymbol{x},\boldsymbol{b}',\boldsymbol{x}'] = \frac{1}{d_f C_f}\left\langle \mathrm{tr}\left(t^c U_{\boldsymbol{b}} U^\dagger_{\boldsymbol{b}'} t^d\right)[\widetilde{U}_{\boldsymbol{x}}\widetilde{U}^\dagger_{\boldsymbol{x}'}]^{cd}\right\rangle, \tag{8.6}$$

$$S^{(2)}[\boldsymbol{v},\boldsymbol{v}'] = \frac{1}{d_f}\left\langle \mathrm{tr}\left(U_{\boldsymbol{v}} U^\dagger_{\boldsymbol{v}'}\right)\right\rangle, \tag{8.7}$$

$$S^{(3)}[\boldsymbol{b},\boldsymbol{x},\boldsymbol{v}'] = \frac{1}{d_f C_f}\left\langle \mathrm{tr}\left(t^c U_{\boldsymbol{b}} t^d U^\dagger_{\boldsymbol{v}'}\right)[\widetilde{U}_{\boldsymbol{x}}]^{cd}\right\rangle, \tag{8.8}$$

$$S^{(3)}[\boldsymbol{b}',\boldsymbol{x}',\boldsymbol{v}]^* = \frac{1}{d_f C_f}\left\langle \mathrm{tr}\left(U_{\boldsymbol{v}} t^c U^\dagger_{\boldsymbol{b}'} t^d\right)[\widetilde{U}^\dagger_{\boldsymbol{x}}]^{cd}\right\rangle. \tag{8.9}$$

We can start simplifying (8.4). Integrating both sides with respect $\boldsymbol{p}'$ creates a Dirac delta in $\boldsymbol{x}-\boldsymbol{x}'$. This leaves us free to perform the $\boldsymbol{x}'$ integral. The main consequence of this is simplifying $S^{(4)}$. The adjoint Wilson lines cancel into a Kronecker delta in cd. Using the fact that $t^c t^d \delta^{cd} = t^c t^c = C_f$, $S^{(4)}[\boldsymbol{b},\boldsymbol{x},\boldsymbol{b}',\boldsymbol{x}']$ simplifies into $S^{(2)}[\boldsymbol{b},\boldsymbol{b}']$. We also write $S^{(3)}$ plus its complex conjugate as twice the real part. We obtain

$$\begin{aligned}\frac{d\sigma(\mathrm{pA}\to qg+\mathrm{X})}{dyd y' d^2\boldsymbol{p}} = K\frac{\alpha_s}{(2\pi)^4}4C_f\int_{\boldsymbol{x}}\int_{\boldsymbol{b}}\int_{\boldsymbol{b}'} e^{-i\boldsymbol{p}\cdot(\boldsymbol{b}-\boldsymbol{b}')}\frac{(\boldsymbol{x}-\boldsymbol{b})\cdot((\boldsymbol{x}-\boldsymbol{b}')}{(\boldsymbol{x}-\boldsymbol{b})^2(\boldsymbol{x}-\boldsymbol{b}')^2}\\ \times\left\{S^{(2)}[\boldsymbol{b},\boldsymbol{b}'] + S^{(2)}[\boldsymbol{v},\boldsymbol{v}'] - 2\mathrm{Re}S^{(3)}[\boldsymbol{b},\boldsymbol{x},\boldsymbol{v}']\right\}.\end{aligned} \tag{8.10}$$

The next step in simplification will be a change of variables, but before we do that, let us examine the elastic scattering (pA $\to$ q+X) cross section, so that we may simplify both in the same way.

This cross section is simply given as [30]

$$\frac{d\sigma(\mathrm{pA}\to q+\mathrm{X})}{dyd^2\boldsymbol{p}} = K\frac{1}{(2\pi)^2}\int_{\boldsymbol{b}}\int_{\boldsymbol{b}'} e^{-i\boldsymbol{p}\cdot(\boldsymbol{b}-\boldsymbol{b}')}\frac{1}{N_c}\left\langle \mathrm{tr}\left[(U_{\boldsymbol{b}}-1)(U^\dagger_{\boldsymbol{b}'}-1)\right]\right\rangle \tag{8.11}$$

Making use of the fact that single Wilson lines are not gauge invariant, their expectation value must be zero. This reduces the Wilson line content of (8.11) to

$$\begin{aligned}\left\langle \mathrm{tr}\left[(U_{\boldsymbol{b}}-1)(U^\dagger_{\boldsymbol{b}'}-1)\right]\right\rangle &= \left\langle \mathrm{tr}(U_{\boldsymbol{b}}U^\dagger_{\boldsymbol{b}'})\right\rangle - \langle \mathrm{tr}(U_{\boldsymbol{b}})\rangle - \left\langle \mathrm{tr}(U^\dagger_{\boldsymbol{b}'})\right\rangle + \langle \mathrm{tr}(1)\rangle\\ &= \left\langle \mathrm{tr}(U_{\boldsymbol{b}}U^\dagger_{\boldsymbol{b}'})\right\rangle - 0 - 0 + \langle \mathrm{tr}(1)\rangle\\ &= \left\langle \mathrm{tr}(U_{\boldsymbol{b}}U^\dagger_{\boldsymbol{b}'})\right\rangle + \langle \mathrm{tr}(1)\rangle.\end{aligned} \tag{8.12}$$

The $\langle \mathrm{tr}(1) \rangle$ term is a constant and turns into a Dirac delta in $\boldsymbol{p}$ when we evaluate the $\boldsymbol{b}$ and $\boldsymbol{b'}$ integrals in (8.11). Since we are working in the large $\boldsymbol{p}$ limit, we can neglect this Dirac delta, simplifying the correlator dependence of (8.11) to that of the humble dipole,

$$\frac{d\sigma(\mathrm{pA} \to q + \mathrm{X})}{dy d^2\boldsymbol{p}} = K \frac{1}{(2\pi)^2} \int_{\boldsymbol{b}} \int_{\boldsymbol{b'}} e^{-i\boldsymbol{p}\cdot(\boldsymbol{b}-\boldsymbol{b'})} \frac{1}{N_c} S^{(2)}[\boldsymbol{b}, \boldsymbol{b'}]. \tag{8.13}$$

Now we are poised to simplify the coordinate dependence of both cross-sections in one fell swoop. We recognize, as argued in [26], that at large p the target can be treated as having infinite transverse size. This implies that the interaction of to disparate Wilson lines is homogeneous in the transverse plane and the coordinate dependence of $S^{(2)}[\boldsymbol{b}, \boldsymbol{b'}]$ can be identified as $S^{(2)}[|\boldsymbol{b'} - \boldsymbol{b}|]$ - it depends only on the relative distance. With that in mind we make the following substitutions: $\boldsymbol{b'} - \boldsymbol{b} \to \boldsymbol{r}$ and $\boldsymbol{x} \to \boldsymbol{x} + \boldsymbol{b'}$.

At last we have gathered the ingredients necessary for calculating the induced gluon spectrum. Simply taking the ratio of (8.10) and (8.13), with the prescribed change of coordinates, yields

$$z\frac{dI}{dz}\Big|_{\mathrm{ind}} = \frac{2C_f\alpha_s}{\pi^2} \frac{\int_{\boldsymbol{r}} e^{i\boldsymbol{p}\cdot\boldsymbol{r}} \int_{\boldsymbol{x}} \frac{\boldsymbol{x}\cdot(\boldsymbol{x}+\boldsymbol{r})}{\boldsymbol{x}^2(\boldsymbol{x}+\boldsymbol{r})^2} \left\{ S^{(2)}(\boldsymbol{r}) - S^{(3)}[\boldsymbol{0}, \boldsymbol{x}+\boldsymbol{r}, z\boldsymbol{x}+\boldsymbol{r}] \right\}}{\int_{\boldsymbol{r}} e^{i\boldsymbol{p}\cdot\boldsymbol{r}} S^{(2)}(\boldsymbol{r})} \tag{8.14}$$

This is the result dubbed as the Master equation in [26]. We reiterate that this expression is valid when $z \ll 1$ and $p \gg Q_s$. From this point the authors proceed to to simplify the expression using assumptions of their model for the dipole to extract the behaviour of the induced gluon spectrum in different limits. We do not need to do this. With the Gaussian truncation we have the power to calculate this spectrum directly.

Recognizing that all the integrals are over transverse coordinates, we switch to polar coordinates. The angle between $\boldsymbol{p}$ and $\boldsymbol{r}$ will be given by θ and the angle between $\boldsymbol{x}$ and $\boldsymbol{r}$ by ϕ. Notice that θ only appears in the Fourier transform, so we can evaluate that integral immediately.

$$\int_0^{2\pi} d\theta e^{ipr\cos\theta} = \frac{1}{2\pi} J_0(pr), \tag{8.15}$$

where $p = |\boldsymbol{p}|$, $r = |\boldsymbol{r}|$ and J_0 is the zero-order Bessel function of the first kind. The presence of the Bessel function presents a great difficulty when attempting to perform numerics. It is highly oscillatory, making it resistant to many numerical integration schemes. It would be the subject of a future work to investigate numerical methods to carry out the full calculation and dedicate the necessary computational resources to the task. All the constituent elements are present, in particular the missing piece of the Wilson line correlators and their rapidity solution are now accounted for thanks to the Gaussian truncation.

Chapter 9

Closing remarks

In the first half of this work we motivated the presence of a CGC and discussed the relevant degrees of freedom in high-energy collisions when the eikonal limit applies (Chapters 1 and 2). These degrees of freedom turned out to be Wilson lines and their correlators (Chapter 3). They are determined through the JIMWLK evolution equation (Chapter 4). However, we have no way of solving the JIMWLK equation for any correlator exactly; it links the evolution of each correlator to all the correlators of a higher order.

The challenge, then, was to find a way of approximating JIMWLK in a manner that closes the evolution equation, making numerical evolution permissible, while preserving salient information about the correlators. The property that we preserve regarding Wilson line correlators is a statement of their gauge invariance: their coincident limits. To that end we introduce the Gaussian truncation: a method for truncating the JIMWLK hierarchy that permits numerical solutions while preserving the coincident limits to all orders in N_c (Chapter 5). Other methods of simplifying JIMWLK may achieve some of these things, but only the Gaussian truncation achieves all of them.

The Gaussian truncation involves the re-parametrization of the rapidity dependence of the correlator onto these "gluon exchange functions", $\mathcal{G}$ and G. We explained how the evolution equation for these functions can be obtained from the evolution equation of dipole and 3-point correlator. We the demonstrated the validity of the Gaussian truncation, by numerically reconstructing the dipoles from which they were obtained (Chapter 6). At this point we could also extract and discuss the relevant length scale in these correlators, the inverse of the saturation scale Q_s.

While the Gaussian truncation has been looked at before and compared to the BK approximation, we have demonstrated how it may be extended to compute any Wilson line correlator, not just the dipole. In chapter 7 we describe and implement the algorithm for using the Gaussian truncation to numerically calculate the amplitude matrix built out of a basis for the 4-point correlators.

From this we could explore a number of properties of the 4-point correlators. We checked that the coincident limits behaved as they should. We demonstrated that the correlators go to zero in particular limits, but also managed to explore non-trivial behaviour, such in the gluon-gluon dipole limit. We investigated two things that go into the BK approximation that don't necessarily hold for correlators more complicated than the dipole: Factorization of correlators and the neglecting of N_c suppressed terms. We have demonstrated that there is a non-trivial factorization error - that correlators cannot be freely factorized out of the average. On top of this the Gaussian truncation actually

predicts a non-trivial solution for correlators that are N_c suppressed.

We also explore the degree to which path dependence matters for the calculation of these correlators. While it may seem a trivial statement that path ordering has an influence on the final result, that is what the analytic solution determines after all, most approximations to JIMWLK evolution neglect this entirely. In particular, the large N_c limit evolution of the 4-point correlators find that the off-diagonal terms vanish. In other words, the matrix amplitude is diagonal and path ordering can be neglected. We see that this is not sufficient, though. When compared with the Gaussian truncation, which does incorporate path ordering, the difference in the diagonal terms is larger than ten percent. Ten percent is the common heuristic of the error induced by using the large N_c limit. Funnily enough, when compared to the rigid exponentiation, which also neglects path ordering, the difference between this and the Gaussian truncation for the diagonal terms is negligible, while the difference for the off-diagonal terms is not.

Finally, we investigated the numerical stability of this Gaussian truncation algorithm and found it to be quite stable.

In chapter 8 we presented an interesting observable: the induced gluon spectrum which goes into the calculation of the energy loss due to cold nuclear matter. This observable has important consequences for things such as the quark gluon plasma, because energy loss is one of the most promising avenues for studying the QGP. Further more, this observable depends on Wilson line correlators, giving us an excellent opportunity to test the Gaussian truncation.

Critical to the discussion on the induced gluon spectrum is the nuclear saturation scale: the effective saturation scale of a nucleus that consists of many protons and neutrons at some references saturation scale. In appendix C we presented a method for extracting the nuclear saturation scale of a given atom. Given how the saturation scale is defined - in reference to the inflection point of the dipole correlator - we can conclude that implementing a higher saturation scale is equivalent to performing a rapidity evolution on the correlator in question. This is another point where the Gaussian truncation comes in handy.

The Gaussian truncation isn't perfect, however. The limitations and open questions on the Gaussian truncation were discussed in 5.4. To briefly summarize, we don't yet know analytically the accuracy granted by the Gaussian truncation or truncations that go beyond this. We would expect to get diminishing returns on the Gaussian truncation as we go to more and more complicated correlators, but this hasn't been firmly established. We know the Gaussian truncation can only access the real part of any correlator, so we must go to a third order truncation or beyond to access this information. Specifying which degrees of freedom are granted as we go to each new order in the generalized truncation is a subject of future research. See [19].

The Gaussian truncation is fertile ground for future research. It grants us access to many observables - all observables that depend on Wilson line correlators and the analytic properties beyond what have been established in this thesis are also rich avenues for discussion.

Appendix A

Vanishing of the gluon 1-point fluctuation $\langle \delta A \rangle_{\delta A}$

In forming the finite difference equation of JIMWLK, we made the claim that the 1-point function of gluons vanishes to leading order. To justify this statement we will expand the QCD action in powers of δA and make use of the fact that we are integrating an odd function to show that it vanishes.

We remind the reader that the averaging procedure is given by

$$\langle ... \rangle_{\delta A} = \int D[\delta A] ... e^{S_{QCD}[b+\delta A]}, \tag{A.1}$$

where δA is a small fluctuation around the background field b. We claim that the following vanishes:

$$\langle \delta A \rangle_{\delta A} = 0. \tag{A.2}$$

To see why this is the case, expand the QCD action up to quadratic order in δ,

$$\begin{aligned} \langle \delta A \rangle_{\delta A} &= \int D[\delta A] \delta A e^{S_{QCD}[b+\delta A]} \\ &= \int D[\delta A] \delta A \exp\left[S_{QCD}[b] + \delta A \frac{\delta}{\delta A} S_{QCD}[b] + \frac{1}{2} \delta A^2 \frac{\delta^2}{\delta A^2} S_{QCD}[b] + \mathcal{O}(\delta A^3) \right]. \end{aligned} \tag{A.3}$$

The $S_{QCD}[b]$ term in the exponential can be factored out of the integral as it is independent of δA. Now, the background field, b, satisfies the classical equations of motion. In other words, b is the field such that the QCD action is minimized and it's variation with respect to a fluctuation is zero. Lastly, the higher order terms can be neglected as this is only used to derive leading order JIMWLK. This leaves us with

$$\langle \delta A \rangle_{\delta A} = e^{S_{QCD}[b]} \int D[\delta A] \delta A \exp\left[\frac{1}{2} \delta A^2 \frac{\delta^2}{\delta A^2} S_{QCD}[b] \right]. \tag{A.4}$$

Notice now that the exponent is quadratic in δA and the exponential is Gaussian in δ. This, of course, means that the exponential is even in δ, while δ, in fact, is an odd function in δA. The product of an odd function and an even function is an odd function. Therefore the integral over the fluctuations is zero, because the integral over an odd function across its domain is zero.

This implies, of course, that all the odd gluon n-point functions are zero. Nevertheless, we have shown that the gluon 1-point function vanishes.

Appendix B

Gluon propagator in the presence of a strong background field

For a gauge field of the form

$$A^{\mu}(x) = g^{\mu}_{+}\delta(x^{-})\beta(x_{\perp}), \tag{B.1}$$

the covariant derivative is given by

$$D^{\mu} = \partial^{\mu} - ig[g^{\mu -}\delta(x^{-})\beta(x_{\perp})]. \tag{B.2}$$

With this we may express the gluon propagator in the presence of a strong background field as [31]

$$\left\langle \delta A^{a+}_{x} \delta A^{b+}_{y} \right\rangle = \frac{\partial^{i}_{x}}{\partial^{-}_{x}} \left[\frac{ig_{\mu\nu}}{(D^{2})} \right] \frac{\partial^{i}_{y}}{\partial^{-}_{y}}. \tag{B.3}$$

The propagator has been written in terms of Green's functions, formal inverses to the differential operators that satisfy $D[\frac{i}{D}]_{xy} = i\delta(x-y)$, where D is an operator and $\frac{1}{D}$ is its Greens function. Thus, to compute the propagator, we must compute these inverse derivatives. The first couple are given by

$$\left[\frac{i}{\partial^{-}} \right]_{xy} = \delta_{x^{-}y^{-}}\delta^{(2)}_{x_{\perp}y_{\perp}} \int \frac{dk^{-}}{2\pi} \frac{1}{k^{-} + i\epsilon} e^{-ik^{-}(x^{+}-y^{+})} \tag{B.4}$$

and

$$\left[\frac{i}{(\partial^{-})^{2}} \right]_{xy} = \delta_{x^{-}y^{-}}\delta^{(2)}_{x_{\perp}y_{\perp}} \int \frac{dk^{-}}{2\pi} \frac{i}{(k^{-})^{2} + i\epsilon} e^{-ik^{-}(x^{+}-y^{+})}. \tag{B.5}$$

These can easily be checked to be the Green's functions by applying their respective differential operators to them. We remind the reader that $\partial^{\pm} = \frac{\delta}{\partial^{\mp}}$. The inverse of the covariant derivative squared is trickier to work out. It can be derived through spectral decomposition like in appendix A of [32]. Instead, we will state the Green's function and prove that it is one by hitting it with its differential operator and obtaining a delta function. The Green's function is given by

$$\begin{aligned} \left[\frac{i}{(D^{2})} \right]^{ab}_{xy} = \lim_{\epsilon \to 0^{+}} \int \frac{dp^{-}}{4\pi p^{-}} \frac{d^{2}q_{\perp}}{(2\pi)^{2}} \frac{d^{2}k_{\perp}}{(2\pi)^{2}} [\theta(x^{-}-y^{-}-\epsilon)\theta(p^{-}) + \theta(y^{-}-x^{-}+\epsilon)\theta(-p^{-})] \\ \times \left[e^{-i(q.x-k.y)} \int d^{2}u_{\perp} e^{-i(q_{\perp}-k_{\perp}).u_{\perp}} \mathcal{P}exp\left[-ig \int_{y^{-}}^{x^{-}} dz^{-} b^{+ab}(z^{-},u) \right] \right], \end{aligned} \tag{B.6}$$

where $p^- = q^- = k^-$ and $p^+ = \frac{p_\perp^2}{2p^-}$,$q^+ = \frac{q_\perp^2}{2q^-}$ and $k^+ = \frac{k_\perp^2}{2k^-}$, because these particles are massless and on-shell. One can abbreviate the path integral as $U(z^-,u)^{ab}$. The colour indices, a, b, will suppressed for the rest of this section. With this we can right the propagator explicitly

$$\begin{aligned}\left\langle \delta A_x^{a+} \delta A_y^{b+} \right\rangle = \lim_{\epsilon\to 0^+} \partial_{x_\perp}\partial_{y_\perp} \int \frac{dp^-}{4\pi(p^-)^3}\frac{d^2q_\perp}{(2\pi)^2}\frac{d^2k_\perp}{(2\pi)^2} \\ \times [\theta(x^- - y^- - \epsilon)\theta(p^-) - \theta(y^- - x^- + \epsilon)\theta(-p^-)] \\ \times \left[e^{-i(q.x-k.y)} \int d^2u_\perp e^{-i(q_\perp - k_\perp).u_\perp} \mathcal{P}exp\left[-ig \int_{y^-}^{x^-} dz^- b^{+ab}(z^-,u) \right] \right],\end{aligned} \tag{B.7}$$

having used integration by parts to move the y derivatives to the left. We have to hit $\left[\frac{i}{D^2}\right]$ with D^2, whose form we first simplify.

$$D^\mu D_\mu = \partial^2 - ig\partial^\mu[g_\mu^- \partial(x^-)\beta(x_\perp)] - ig[g^{\mu-}\partial(x^-)\beta(x_\perp)]\partial_\mu + (ig)^2 g^{\mu-}g_\mu^-[\delta(x^-)\beta(x_\perp)]^2. \tag{B.8}$$

Making use of the following properties in light-cone coordinates: $\partial^\pm = \partial_\mp$, $\partial^{\pm\mu} = g^\mu_\mp$ and $g^{\mu-} = \delta^{\mu+}$, we get

$$D^\mu D_\mu = \partial^2 - 2ig[\delta(x^-)\beta(x_\perp)]\partial_+. \tag{B.9}$$

We break the calculation into parts. First we examine the action of the D'Alembertian on the following piece of the Greens function:

$$\begin{aligned}&\partial^2\left(e^{-iq.x}\theta(x^- - y^-)U(z^-,u_\perp)\right) \\ =&(\partial^2 e^{-iq.x})\theta(x^- - y^-)U(z^-,u_\perp) + e^{-iq.x}\underbrace{(\partial^2\theta(x^- - y^-))}_{=0}U(z^-,u_\perp)_{=0} \\ &+ e^{-iq.x}\theta(x^- - y^-)\underbrace{(\partial^2 U(z^-,u_\perp))}_{=0} + 2(\partial_\mu e^{-iq.x})(\partial^\mu\theta(x^- - y^-))U(z^-,u_\perp) \\ &+ 2(\partial_\mu e^{-iq.x})\theta(x^- - y^-)(\partial^\mu U(z^-,u_\perp)) + 2e^{-iq.x}\underbrace{(\partial_\mu\theta(x^- - y^-))(\partial^\mu U(z^-,u_\perp))}_{=0} \\ =&\underbrace{(-iq)^2}_{=m^2=0} e^{-iq.x}\theta(x^- - y^-)U(z^-,u_\perp) \\ &+ 2(-iq_\mu e^{-iq.x})(\delta_-^\mu\delta(x^- - y^-))U(z^-,u_\perp) \\ &+ 2e^{-iq.x}(\delta_-^\mu\delta(x^- - y^-))(\partial_\mu U(z^-,u_\perp))\end{aligned} \tag{B.10}$$

Several terms go to zero because they involve a derivative with respect to the x^+ direction, of which none of the terms have any dependence on. We also used the fact that the on-shell gluon is massless, implying $q^2 = 0$. This leaves us with the following expression

$$2\underbrace{(-iq_- e^{-iq.x})(\delta(x^- - y^-))U(z^-,u_\perp)}_{\text{(i)}} + 2\underbrace{e^{-iq.x}(\delta(x^- - y^-))(\partial_- U(z^-,u_\perp))}_{\text{(ii)}} \tag{B.11}$$

We explore term (ii) first and show that it cancels against gauge field term of D^2. The derivative of the Wilson line, U, taking care to employ the Leibniz integral rule, is given by

$$\partial_- U = -ig\beta(z_\perp)[\delta(x^-)\theta(-y^-) + \delta(-x^-)\theta(y^-)]U. \tag{B.12}$$

When one considers the presence of both $\delta(x^-)$ and $\delta(x^- - y^-)$, we see that this term of the Green's function only has support where $x^- = y^- = 0$. This trivializes the $d^2q_\perp$ integral into a Dirac delta in $x_\perp - z_\perp$. Thus this term is the same, but with opposite sign, as the one obtained by applying the second term of (B.9). Hence, they cancel.

We see now that $D^2\left[\frac{i}{D^2}\right] \sim$ (i). More explicitly, we have

$$\begin{aligned} D^2\left[\frac{i}{D^2}\right] = \lim_{\epsilon\to 0^+}\int \frac{dp^-}{4\pi p^-}\frac{d^2q_\perp}{(2\pi)^2}\frac{d^2k_\perp}{(2\pi)^2}(-2iq^-) \\ \times\left[\delta(x^- - y^- + \epsilon)\theta(p^-) - \delta(y^- - x^- + \epsilon)\theta(-p^-)\right] \\ \times e^{-i(q.x-k.y)}\int d^2u_\perp e^{-i(q_\perp - k_\perp).u_\perp}\mathcal{P}exp\left[-ig\int_{y^-}^{x^-} dz^-\delta(x^-)\beta(u_\perp)\right]. \end{aligned} \tag{B.13}$$

Immediately we may cancel the q^- and p^-, as they are equal. The next step is to perform the $q_\perp$ and $k_\perp$ integrals. They are for displaced, complex Guassians, so it is assumed that the integration variables have small positive imaginary parts so that the integrals are well defined at infinity. We perform the first integral, cognisant of the fact that $q^+ = \frac{q_\perp^2}{2q^-}$.

$$\int dq_1 e^{-i(\frac{x^-}{2q^-}q_1^2 + (x_1+u_1)q_1)} = \sqrt{\frac{-2\pi i q^-}{x^-}}e^{\frac{i(x_1+u_1)^2q^-}{2x^-}}. \tag{B.14}$$

From this result, and the equality of q^-, k^- and p^-, it's easy to see that performing all four integrals gives us

$$\begin{aligned} \int dq_\perp^2 e^{-i(\frac{x^-}{2q^-}q_\perp^2 + (x_\perp+u_\perp).q_\perp)} &= \frac{-2\pi i p^-}{x^-}e^{\frac{i(x_\perp+u_\perp)^2p^-}{2x^-}} \\ \int dk_\perp^2 e^{i(\frac{y^-}{2k^-}k_\perp^2 + (y_\perp+u_\perp).k_\perp)} &= \frac{2\pi i p^-}{y^-}e^{\frac{-i(y_\perp+u_\perp)^2p^-}{2y^-}}. \end{aligned} \tag{B.15}$$

This is the current status of our calculation

$$\begin{aligned} D^2\left[\frac{i}{D^2}\right] = \lim_{\epsilon\to 0^+}\int \frac{p^-}{2\pi}\frac{1}{2\pi}\frac{1}{2\pi}(-i)e^{-ip^-(x^+-y^+)} \\ \times\left[\delta(x^- - y^- + \epsilon)\theta(p^-) - \delta(y^- - x^- + \epsilon)\theta(-p^-)\right] \\ \times\frac{-(ip^-)^2}{x^-y^-}\int d^2u_\perp e^{\frac{i(x_\perp+u_\perp)^2p^-}{2x^-}}e^{\frac{-i(y_\perp+u_\perp)^2p^-}{2y^-}} \\ \times\mathcal{P}exp\left[-ig\int_{y^-}^{x^-} dz^-\delta(x^-)\beta(u_\perp)\right]. \end{aligned} \tag{B.16}$$

The next computational step is to examine the Wilson line. We actually evaluate the integral in the exponent, but the calculation is subtle. Its path from x^- to y^- is a straight

line path that can be parametrized in terms of an affine parameter, $\tau \in [0,1]$, such that $z^-(\tau) = \tau x^- + (1-\tau)y^-$. The exponent of the Wilson line that evaluates as

$$\begin{aligned}\int_{y^-}^{x^-} dz^- \delta(x^-)\beta(u_\perp) &= \int_0^1 d\tau \frac{\partial z^-}{\partial \tau}\delta(z^-)\beta(u_\perp) \\ &= \int_0^1 d\tau (x^- - y^-)\delta(z^-)\beta(u_\perp) \\ &= \int_0^1 d\tau (x^- - y^-)\frac{\delta(\tau-\tau_0)}{|x^- - y^-|}\beta(u_\perp),\end{aligned} \tag{B.17}$$

where we have change variables in the argument of the Dirac delta. The choice of τ_0 is irrelevant; if it lies outside the range of the integral, the integral trivially evaluates to zero, if not, the integral non-trivially evaluates to zero, as will be shown. If both x^- and y^- where on the same side of 0, this integral would be trivially 0. Thus we are left with the cases of $x^- < 0 < y^-$ and $y^- < 0 < x^-$. Taking this into consideration, the integral evaluates to

$$\int_{y^-}^{x^-} dz^- \delta(x^-)\beta(u_\perp) = [\theta(y^-)\theta(-x^-) - \theta(-y^-)\theta(x^-)]\beta(u_\perp), \tag{B.18}$$

which, given the the presence of $\delta(x^- - y^-)$, has no support and we see that this exponent must be zero. The penultimate step is to perform the $d^2u_\perp$ integral. Once again, it is a displaced Gaussian integral and once again we let $u_\perp$ have a small imaginary part so that the integral is well defined. After some manipulation we obtain

$$\int d^2u_\perp e^{\frac{i(x_\perp+u_\perp)^2 p^-}{2x^-}} e^{\frac{-i(y_\perp+u_\perp)^2 p^-}{2y^-}} = \frac{-2\pi i x^- y^-}{p^-(x^- - y^-)} e^{i\frac{p^-}{2}\frac{(x_\perp - y_\perp)^2}{x^- - y^-}}. \tag{B.19}$$

The calculation is now in the following state:

$$\begin{aligned}D^2\left[\frac{i}{D^2}\right] = &-\lim_{\epsilon\to 0}\int dp^- \frac{1}{2\pi}\frac{1}{2\pi}e^{-ip^-(x^+ - y^+)} \\ &\times \left[\delta(x^- - y^- + \epsilon)\theta(p^-) - \delta(y^- - x^- + \epsilon)\theta(-p^-)\right] \\ &\times \frac{p^-}{x^- - y^-} e^{\frac{i(x_\perp - y_\perp)^2}{2(x^- - y^-)/p^-}}.\end{aligned} \tag{B.20}$$

It may not look like it, but we're almost there. The reason for the epsilon limit will be made clear as we make use of one final identity:

$$\delta(x) = \lim_{\epsilon\to 0^+}\frac{1}{\sqrt{2\pi i\epsilon}} e^{\frac{ix^2}{2\epsilon}}. \tag{B.21}$$

For our purposes, the role of ϵ in (B.21) is played by $\frac{x^- - y^-}{p^-}$. However, we need this term to approach zero from the positive direction. To this end the p^- contour has been split into two halves by the Heaviside functions. In the firs half, p^- is positive and $x^- - y^-$ approaches zero from the positive direction according to $\lim_{\epsilon\to 0^+}\delta(x^- - y^- + \epsilon)$. In

the second half of the contour, p^- is negative, but $x^- - y^-$ approaches zero from the negative side according to $\lim_{\epsilon\to 0^+}\delta(y^- - x^- + \epsilon)$. Therefore, the identity is applicable in both halves, although a minus sign is picked up in the second half.

$$\begin{aligned}
&\int_0^\infty dp^- \frac{p^-}{x^- - y^-} e^{\frac{i(x_\perp - y_\perp)^2}{2(x^- - y^-)/p^-}} \\
&- \int_{-\infty}^0 dp^- \frac{p^-}{x^- - y^-} e^{\frac{i(x_\perp - y_\perp)^2}{2(x^- - y^-)}} \\
=&2\pi i \int_0^\infty dp^- \delta(x_\perp - y_\perp) + 2\pi i \int_{-\infty}^0 dp^- \delta(x_\perp - y_\perp)
\end{aligned} \tag{B.22}$$

Bringing it altogether, we are safely able to evaluate the ϵ limit. We are left with an expression involving the Fourier representation of the delta function,

$$\begin{aligned}
D^2\left[\frac{i}{D^2}\right] &= -i\delta(x^- - y^-)\delta^{(2)}(x_\perp - y_\perp)\int dp^- e^{-ip^-(x^- - y^-)} \\
&= -i\delta^{(4)}(x - y).
\end{aligned} \tag{B.23}$$

Thus we have shown that this is indeed the appropriate Green's function.

Appendix C

Nuclear Saturation Scale

There are a number of interesting observables that depend on Wilson line correlators, from energy loss in cold nuclear matter [26], to dijet processes in pA collisions [25]. Therefore there is a great need for a way to calculate these correlators. Unfortunately, they have a non-trivial energy dependence [4] which leaves us without any analytical expression and most numerical approximations abandon vital properties of these correlators. Most, but not the Gaussian truncation which gives us approximate access to any Wilson line correlator and its energy evolution whilst preserving many fundamental properties [18]. We now have, in principle, the tools calculate these observables, but an important concept that enters this discussion is: what saturation scale should we compute these Wilson line correlators for?

The saturation scale gives a characteristic energy scale at which the Wilson line correlator corresponding to the $q\bar{q}$ dipole becomes uncorrelated. It is determined by the experimental set-up with a proton target.

For a nucleus, however, there is a subtlety for how the saturation scale is calculated. When a given batch of Wilson lines pierces a nucleus, the saturation scale is determined by the number of nucleons they pass through by [24]

$$Q^2_{s0,\text{nucleus}}(\text{R}) = N(\text{R})Q^2_{s0,\text{proton}}, \tag{C.1}$$

where N is the number of nucleons pierced and R is the position in the transverse plane of the nucleus where it is pierced. So the greater the number of nucleons pierced, the greater the saturation scale. In fact, the nucleus saturation scale goes like $\sqrt{N(\text{R})}Q_{s0,\text{proton}}$. Then how many nucleons would be pierced if the target were a lead nucleus? Not 208. That would imply all the nucleons were in a straight line. One? That's possible if the Wilson lines strike the periphery of the nucleus. In truth, the Wilson lines can pierce the nucleus anywhere and they have different chances of hitting places with different numbers of overlapping nucleons. The challenge is to determine how often a Wilson line hits different regions of the nucleus with different nucleon numbers.

Once this is determined, what is left to be done is to compute the observable at different saturation scales and weight them by how likely it is that the Wilson lines enter with those saturation scales. This brings us to the point of this section. Here we present the algorithm for determining how often each modified saturation scale is needed so that we may calculate observables with larger nucleus targets.

It should be said that the transverse dependence of a batch of Wilson lines only cares about the saturation scale, the rest of the position dependence sees only position of

Wilson lines relative to each other. Given that in a particular region of overlapping nucleons, the saturation scale is constant in this region, so we may work out the average value of a correlator, $S(Q_{s,i})$, where i denotes different saturation scales as such

$$\begin{aligned}\langle S\rangle &= \frac{1}{n}\sum_{j}^{n}\sum_{i}\frac{A_{ij}}{T_j}S(Q_{s,i}) \\ &=: \sum_{i}\langle A\rangle_i S(Q_{s,i}),\end{aligned} \tag{C.2}$$

In other words, we can construct the average value of this correlator inside a nucleus as such

$$\langle S\rangle = \langle A\rangle_1 S(Q_{s,1}) + \langle A\rangle_2 S(Q_{s,2}) + ... + \langle A\rangle_n S(Q_{s,n}) + ... \tag{C.3}$$

where A_i are the areas of different regions of the nucleus with different saturation scales. j is the ensemble member index, a particular nucleus configuration that we sum over to get an average proportion of the nucleus taken up by each region, and n is the number of ensemble members. $\langle A\rangle_i$ is the average probability of piercing i nucleons.

This factorisation assumes that within a batch of Wilson lines, all the Wilson lines pierce the same region in the nucleus. In other words, for a single correlator, any two Wilson lanes carry the same saturation scale.

C.1 Relative Frequency of Saturation Scales

Here we will present how to calculate the relative frequency of different saturations scales that arise due to interactions with a large nucleus. The algorithm can be broken into 5-parts

- Generate a nucleus from the Woods-Saxon distribution
- Flatten this nucleus into the plane transverse to the path of the Wilson line
- Separate this flattened image into regions of n overlapping nucleons for each n
- Measure the area of each region relative to the total transverse area of the nucleus to obtain the probability of piercing that region
- Repeat this process for many generated nuclei to find the average probability of piercing n nucleons for each n

C.2 Nucleus generation

The first step is to generate a nucleus with nucleons distributed within it in an appropriately random way. The distribution we draw our nucleus from is the Woods-Saxon distribution [33]:

$$p(r) = \frac{\rho_0}{1 + e^{\frac{r-R}{a}}}, \tag{C.4}$$

where $R = r_0 A^{1/3}$, r_0 is the typical nucleon-nucleon distance in a large nucleus. As a slight simplification, we will take it to be the radius of a proton. A is the nucleon

number. a is the diffuseness. ρ_0 is the normalization so that this distribution integrates to one. For our purposes we use the following values for a lead nucleus:

- $\rho_0 = 0.0005623529449722396$
- $r_0 = 1.25fm$
- $A = 208$
- $a = 0.5fm$

Drawing 208 nucleons from this distribution gives us the following nucleus

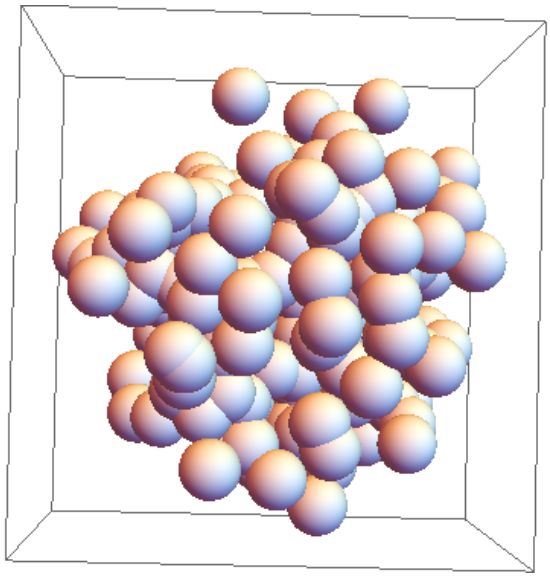

FIGURE C.1: Sample nucleus generated from the Woods-Saxon distribution.

C.3 Nucleus Flattening

From the perspective of an incoming parton, we only care about the transverse distribution of nucleons. Specifically, we care about the number of overlapping nucleons at any given point on the transverse plane. The function describing this distribution is given by

$$N(x,y) = \sum_i \frac{1}{2}\left(\theta(r_0 - \sqrt{(x-x_i)^2 + (y-y_i)^2}) - \theta(\sqrt{(x-x_i)^2 + (y-y_i)^2} - r_0) + 1\right), \tag{C.5}$$

where i sums over each nucleon and θ is the the Heaviside function. Here we are treating every nucleon as as a thin cylindrical disk. In other words, glancing blows off nucleons are treated the same as when the parton pierces straight through the equator. Is this a reasonable assumption? This is in line with the assumptions used to derive JIMWLK, where the target proton is Lorentz contracted into a flat disk. This gives the following picture

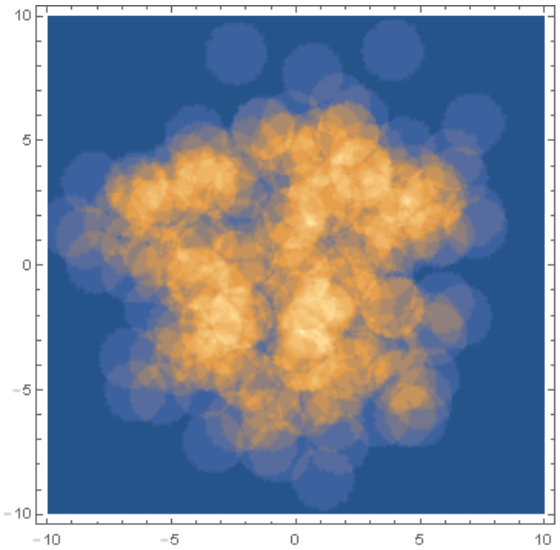

FIGURE C.2: Transverse distribution of nucleons inside a nucleus. Brighter regions correspond to regions with a greater number of overlapping nucleons. Axes are in units of proton diameter.

C.4 Nucleus level slicing

What matters for the purpose of calculating the average of our function (C.2) is the relative size of each region corresponding to each number of overlapping nucleons. It is simple enough to separate these regions, since they all live on a different level in (C.5). I.e. the region $x, y \in \mathbb{R}$ s.t. $N(x, y) = n$ corresponds to the region where there are n overlapping nucleons. This gives us the following regions for each level of cut

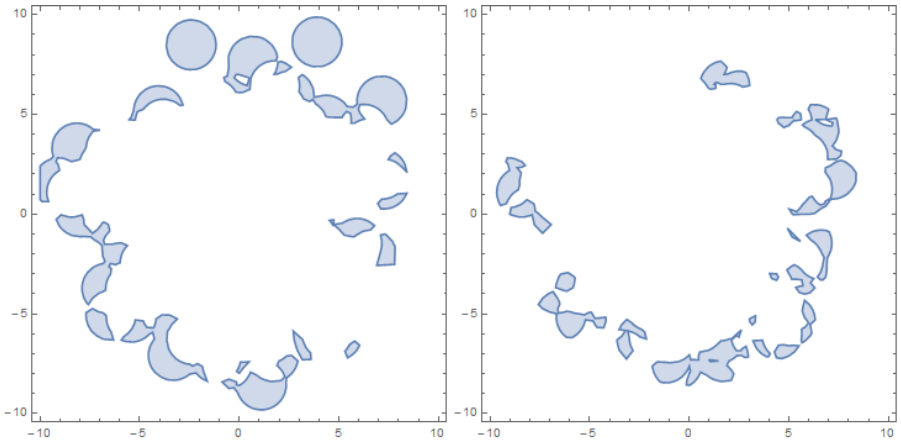

FIGURE C.3: On the left (right) is the transverse area of the nucleus with one (two) overlapping nucleons.

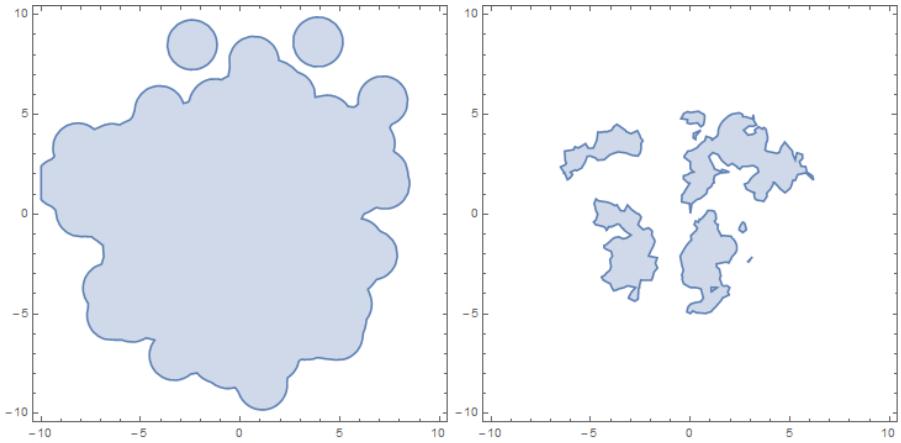

FIGURE C.4: On the left is the entire transverse area of the nucleus. One the right is the total area of levels eight and above.

We use Mathematica to calculate the area of each of these levels. If you take the ratio of one of these areas to the total transverse area of the nucleus, you obtain the probability that an incoming parton pierces the corresponding number of nuclei and the probability that the associated saturation scale should be used.

C.5 Averaging Over an Ensemble of Nuclei

It is not enough to perform this process for one nucleus, one must average over the different possible nucleus configurations. So we repeat the process, generating a new nucleus each time and averaging the probabilities of piercing each number of nucleons until the values start to converge. When we performed this for 200 different nucleons, we obtained the following probabilities for each nucleon level.

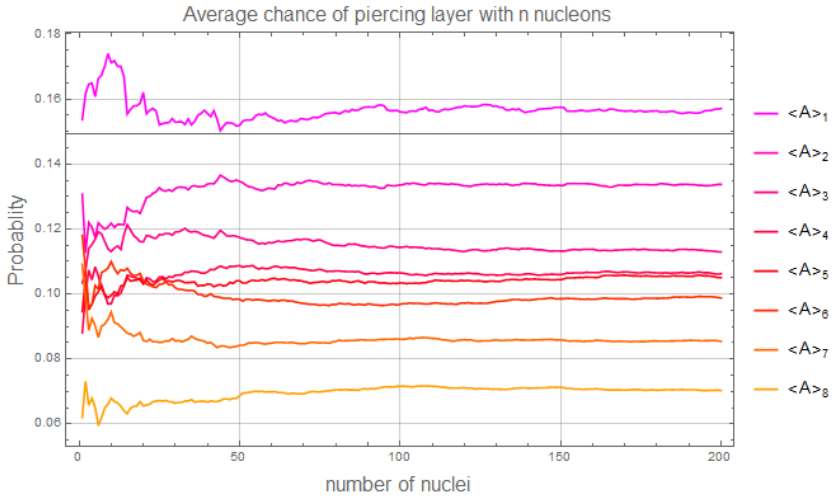

FIGURE C.5: Average proportion of each level of the nucleus as we incorporate more nuclei into our ensemble.

With the final results being

	$\langle A\rangle_1$	$\langle A\rangle_2$	$\langle A\rangle_3$	$\langle A\rangle_4$	$\langle A\rangle_5$	$\langle A\rangle_6$
Mean	0.157103	0.133774	0.112981	0.106279	0.105084	0.098786
u(Mean)	0.00310584	0.00176138	0.00148077	0.00128249	0.00132928	0.00114936

	$\langle A\rangle_7$	$\langle A\rangle_8$	$\langle A\rangle_9$	$\langle A\rangle_10$	$\langle A\rangle_{11}$	$\langle A\rangle_{12}$
Mean	0.0854347	0.0703006	0.0514948	0.0348951	0.0203723	0.0112758
u(Mean)	0.0010376	0.000935931	0.000742466	0.00065575	0.000567131	0.000426276

	$\langle A\rangle_{13}$	$\langle A\rangle_{14}$	$\langle A\rangle_{15}$	$\langle A\rangle_{16}$	$\langle A\rangle_{17}$	$\langle A\rangle_{18}$
Mean	0.0062397	0.00345083	0.00151097	0.000578431	0.000359289	0.0000686582
u(Mean)	0.000338593	0.00028663	0.000156229	0.000086987	0.0000874962	0.0000313536

(C.6)

With these values we may construct the average value of the operator S (C.3).

C.6 Effective Rapidity Evolution

How do we use this information to calculate observables with large nucleus targets, such as the induced gluon spectrum (8.14)? Throughout this work we have not been dealing with saturation scale evolution, but rapidity evolution. We take data for the dipole correlator at some initial rapidity and saturation scale and evolve it in rapidity. However, when we evolve in rapidity, the saturation scale changes too. There is a one-to-one map between the two that we have determined in figure 6.3, which we repeat here for convenience.

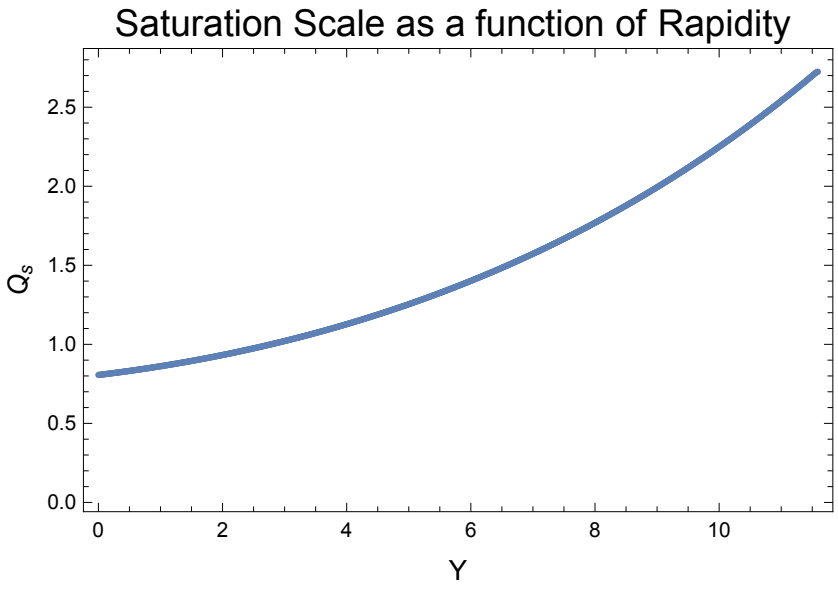

FIGURE C.6: The saturation scale, Q_s, of the dipole correlator as a function of rapidity, Y.

This implies that, in order to calculate an observable at a new saturation scale, we must simply evolve it in rapidity to the appropriate value prescribed by C.6. One can do this to calculate an observable at all the saturations scales needed to calculate the

average (C.3). Thus, even nucleus target observables are accessible to us.

In summary, in order to calculate an observable with a large nucleus target, we do the following: Start with knowledge about the saturation scale of a single nucleon in the target and the associated dipole correlator for that scale. Through the Gaussian truncation one may use this dipole to calculate any correlator at any rapidity. Calculate the correlator associated with the relevant observable at the rapidities prescribed by C.6 so that we have the correlator at the saturation scales prescribed by (C.1). Finally, if the target is lead, average these correlators at different saturation scales according to table (C.6) and you will have computed the correlator for large nucleus target. Other tables would need to be generated for other target nuclei.

Appendix D

SU(N_c) Identities

This is a small collection of $SU(N_c)$ identities, many of which are used to proves statements throughout this text. Sources one may look to for further reading include standard QFT textbooks like Peskin and Schroeder [2], Cvitanovic's book on group theory and birdtracks [21] and a handy summary of useful $SU(N_c)$ identities written by Howard Haber [34].

We start by reminding the reader that the defining characteristic of the special unitary group is that its elements obey properties (3.7) and (3.8), they are of unit norm and unitary. The generators of the special unitary algebra, $su(N_c)$, are given by T_R^a, where R is the representation of the generator. We will mostly be working with the fundamental, $T_{R=f}^a =: t^a$, and adjoint, $(T_{R=A}^{ab})^c = if^{abc}$, representations. Then any element of $SU(N_c)$ can be expressed via the exponential map of a linear combination, $U_R = \exp[T_R^a A^a]$, where A^a are arbitrary constants.

The inner product for two elements of $SU(N_c)$, U, V, is given by

$$U \cdot V = \text{tr}(U^\dagger V). \tag{D.1}$$

The normalization condition of the generators is given by

$$\text{tr}(T_R^a T_R^b) = \frac{1}{2}\delta^{ab}. \tag{D.2}$$

The adjoint representation is related to every other representation the same way it is related to the fundamental representation, by the following commutation relation:

$$[t^a, t^b] = if^{abc}t^c. \tag{D.3}$$

Another way of expressing the adjoint generator is in terms of the trace of three generators:

$$\frac{1}{2}if^{abc} = \text{tr}\left(t^a t^b t^c\right) - \text{tr}\left(t^b t^a t^c\right) \tag{D.4}$$

The proof is as follows:

$$\begin{aligned}
&\text{tr}\left(t^a t^b t^c\right) - \text{tr}\left(t^b t^a t^c\right) \\
=&\text{tr}\left(t^a t^b t^c\right) - \text{tr}\left(t^a t^b t^c\right) + \text{tr}\left([t^a, t^b] t^c\right) \\
=&\text{tr}\left([t^a, t^b] t^c\right) \\
=&if^{abd}\text{tr}\left(t^d t^c\right) \\
=&if^{abd}\frac{1}{2}\delta^{dc} \\
=&\frac{1}{2}if^{abc}.
\end{aligned} \tag{D.5}$$

A constant that often comes up is the quadratic Casimir, C_R, of a representation, R, defined as

$$T_R^a T_R^a = C_R \mathbb{1} \tag{D.6}$$

The quadratic Casimir for the fundamental and adjoint representations are given by $C_f = \frac{N_c^2-1}{2N_c}$ and $C_A = \frac{1}{2}$ respectively [2, 21].

An identity involving the Casimirs involving a generator that is inserted between two generators that are being summed over is given by the following:

$$t^i_{\mathcal{R}} t^a_{\mathcal{R}} t^i_{\mathcal{R}} = t^a_{\mathcal{R}} \left(C_{\mathcal{R}} - \frac{N_c}{2}\right) \tag{D.7}$$

The proof of which is as follows:

$$\begin{aligned}
t^i t^a t^i =& t^a t^i t^i + [t^i, t^a] t^i \\
=& t^a C_{\mathcal{R}} + if^{iak} t^k t^i = t^a C_{\mathcal{R}} + if^{iak}\frac{1}{2}if^{kij}t^j = t^a\left(C_{\mathcal{R}} - \frac{N_c}{2}\right).
\end{aligned} \tag{D.8}$$

The $f^{abc\prime}$s are the totally anti-symmetric rank 3 colour structures. We can correspondingly define the totally symmetric colour structures through the anti-commutator

$$\{t^a, t^b\} = \frac{1}{2N_c}\delta^{ab} d^{abc} t^c, \tag{D.9}$$

where $\{t^a, t^b\}$ is the anti-commutator of two generators. The Kronecker delta and symmetric tensor constitute the trace-full and traceless parts of the anti-commutator respectively.

One can decompose the product of two generators into an expression involving the symmetric and anti-symmetric colour structures:

$$t^a t^b = \frac{1}{2N_c}\delta^{ab} + \frac{1}{2}(if^{abd} + d^{abd})t^d \tag{D.10}$$

A corollary of equation (D.10) is the following identity.

$$f^{abc}t^a t^b = f^{abc}\frac{1}{2}if^{abd}t^d, \tag{D.11}$$

which one obtains by substituting the decomposition of the product of generators in,

$$\begin{aligned} f^{abc}t^a t^b =& f^{abc}\left(\frac{1}{2N_c}\delta^{ab} + \frac{1}{2}(if^{abd} + d^{abd})t^d\right) \\ =& f^{abc}\frac{1}{2}if^{abd}t^d, \end{aligned} \tag{D.12}$$

where we have made use of the fact that the product of a symmetric matrix with an anti-symmetric matrix is zero.

Another way of decomposing the product of two generators is through using what is known as the Fierze identity

$$t^c_{ij}t^c_{kl} = \frac{1}{2}(\delta_{il}\delta_{jk} - \frac{1}{Nc}\delta_{ij}\delta_{kl}) \tag{D.13}$$

To start the proof of this, we remind the reader that the dimension of traceless Hermitian matrices is the same as the space of Hermitian matrices minus one. This is simply because the trace condition removes one degree of freedom:

$$\dim(\mathcal{H}) = \dim(SU(N_c)) + 1. \tag{D.14}$$

A consequence of this is that any Hermitian matrix, H, can be decomposed into a linear combination of the traceless Hermitian matrices, t^a, and the identity matrix,

$$H = c^0\mathbb{1} + c^a t^a, \tag{D.15}$$

where the extra degree of freedom in the trace is recovered in c^0. Using D.2 we can work out these coefficients exactly

$$c^0 = \frac{1}{N_c}\text{tr}(H), \qquad c^a = 2\text{tr}(Ht^a). \tag{D.16}$$

With this we may rewrite D.14 with the coefficients in place,

$$H = \frac{1}{N_c}\text{tr}(H)\mathbb{1} + 2\text{tr}(Ht^a)t^a. \tag{D.17}$$

If we write this with the indices explicit, we'll find that the identity we desire can be factored out,

$$H_{ij} = \frac{1}{N_c}H_{kk}\delta_{ij} + 2H_{kl}t^a_{lk}t^a_{ij}. \tag{D.18}$$

We introduce Kronecker delta in order to permit a factoring of H_{kl},

$$\delta_{ik}\delta_{jl}H_{kl} = \frac{1}{N_c}\delta_{lk}H_{kl}\delta_{ij} + 2H_{kl}t^a_{lk}t^a_{ij}. \tag{D.19}$$

We may finally factorize,

$$\left(t^a_{lk}t^a_{ij} - \frac{1}{2}\left(\delta_{ik}\delta_{jl}H_{kl} - \frac{1}{N_c}\delta_{lk}\delta_{ij}\right)\right)H_{kl} = 0. \tag{D.20}$$

This must hold for any Hermitian matrix and thus for any H_{kl}. Therefore we may safely divide it out and we are left with

$$t^a_{lk}t^a_{ij} - \frac{1}{2}\left(\delta_{ik}\delta_{jl}H_{kl} - \frac{1}{N_c}\delta_{lk}\delta_{ij}\right) = 0, \tag{D.21}$$

and the theorem is proven. This can also be efficiently proven using birdtracks, as in [21].

A corollary of the Fiertz identity is the following:

$$\text{tr}(t^a A t^a B) = \frac{1}{2}\text{tr}(A)\text{tr}(B) - \frac{1}{2N_c}\text{tr}(AB) \tag{D.22}$$

So far, we've only talked about Wilson lines as elements of $SU(N_c)$. In actuality, Wilson lines are fields, as in, the have a coordinate dependence. We have already covered the derivatives of Wilson lines in section 3.50, but another identity involving the derivatives of Wilson lines is the following:

$$U^\dagger(v)(\partial_i U(v)) = -(\partial_i U^\dagger(v))U(v). \tag{D.23}$$

This is a trivial consequence of the unitary property of Wilson lines. To prove it, consider the derivative of the identity element:

$$\begin{aligned} \mathbb{1} &= U^\dagger(v)U(v) \\ \Rightarrow \partial_i\mathbb{1} &= \partial_i(U^\dagger(v)U(v)) \\ 0 &= U^\dagger(v)(\partial_i U(v)) + (\partial_i U^\dagger(V))U(v) \\ \Rightarrow U^\dagger(v)(\partial_i U(v)) &= -(\partial_i U^\dagger(V))U(v) \end{aligned} \tag{D.24}$$

In section 3.1.1, we introduced the Lie derivatives of $SU(N_c)$. We claimed that they have the properties (3.22) and (3.23):

$$[i\nabla^a_x, i\nabla^b_y] = if^{abc}i\nabla^c_x\delta_{xy}; \qquad [i\bar{\nabla}^a_x, i\bar{\nabla}^b_y] = if^{abc}i\bar{\nabla}^c_x\delta_{xy}$$

and

$$[i\nabla^a_x, i\bar{\nabla}^b_y] = 0,$$

where $\delta_{xy} = \delta(x-y)$ is the Dirac delta function. To prove the first identity, we simply compute the commutator:

$$\begin{aligned} [i\nabla^a_x, i\nabla^b_y] &= i\nabla^a_x i\nabla^b_y - i\nabla^b_y i\nabla^a_x \\ &= [U_x t^a]_{ij}\frac{\delta}{\delta U_{x,ij}}\left([U_y t^b]_{kl}\frac{\delta}{\delta U_{y,kl}}\right) - [U_y t^b]_{ij}\frac{\delta}{\delta U_{y,ij}}\left([U_x t^a]_{kl}\frac{\delta}{\delta U_{x,kl}}\right) \end{aligned} \tag{D.25}$$

We must not forget that the functional derivative, $\frac{\delta}{\delta U_{ij}}$, acts on both factors in the parentheses via the product rule. However, the functional derivative commutes with the second derivative, so the contribution from this term to the commutator is zero. This leaves us with only

$$[i\nabla^a_x, i\nabla^b_y] = U_{x,in}t^a_{nj}\left(\frac{\delta U_{y,km}}{\delta U_{y,ij}}\right)t^b_{ml}\frac{\delta}{\delta U_{y,kl}} - U_{y,in}t^b_{nj}\left(\frac{\delta U_{x,km}}{\delta U_{y,ij}}\right)t^a_{ml}\frac{\delta}{\delta U_{x,kl}}. \tag{D.26}$$

Now we use the fact that $\frac{\delta U_{x,km}}{\delta U_{y,ij}} = \delta_{ki}\delta_{nj}\delta_{xy}$, resulting in

$$\begin{aligned}
[i\nabla^a_x, i\nabla^b_y] &= U_{x,in}t^a_{nj}t^b_{jl}\frac{\delta}{\delta U_{y,il}}\delta_{xy} - U_{y,in}t^b_{nj}t^a_{jl}\frac{\delta}{\delta U_{x,il}}\delta_{xy} \\
&= U_{x,in}[t^a,t^b]_{nl}\frac{\delta}{\delta U_{x,il}}\delta_{xy} \\
&= f^{abc}U_{x,in}t^c_{nl}\frac{\delta}{\delta U_{x,il}}\delta_{xy} \\
&= f^{abc}i\nabla^c_x\delta_{xy} \qquad\qquad \square,
\end{aligned} \tag{D.27}$$

as per the commutation relations of the generators of $SU(N_c)$. The proof for the right invariant vector field follows the same path. To prove that the two Lie derivatives commute among themselves is similar. We start by expanding the commutator

$$\begin{aligned}
[i\bar{\nabla}^a_x, i\nabla^b_y] &= -[t^aU_x]_{ih}\frac{\delta}{\delta U_{x,ij}}\left([U_yt^b]_{kl}\frac{\delta}{\delta U_{y,kl}}\right) \\
&= -[t^aU_x]_{ij}\delta_{ik}\delta_{jm}t^b_{ml}\frac{\delta}{\delta U_{y,kl}}\delta_{xy} + [U_yt^b]_{ij}t^a_{km}\delta_{im}\delta_{jl}\frac{\delta}{\delta U_{x,kl}}\delta_{xy} \\
&= -[t^aU_x]_{ij}t^b_{jl}\frac{\delta}{\delta U_{y,il}}\delta_{xy} + [U_yt^b]_{ij}t^a_{ki}\frac{\delta}{\delta U_{x,kj}}\delta_{xy}.
\end{aligned} \tag{D.28}$$

To compute the next step, we relabel the indices of the first term as $il \leftrightarrow kj$. We are free to do this since those are dummy indices that are being summed over. This makes it easier to compare the two terms. We also expand $[Ut^b]_{ij}$ as $U_{in}t^b_{nj}$ and $[t^aU]_{kl}$ as $t^a_{kn}U_{nl}$. This results in

$$\begin{aligned}
[i\bar{\nabla}^a_x, i\nabla^b_y] &= U_{x,in}t^b_{nj}t^a_{ki}\frac{\delta}{\delta U_{y,kj}}\delta_{xy} - t^a_{kn}U_{y,nl}t^b_{lj}\frac{\delta}{\delta U_{x,kj}}\delta_{xy} \\
&= \left([t^aU_xt^b]_{kj} - [t^aU_xt^b]_{kj}\right)\frac{\delta}{\delta U_{x,kj}}\delta_{xy} \\
&= 0,
\end{aligned} \tag{D.29}$$

which completes the proof.

Bibliography

[1] Aaboud el al. Search for pair production of higgs bosons in the $b\bar{b}b\bar{b}$ final state using proton-proton collisions at $\sqrt{s} = 13$ TeV with the atlas detector. *Phys. Rev. D*, 94:052002, Sep 2016.

[2] M.E. Peskin and D.V. Schroeder. *An Introduction To Quantum Field Theory*. Frontiers in Physics. Avalon Publishing, 1995.

[3] Schwartz, M.D. *Quantum Field Theory and the Standard Model*. Quantum Field Theory and the Standard Model. Cambridge University Press, 2014.

[4] Heribert Weigert. Evolution at small x(bj): The Color glass condensate. *Prog. Part. Nucl. Phys.*, 55:461–565, 2005.

[5] Yuri V. Kovchegov, Janne Kuokkanen, Kari Rummukainen, and Heribert Weigert. Subleading-N(c) corrections in non-linear small-x evolution. *Nucl. Phys.*, A823:47–82, 2009.

[6] Alan D. Martin. Proton structure, Partons, QCD, DGLAP and beyond. *Acta Phys. Polon.*, B39:2025–2062, 2008.

[7] Sergey E. Derkachov and R. Kirschner. Parton interactions in the Bjorken limit of QCD. *Phys. Rev.*, D64:074013, 2001.

[8] Ringaile Placakyte. Parton Distribution Functions. In *Proceedings, 31st International Conference on Physics in collisions (PIC 2011): Vancouver, Canada, August 28-September 1, 2011*, 2011.

[9] Alexander Van-Brunt and Matt Visser. Explicit baker-campbell-hausdorff formulae for some specific lie algebras. *arXiv preprint arXiv:1505.04505*, 2015.

[10] Jian-Hua Gao. A Derivation of the Gauge Link in Light Cone Gauge. *Phys. Rev.*, D82:014018, 2010.

[11] C. J. Bomhof, P. J. Mulders, and F. Pijlman. The Construction of gauge-links in arbitrary hard processes. *Eur. Phys. J.*, C47:147–162, 2006.

[12] Judith Alcock-Zeilinger. Symmetry implications for wilson line correlators in qcd at high energies. 2017.

[13] Rikkert Frederix. Wilson lines in qcd. 2005.

[14] F. Fiorani, G. Marchesini, and L. Reina. Soft Gluon Factorization and Multi - Gluon Amplitude. *Nucl. Phys.*, B309:439–460, 1988.

[15] I. Balitsky. Operator expansion for high-energy scattering. *Nucl. Phys.*, B463:99–160, 1996.

[16] Heribert Weigert. Unitarity at small Bjorken x. *Nucl. Phys.*, A703:823–860, 2002.

[17] E. Iancu and D. N. Triantafyllopoulos. Higher-point correlations from the JIMWLK evolution. *JHEP*, 11:105, 2011.

[18] Cyrille Marquet and Heribert Weigert. New observables to test the Color Glass Condensate beyond the large-N_c limit. *Nucl. Phys.*, A843:68–97, 2010.

[19] Robert Moerman. A gauge-invariant, symmetry-preserving truncation of jimwlk. 2017.

[20] Janne Kuokkanen, Kari Rummukainen, and Heribert Weigert. HERA-Data in the Light of Small x Evolution with State of the Art NLO Input. *Nucl. Phys.*, A875:29–93, 2012.

[21] Cvitanović, P. *Group Theory: Birdtracks, Lie's, and Exceptional Groups*. Princeton University Press, 2008.

[22] T. Lappi, A. Ramnath, K. Rummukainen, and H. Weigert. Jimwlk evolution of the odderon. *Phys. Rev. D*, 94:054014, Sep 2016.

[23] Javier Albacete. Numerics of gluon exchange functions.

[24] Javier L. Albacete, Adrian Dumitru, Hirotsugu Fujii, and Yasushi Nara. CGC predictions for p + Pb collisions at the LHC. *Nucl. Phys.*, A897:1–27, 2013.

[25] Fabio Dominguez, Cyrille Marquet, Bo-Wen Xiao, and Feng Yuan. Universality of Unintegrated Gluon Distributions at small x. *Phys. Rev.*, D83:105005, 2011.

[26] Stéphane Munier, Stéphane Peigné, and Elena Petreska. Medium-induced gluon radiation in hard forward parton scattering in the saturation formalism. *Phys. Rev.*, D95(1):014014, 2017.

[27] Magdalena Djordjevic and Marko Djordjevic. Generalization of radiative jet energy loss to non-zero magnetic mass. *Phys. Lett.*, B709:229–233, 2012.

[28] Cyrille Marquet. Forward inclusive dijet production and azimuthal correlations in p(A) collisions. *Nucl. Phys.*, A796:41–60, 2007.

[29] Edmond Iancu and Julien Laidet. Gluon splitting in a shockwave. *Nucl. Phys.*, A916:48–78, 2013.

[30] Adrian Dumitru and Jamal Jalilian-Marian. Forward quark jets from protons shattering the colored glass. *Phys. Rev. Lett.*, 89:022301, 2002.

[31] Alex Kovner, J. Guilherme Milhano, and Heribert Weigert. Relating different approaches to nonlinear QCD evolution at finite gluon density. *Phys. Rev.*, D62:114005, 2000.

[32] Martin Hentschinski. Exclusive methods in qcd at high energies. Feb 2005.

[33] Michael L. Miller, Klaus Reygers, Stephen J. Sanders, and Peter Steinberg. Glauber modeling in high energy nuclear collisions. *Ann. Rev. Nucl. Part. Sci.*, 57:205–243, 2007.

[34] Haber, H. *Useful relations involving the generators of su(N)*. 2016.